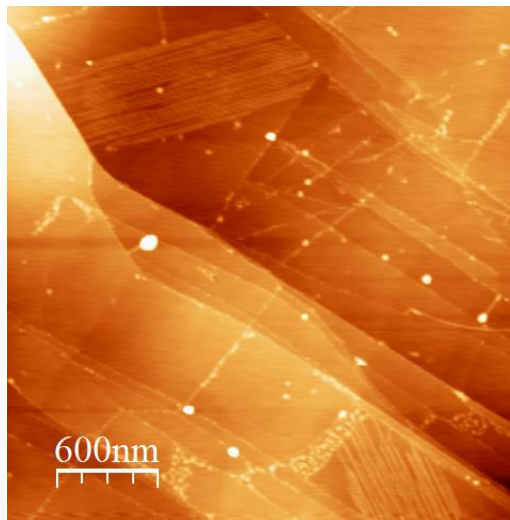


Functionalisation of Graphite Surfaces with Varying Concentrations of Nitric Acid and Aqua Regia, and their Effect on the Deposition of Gold Nanoparticles



By
Daniel J. Wotton

MPhil Thesis
Department of Chemistry
Cardiff University
October 2017

Abstract

The surface science of graphite surfaces for real world applications currently is poorly understood but shows promise in certain chemical industries such as acetylene hydrochlorination and thiosulfate leaching of preg-robbing ores. In this work the role of oxygen functional groups on the surface of HOPG introduced through acid treatment with nitric acid, aqua regia and sulfuric acid has been explored to determine how these functionalities influence the deposition of gold nanoparticles.

Previous work by Cardiff University has determined that acid treatment with 0.5 mol dm^{-3} nitric acid introduces hydroxyl groups onto the surface determined by selective derivatization. Heating of these surfaces creates ketones and ethers and that these differences in functionality change how gold is deposited on the surface.

HAuCl_4 treatment of HNO_3 activated HOPG resulted in very little gold deposition on the surface when using low concentrations of nitric acid or no nitric acid. At nitric acid concentrations of 1.0M or higher there is a large increase in the quantities of gold on the surface. Higher concentrations showed an increase in the ratio of Au(III) to Au(0) deposited.

In aqua regia treated surfaces higher concentrations resulted in more ketone present on the surface as determined by selective derivatization. This effected gold deposition by showing a large increase in Au(0) deposited at these higher aqua regia concentrations.

Sulfuric acid activated samples showed sulfur being incorporated into the HOPG samples. Dilute concentrations of sulfuric acid were required to deposit large amounts of gold and all gold deposited was in the form of Au(0).

The results and conclusions derived from them give insight into the effect of acid washing with different acids and their effect on the subsequent loading of the active gold ion.

Acknowledgements

I would like to thank my supervisor Philip Davies as well as David Morgan for their continuous support and guidance throughout the course of this research. Philip Davies for always being available and David Morgan for his assistance in obtaining XPS results.

I would also like to thank my friends Vaughn Roberts, Alice Josephine Schmitz and Emir Bouleghlimat for their support over this course.

Contents

1. Introduction	8
1.1 Surface Science and Heterogeneous Catalysis.....	8
1.1.1 Activation Energy of Catalysed Reactions.....	11
1.2 Catalysis at Surfaces.....	12
1.3 Catalysis by Gold	13
1.4 The Physical and Chemical Properties of Gold	14
1.5 Physical Properties and Characterisation of Small Gold Particles	14
1.6 Acetylene Hydrochlorination	16
1.7 Acetylene Hydrochlorination Using Mercury Catalysts	17
1.8 Studies of the Activities of Metal Chlorides as Catalysts for Acetylene Hydrochlorination .	18
1.9 Acid Washing of HOPG and its Effect on the Deposition of Au Metal Nanoparticles.....	22
1.10 Atomic Force Microscopy (AFM).....	24
1.11 Introduction to AFM Theory	24
1.12 AFM Scanning Modes	25
1.12.1 Contact Mode	25
1.12.2 Non-contact Mode.....	26
1.12.3 Tapping Mode	27
1.13 AFM Images.....	27
1.13.1 Surface Topography	27
1.13.2 Deflection Images	28
1.14 X-ray Photoelectron Spectroscopy (XPS)	29
1.15 Introduction to XPS Theory.....	29
1.15.1 Photoelectric Effect.....	30
1.15.2 Electron Mean Free Path	31
1.15.3 Koopmans' Theorem.....	32
1.15.4 XPS Instrument.....	32
1.16 Initial and Final State Effects on XPS Spectra.....	34

1.16.1	Chemical Environment, Oxidation States and Chemical Bonds.....	34
1.16.2	Surface Charging	34
1.16.3	Spin-Orbit Coupling.....	35
1.17	XPS – Quantitative Analyses	36
1.17.1	Determining Surface Concentration of Adsorbed Species.....	36
1.18	Selective Derivatization for Determination of Oxygen Functionalities	37
2	Experimental.....	39
2.1	Graphite Samples.....	39
2.2	Nitric Acid, Aqua Regia, Sulphuric Acid, Chloroauric Acid & Mixed Solutions.....	39
2.3	UPW Treatment for Creating References	40
2.4	Nitric Acid Treatment.....	40
2.5	Gold Treatment.....	40
2.6	Gold in Acid Treatment.....	40
2.7	Selective Derivatization of Oxygen Functionalities.....	40
3	Results and Discussion	42
3.1	Clean HOPG Treated with UPW	42
3.2	HNO ₃ Treatment on HOPG.....	44
3.2.1	0.25M HNO ₃ Treated HOPG.....	45
3.2.2	0.5M HNO ₃ Treated HOPG	46
3.2.3	1.0M HNO ₃ Treated HOPG	47
3.2.4	2.0M HNO ₃ Treated HOPG	48
3.2.5	5.0M HNO ₃ Treated HOPG	49
3.3	HAuCl ₄ (2x10 ⁻⁶ moldm ⁻³) Treatment of HNO ₃ Treated HOPG	52
3.3.1	Clean HOPG Treated with UPW before Treatment with HAuCl ₄ (2x10 ⁻⁶ M).....	53
3.3.2	HNO ₃ (0.25M) – HAuCl ₄ (2x10 ⁻⁶ M)	54
3.3.3	HNO ₃ (0.5M) – HAuCl ₄ (2x10 ⁻⁶ M)	55
3.3.4	HNO ₃ (1.0M) – HAuCl ₄ (2x10 ⁻⁶ M)	55
3.3.5	HNO ₃ (2.0M) – HAuCl ₄ (2x10 ⁻⁶ M)	56

3.3.6	HNO ₃ (5.0M) – HAuCl ₄ (2x10 ⁻⁶ M)	56
3.4	Aqua Regia (AR) Treatment of HOPG.....	59
3.4.1	0.25M AR Treated HOPG.....	60
3.4.2	0.5M, 1.0M, 2.0M and 5.0M AR Treated HOPG.....	60
3.4.3	Fluorinating Hydrophilic Groups on AR Treated HOPG for Determination the Identity of the Oxygen Functionalities	62
3.5	HAuCl ₄ (2x10 ⁻⁶ moldm ⁻³) Treatment of AR Treated HOPG	65
3.5.1	AR (0.25M) – HAuCl ₄ (2x10 ⁻⁶ M).....	66
3.5.2	AR (0.5M) – HAuCl ₄ (2x10 ⁻⁶ M).....	67
3.5.3	AR (1.0M) – HAuCl ₄ (2x10 ⁻⁶ M).....	67
3.6	Comparison of HAuCl ₄ Treated HNO ₃ Activated HOPG with HAuCl ₄ Treated AR Activated HOPG	69
3.7	Heat Treatment of AR Activated HOPG and Its Effect on the Deposition of HAuCl ₄	74
3.7.1	UPW – Heat (473K) – HAuCl ₄ (2x10 ⁻⁶ M).....	74
3.7.2	AR (xM) – Heat (473K) – HAuCl ₄ (2x10 ⁻⁶ M).....	75
3.8	H ₂ SO ₄ Treatment on HOPG	78
3.8.1	0.1M H ₂ SO ₄ Treated HOPG.....	79
3.8.2	0.2M H ₂ SO ₄ Treated HOPG.....	81
3.8.3	0.3M H ₂ SO ₄ Treated HOPG.....	83
3.9	HAuCl ₄ (2x10 ⁻⁶ moldm ⁻³) Treatment of H ₂ SO ₄ Treated HOPG.....	86
3.9.1	UPW – HAuCl ₄ (2x10 ⁻⁶ M).....	86
3.9.2	2x10 ⁻⁶ M HAuCl ₄ on 0.1M H ₂ SO ₄ Treated HOPG	86
3.9.3	2x10 ⁻⁶ M HAuCl ₄ on 0.2M H ₂ SO ₄ Treated HOPG	88
3.9.4	2x10 ⁻⁶ M HAuCl ₄ on 0.3M H ₂ SO ₄ Treated HOPG	90
3.10	Effect of H ₂ SO ₄ on the bulk of HOPG	94
3.11	H ₂ SO ₄ & HAuCl ₄ (2x10 ⁻⁶ moldm ⁻³) Solution Treatment of HOPG	95
3.11.1	H ₂ SO ₄ (0.1 moldm ⁻³) & HAuCl ₄ (2x10 ⁻⁶ moldm ⁻³) Solution Treatment of HOPG	96
3.11.2	H ₂ SO ₄ (0.2 moldm ⁻³) & HAuCl ₄ (2x10 ⁻⁶ moldm ⁻³) Solution Treatment of HOPG	97

3.11.3	H_2SO_4 (0.3 mol dm^{-3}) & HAuCl_4 ($2 \times 10^{-6} \text{ mol dm}^{-3}$) Solution Treatment of HOPG	99
4	Conclusion.....	103
5	Further Work.....	106
6	References	108

1. Introduction

1.1 Surface Science and Heterogeneous Catalysis

The work presented in this thesis relates to the investigation of the bonding of gold nanoparticles to an engineered graphite surface.

In the early years of the 19th century, when many of the most important discoveries in the fields of chemistry and physics were being made, it was observed that a number of chemical reactions were significantly affected by trace amounts of substances that were not consumed during the reaction. It was noticed that traces of acid could bring around the hydrolysis of starch, and that low concentrations of metal ions (not then recognized as metal ions) affected the decomposition of hydrogen peroxide into water and hydrogen.[1]

The scientific observations could not be rationalised with what was known about chemical reactivity at the time and it was many years before methods were developed for the accurate measurement of the rates of reactions. The first attempt at rationalization of these findings was made by J. J.

Berzelius who stated

'I shall therefore call it the catalytic power of substances, and the decomposition by means of this power catalysis, just as we use the word analysis to denote the separation of the component parts of bodies by means of ordinary chemical forces. Catalytic power actually means that substances are able to awake affinities which are asleep at this temperature by their mere presence and not by their own affinity.' [1]

Today, catalysts play a highly prominent role in society where the vast majority of all chemicals and fuels produced within the chemical industry involves catalysis in one or more steps of its synthesis. Catalysis has also made important strides in environmental pollution control where selective catalytic routes have replaced stoichiometric processes that generate high quantities of waste. A very common example used in everyday life, is in the three-way catalysts that lead to an effective reduction in the pollution emitted from car exhausts. [2]–[4]. Catalysis has been used in nature long before humans discovered the first catalysts to be used in artificial synthesis. These catalysts are called enzymes and are important in the lives and health of all living things as they are integral to important biological reactions in the body. Enzymes are biological catalysts that are usually made from complex structures of proteins, which sometimes have a metal atom containing a prosthetic group such as a chlorophyll or haem molecule. Enzymes are incredibly effective biocatalysts and are often seen as the pinnacle of catalytic power and as such all synthetic catalysts strive to emulate their performance.[5]

Catalysis is the increase in the rate of a reaction without modifying the overall standard Gibbs energy change in the reaction, and involves changing the pathway of a reaction to one that is faster and requires a lower activation energy, the catalyst is also not used up in the reaction.[6] The energy vs reaction path diagram shown in figure 1 provides an illustrated example of the effect catalysts have on the energy required to reach a reactions transition state.

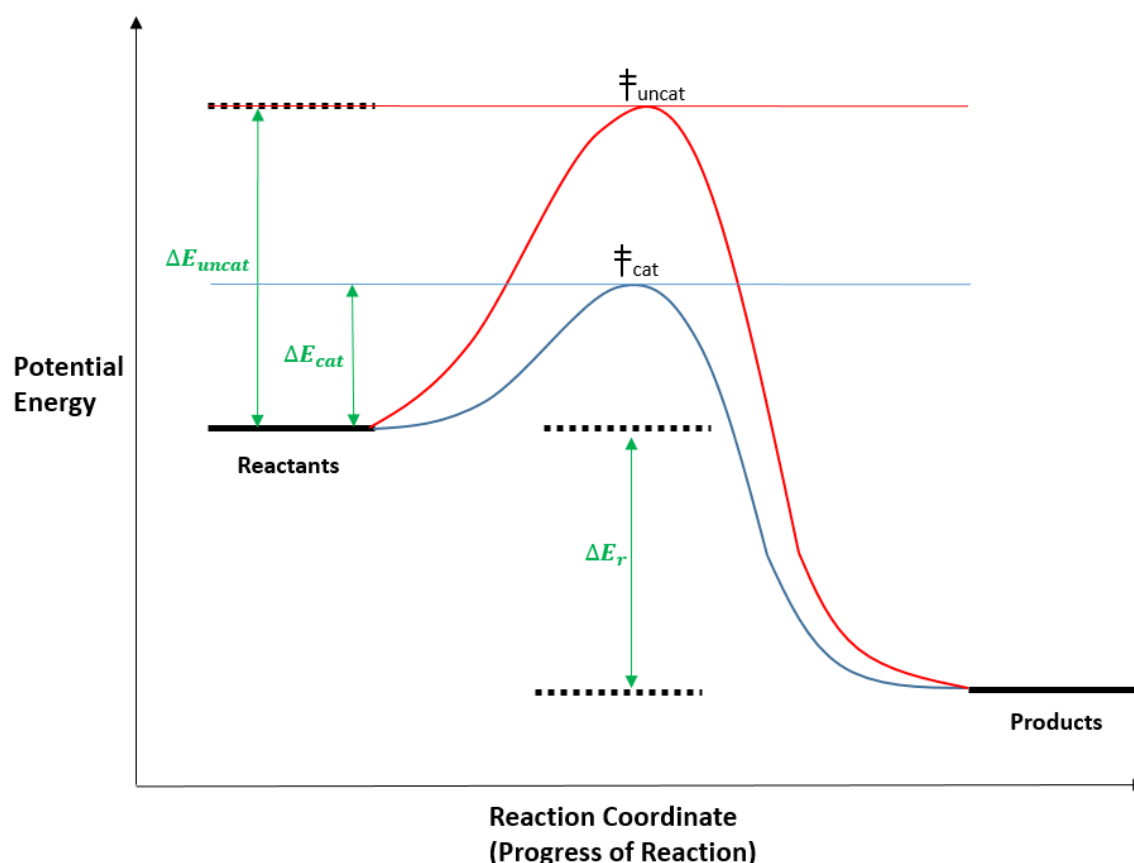


Figure 1 – The energy vs reaction path diagram representing the effect a catalyst has to lower the reaction activation energy from ΔE_{uncat} to ΔE_{cat} allowing the reaction to occur upon a more favourable pathway.

Catalysis can be classified into homogeneous and heterogeneous catalysis. Homogeneous catalysis involves a reaction where the catalyst and reactants are of the same phase, either liquid or gas. By contrast, heterogeneous catalysis involves a reaction where the phase of the catalyst and reactants are different and reactions occur at, or near, interfaces between the phases.

Heterogeneous catalytic reaction begins with the adsorption of the reacting gases or liquids onto the surface of the catalyst. After adsorption intramolecular bonds are broken or weakened before reacting on the surface, often in a number of consecutive steps. The final stage involves desorption of the products from the surface of the catalyst thereby regenerating the active site on the surface for the following catalytic cycle. The function of the catalyst is to provide an energetically favourable pathway for the reaction where the activation barriers of all the intermediate steps are low

compared to the activation energy of the gas phase reactants. An example of the catalytic oxidation of carbon monoxide is illustrated schematically in Figure 2. During this reaction the key role of the catalyst is to dissociate the O₂ molecule which binds to the surface of many metals. [7], [8]

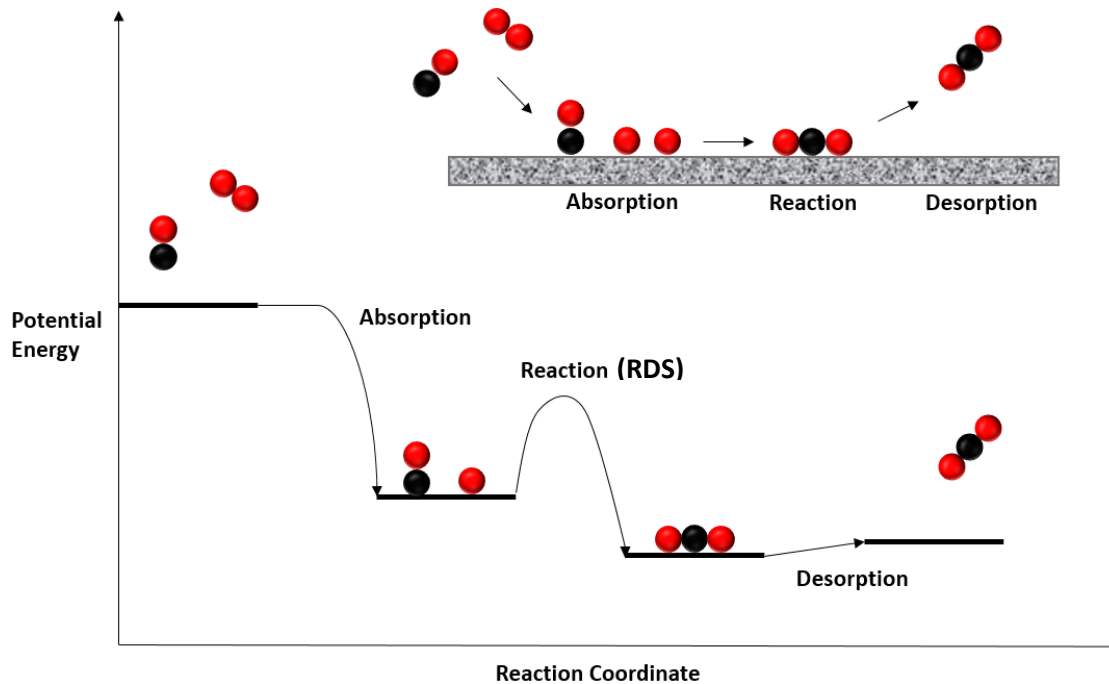


Figure 2 - Schematic representation of a well-known catalytic reaction, the oxidation of carbon monoxide on noble metal catalysts with the overall reaction being $CO + \frac{1}{2}O_2 \rightarrow CO_2$.

The catalytic reaction of the oxidation of carbon monoxide on noble metal catalysts begins with the associative adsorption of O₂ onto the surface. As adsorption is always exothermic the potential energy decreases. In the reaction step, the CO and O molecules combine to form an adsorbed CO₂ molecule. This is the rate determining step, in the catalytic sequence. The adsorbed CO₂ molecule desorbs almost instantly, thereby liberating adsorption sites for the next reaction and conversion of CO to CO₂. This regeneration of sites distinguishes catalytic reactions from stoichiometric ones.[7]

1.1.1 Activation Energy of Catalysed Reactions

In any catalysed reaction, the overall process can be divided into five constituent steps

- i. Transport of the reactants to the catalyst.
- ii. Adsorption of reactants on the catalyst.
- iii. Interactions of adsorbed reactants.
- iv. Desorption of products from the catalyst
- v. Transport of products away from the catalyst

Steps (i) and (v) involve no chemical change but are often the rate limiting step, especially with highly porous catalysts. Steps (ii), (iii) and (iv) do involve a chemical reaction and provided that any one of these steps are rate limiting, the reaction will obey the Arrhenius equation.

$$k = Ae^{\frac{-\Delta E}{RT}}$$

Where k is the rate constant, A is the so-called pre-exponential factor and E is the activation energy. This equation can also be expressed in the form

$$\ln(k) = \ln(A) - \frac{E}{R} \cdot \frac{1}{T}$$

When looking at the equation in this form it appears that A is the hypothetical value of the rate constant at infinite temperature. However from the standpoint of collision theory, A may also be equated to the product of the collision number, Z and a steric factor, P .

If hypothetically a unimolecular reaction occurs where the rate determining step is the formation of the catalyst-reactant complex, step (ii), then the collision number in question is the number of collisions per unit time between the catalytic sites or species and the reactant molecules. Now the concentration of the catalytic sites is normally very small. Therefore the number of relevant collisions (collisions between reactants and catalytically active sites) is smaller by a factor of about 10^{12} when compared to non-relevant collisions (collisions between reactant molecules with reaction molecules). Because of this huge difference in the number of collisions, for the catalysed reaction to compete with the uncatalysed reaction then the exponential term has to be some 10^{12} times larger than in the catalysed reaction. If the required factor is exactly 10^{12} then the activation energy for the catalysed reaction must be about 67 kJmol^{-1} less than that for the uncatalysed reaction for the catalysed reaction to be as fast as the uncatalysed reaction. For efficient catalysis then the activation energy difference has to be greater still and preferably exceed 83 kJmol^{-1} . [9]

These statements are illustrated graphically in Figure 1 and some experimental values for the activation energy of catalysed and uncatalysed reactions are given in Table 1.

Reaction	$E_{\text{uncatalysed}} \text{ (kJmol}^{-1}\text{)}$	$E_{\text{catalysed}} \text{ (kJmol}^{-1}\text{)}$	Catalyst
$2HI \rightarrow H_2 + I_2$	184	105	Au
		59	Pt
$2N_2O \rightarrow 2N_2 + O_2$	245	121	Au
		134	Pt
Pyrolysis of diethyl ether	224	144	I ₂ vapour

Table 1 - Activation energies of catalysed and uncatalysed reactions[9]

1.2 Catalysis at Surfaces

Most large scale, industrially catalysed processes are heterogeneous and involve the application of a solid catalyst in contact with the gas or liquid phase reactants. For these type of reactions the nature of the interface is crucial for changing the efficiency of the process. The nature of the top layer of atoms can have a drastic effect on the rate a catalytic reaction occurs and small amounts of additives can either reduce (poison) or enhance (promote) the reaction.

Since the nature of the surface involved in heterogeneous catalysis is crucial to its performance the structure is important to consider as a starting point for the discussion of catalytic properties.

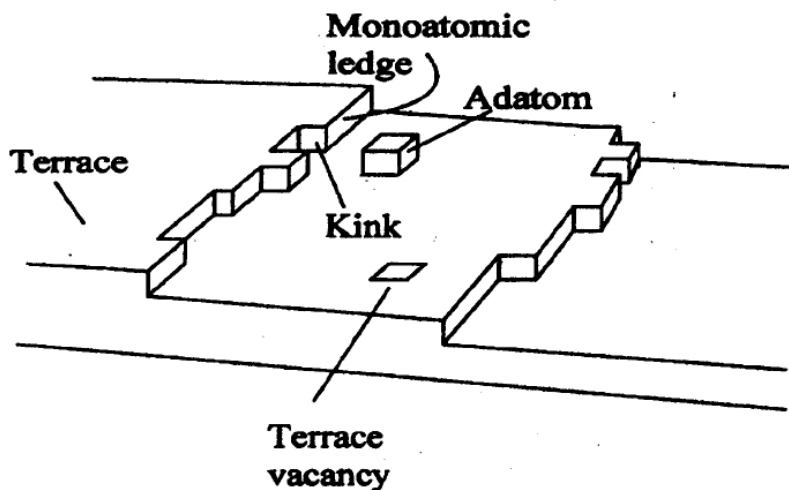


Figure 3 – The Terrace-Step-Kink (TSK) schematic, representation of a single crystal surface showing different defects on the surface.[10]

On real single crystal surfaces, ideal surface planes are perturbed by relaxation effects and the presence of atomic-scale defects. It is therefore more appropriate to think of single crystal surfaces as being composed of terraces of stable planes separated by atomic-scale steps or ledges that contain kinks. In addition, various point defects such as atomic vacancies or surface adatoms are often present. Figure 3 shows a schematic representation of this single crystal surface.

1.3 Catalysis by Gold

Gold is an element that has fascinated mankind for thousands of years. It is viewed as immutable, unchanging and has been the ultimate symbol of wealth and prosperity in civilizations across the world. The constancy of gold is a result of its chemical inertness when in its bulk form.

During the 19th century one of the most interesting catalytic effects were shown by the noble metals platinum and palladium, which had only recently become available and were considered highly inert chemicals. Michael Faraday managed to demonstrate that a platinum sponge was capable of sustaining the oxidation of ethanol vapour. Meanwhile J . W. Döbereiner discovered that platinum could bring about the oxidation of hydrogen which he later developed into a device which acted as a lamp lighter, and in 1831 Peregrine Phillips patented the role of platinum in the oxidation of sulfur dioxide which later became the basis of industrial scale sulfuric acid manufacturing.[1] This showed the potential for noble metals in catalysis and paved the way for experiments using gold nanoparticles.

1.4 The Physical and Chemical Properties of Gold

It is important to discuss the physical and chemical properties of gold to understand how gold works as a catalyst. Whilst it would be simple to list different properties of gold it is important to discuss how and why the properties of gold differ from the properties of its neighbouring elements, particularly those elements preceding it in group 11, to gain an appreciation of their full significance.[7]

Heterogeneous catalysis is a phenomenon whereby a chemical reaction proceeds on a surface, before these reactions can occur the molecules must adsorb to the surface as discussed and illustrated in the oxidative reaction of carbon monoxide as shown in Figure 2.

Since chemisorption is necessary before catalysis, the chemical and physical properties of gold are important to help determine not only what it can and can't catalyse, but also what the levels of activity are likely to be. At various times catalytic activity has been associated with either geometric structure or electronic constitution or energetic parameters such as latent heat of sublimation before it was finally appreciated that these and many other properties of metals are themselves related. Therefore, catalytic activity cannot be ascribed to a single metallic property. It is therefore likely that a number of factors work synergistically to determine the types and strengths of bonds formed between the metal and the molecules at the surface. All the properties of gold therefore become a proper subject for enquiry.

There is one major difference between the catalytic properties of gold compared with other metals, and that is that its catalytic ability in carbon monoxide oxidation and several other reactions is a steep function of the size of the metal particle responsible. It is therefore important to examine how the properties of gold depend on the size and assembly of atoms.

Whilst every element is unique in some respects, gold occupies a position at one extreme of the range of metallic properties. Its exceptional chemical inertness is attributed to chemical features that surpass any other metal.

1.5 Physical Properties and Characterisation of Small Gold Particles

Despite occasional references in older literature to the ability of gold to catalyse certain reactions, the metal has, until recent years, had the reputation of being one of the least catalytically active or useful. It wasn't until the discovery that supported gold nanoparticles could significantly affect the oxidation of carbon monoxide at or below room temperature, that gold became the focus of attention for a lot of the scientific community that studied catalysis.[7]

Supported gold and gold alloy nanoparticles have been found to be highly catalytically active and selective in a variety of important catalytic reactions, particularly when the particles are only a few nm in size.[11]–[18] The change in catalytic activity between inert bulk gold and supported gold nanoparticles has been ascribed to a variety of mechanisms. This includes the fact that individual gold atoms have far fewer neighbouring atoms (ie. a high degree of coordinative unsaturation),[19]–[22] quantum size effects which alter the electronic band structure, electronic modification of the charge on the gold atoms by their interaction with the underlying oxide in metal oxide supported gold nanoparticles,[23]–[25] or the combined effect of sites on the oxide (vacancies or other defects), possibly modified by the presence of nearby gold, working together with sites on the gold nanoparticles.

Whilst the surface of large gold particles exhibit some modest catalytic properties, with highly dispersed forms of gold the catalytic activity per unit mass of metal; is dependent upon the fraction of atoms at the surface and this of course increases as the mean particle size is made smaller. This fraction is called the ‘degree of dispersion’, and the way in which it varies with particle size can be calculated if it is assumed that the unit mass is converted into structureless spheres of uniform size.[26]–[28] This is shown in Figure 4 and shows how the particles size affects the fraction of gold atoms exposed on the surface, this relationship was found to be similar for other nanoparticle shapes as well such as cubes with 5 exposed faces and perfect cubo-octahedra.

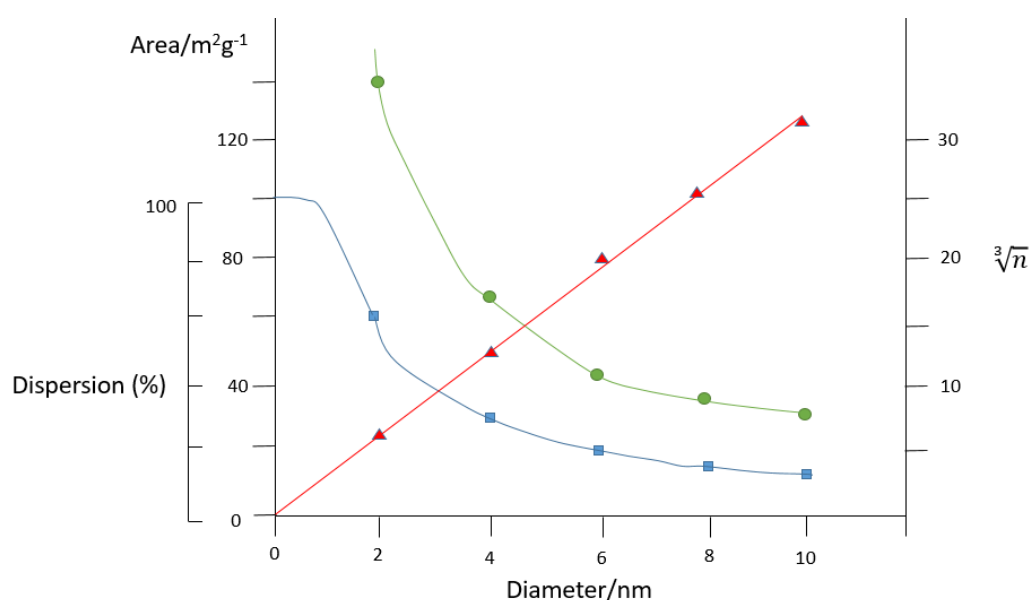


Figure 4 -Dependence of surface area (●), dispersion (■) and $\sqrt[3]{n}$ (where n = the number of atoms per particle) (▲) on particle diameter for uniform spheres of gold.[5] (Data redrawn from reference [5])

1.6 Acetylene Hydrochlorination

Vinyl chloride monomer (VCM), is a major commodity chemical produced on an industrial scale with 40 million tons of it being produced annually. One of the key reasons for such high levels of production is that it is the monomer for the production of polyvinyl chloride (PVC) a major non-biodegradable polymer with numerous uses. PVC is currently the third highest selling polymer because of its relatively low production cost, biological and chemical resistance and workability which make it particularly useful in the construction industry, for applications such as in piping and electric cable insulation.[29]

VCM has been manufactured on a large scale since the 1950's when the initial process was based on the hydrochlorination of acetylene using mercuric chloride supported on carbon as the catalyst. Acetylene is produced from coal via calcium carbide as an intermediate. The HCl then undergoes electrophilic addition across the acetylene triple bond.



Subsequently, a newer route, often referred to as the balanced process, was developed in which ethene is converted to ethylene dichloride (EDC) via chlorination and oxychlorination reactions, after which the EDC is thermally cracked to VCM.

- i. $\text{CH}_2=\text{CH}_2 + 2\text{HCl} + \frac{1}{2}\text{O}_2 \rightarrow \text{CH}_2\text{Cl}-\text{CH}_2\text{Cl} + \text{H}_2\text{O}$
- ii. $\text{CH}_2=\text{CH}_2 + \text{Cl}_2 \rightarrow \text{CH}_2\text{Cl}-\text{CH}_2\text{Cl}$
- iii. $\text{CH}_2\text{Cl}-\text{CH}_2\text{Cl} \rightarrow \text{CH}_2=\text{CHCl} + \text{HCl}$

In recent decades, western economies has shifted the production of VCM almost exclusively from ethene due to the increase in the availability of oil lowered the price of ethene.

However the availability of inexpensive coal from China has led to a resurgence in producing VCM from the hydrochlorination of acetylene again. At present over 13 million tons of VCM are being manufactured annually in China from acetylene hydrochlorination using mercury catalysts. This has prompted a resurgence in the interest of the hydrochlorination of the acetylene reaction, especially in the design of non-mercury catalysts and gold has become the new catalyst of choice for the synthesis of this very important monomer.

1.7 Acetylene Hydrochlorination Using Mercury Catalysts

Mercury was selected as a catalyst at the outset of VCM production from acetylene. The catalysts use a high area activated carbon ($1000-2000 \text{ m}^2\text{g}^{-1}$) on which mercuric chloride is deposited by adsorption from aqueous solution and a 10 wt % mercuric chloride catalyst is typically utilized. High surface area activated carbons are used since they remain stable in the presence of HCl and HNO_3 at high temperatures, therefore maintaining a high surface area. In addition, activated carbon is very effective in adsorbing mercuric chloride (HgCl_2). As such virtually all studies on the hydrochlorination of acetylene utilize carbon as the support.

The mercuric chloride catalyst has a number of major disadvantages. One is the volatility of mercuric chloride at the reaction temperature which results in a high loss of mercury from the catalyst leading to an exceptionally short catalytic lifetime. Secondly mercury may catalyse the secondary, addition of HCl to vinyl chloride leading to a loss in selectivity. This downstream ethane dichloride cracking unit can be used to obtain VCM, but this has its own obvious disadvantages whereby the process becomes more complex and expensive.[30], [31]

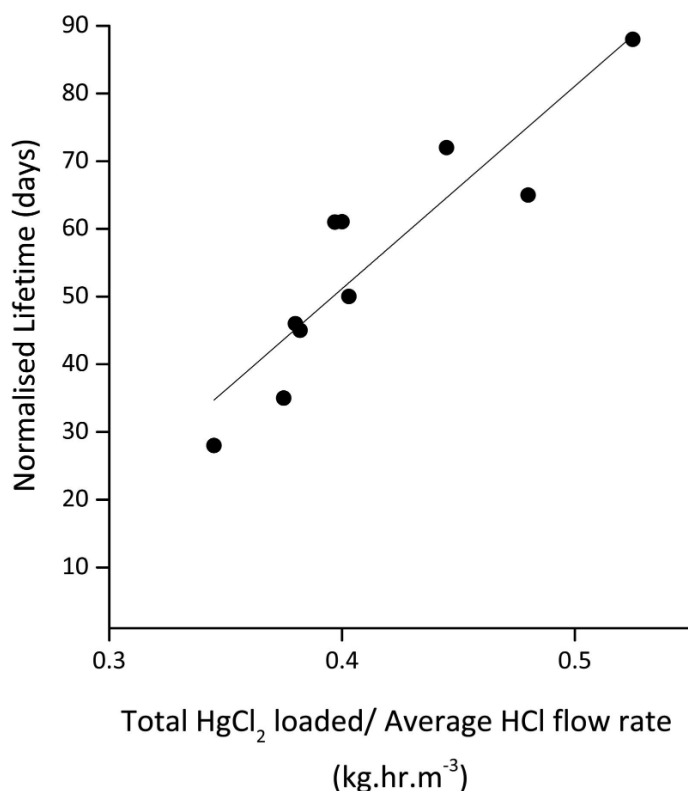


Figure 5 - Catalyst lifetime of mercuric chloride catalysts showing the relationship with $[\text{HgCl}_2]$ and the reactant flow rate. (Data redrawn from reference 12[30])

Commercial production of VC in these units requires 600-1000 tonnes of Hg per annum. It has not been possible to trap mercury effectively and therefore the mercury escapes the production units leading to significant environmental problems. At present, around 60% of annual mercury production is used in the manufacture of this VCM catalyst. This is a highly unsustainable situation due to the environmental and health risks of mercury being released into the environment and the fact that mercury deposits are rapidly becoming depleted. However with the wide availability of cheap coal from China, acetylene hydrochlorination is still a very attractive method for PVC production, as such there is a need to produce a new non-mercury containing catalyst for the process.

1.8 Studies of the Activities of Metal Chlorides as Catalysts for Acetylene Hydrochlorination

A very important paper in the identification of an improved catalyst for acetylene hydrochlorination is one by Shinoda[32] where the vapour-phase hydrochlorination of acetylene was studied over a series of metal chlorides supported on carbon and silica. Shinoda evaluated over 30 metal chlorides and attempted to correlate the catalysts activity with the electron affinity of the metal cation.

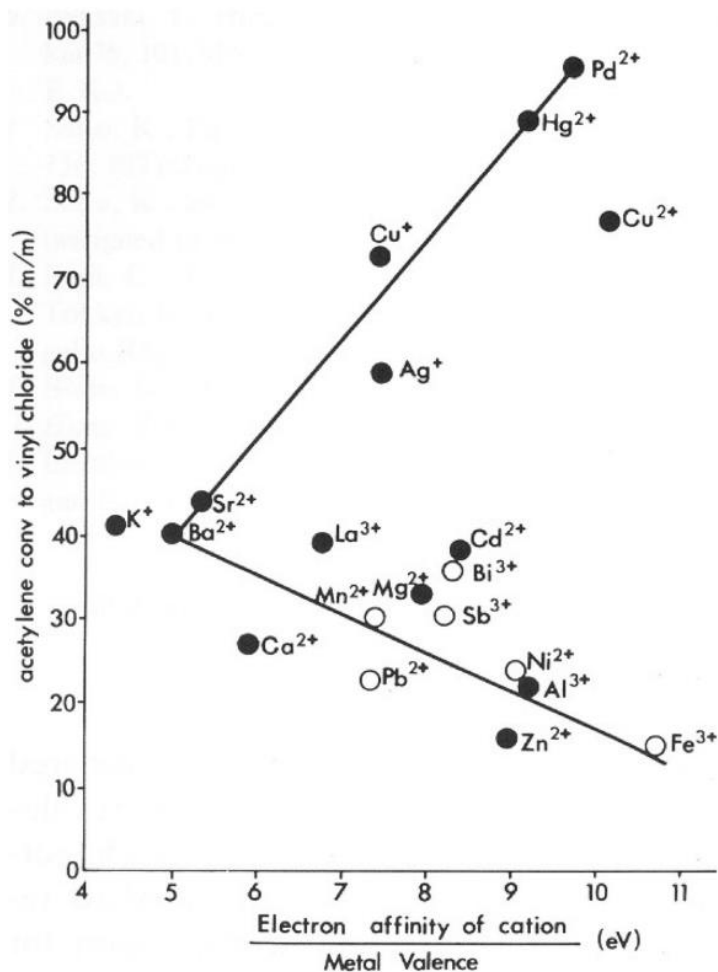


Figure 6 - Graph showing the divalent correlation of the reactivity for acetylene hydrochlorination with the electron affinity of the catalyst cation. (Data redrawn from reference [32])

The data did not statistically correlate with the metal ions electron affinity. For example, the metal cations Zn²⁺, Cd²⁺ and Hg²⁺ span from most to least active but all have similar electron affinities as seen in Figure 6. As such, the data presented in Figure 6 cannot be used in a predictive manner and therefore would not be very useful in predicting the activity of a new metal chloride and would have to be determined experimentally.

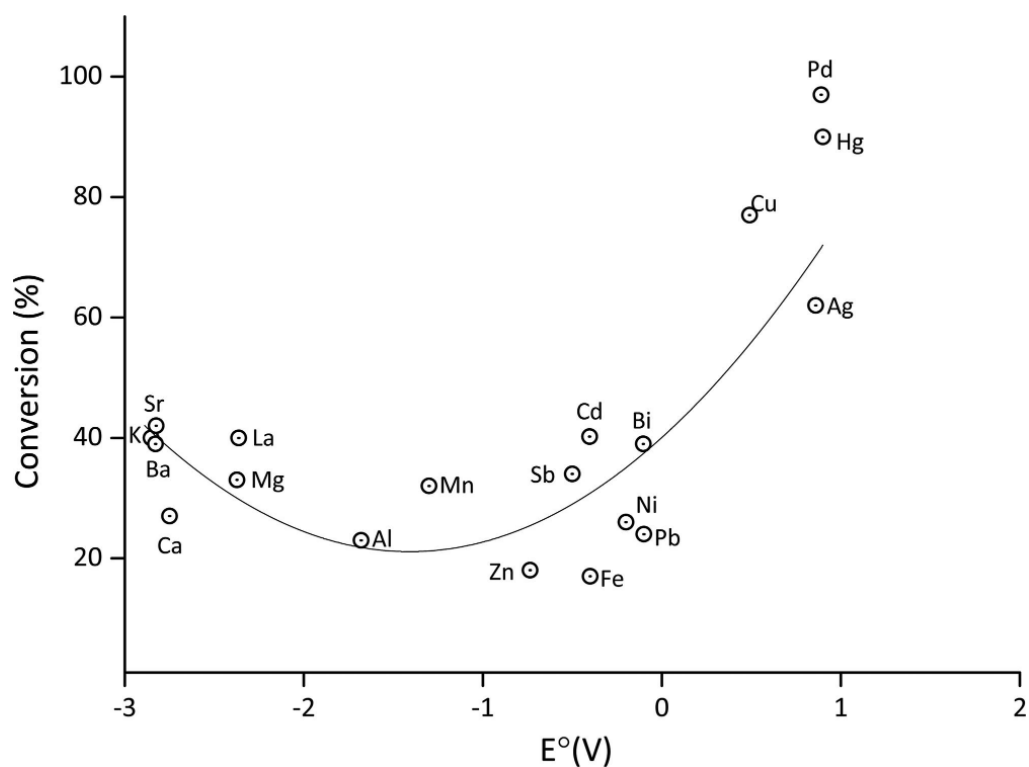


Figure 7 - A graph showing the correlation between percentage of acetylene conversion to vinyl chloride and the standard electrode potential (data replotted from Figure 6 and redrawn from reference [33])

Hutchings made a significant improvement on Shinoda's approach to determining the standard electrode potential of cations and is shown in Figure 7. The graph shows a general correlation between the activity of the metal ion to acetylene conversion to vinyl chloride and the standard electrode potential.[33] This correlation suggests that catalysts with the highest standard electrode potentials would be the most effective catalysts allowing the trend seen in Figure 7 to be used to predict that gold would be a very effective catalyst for this reaction. Gold was used experimentally and was shown to be a very effective catalyst for the hydrochlorination of acetylene.[34]

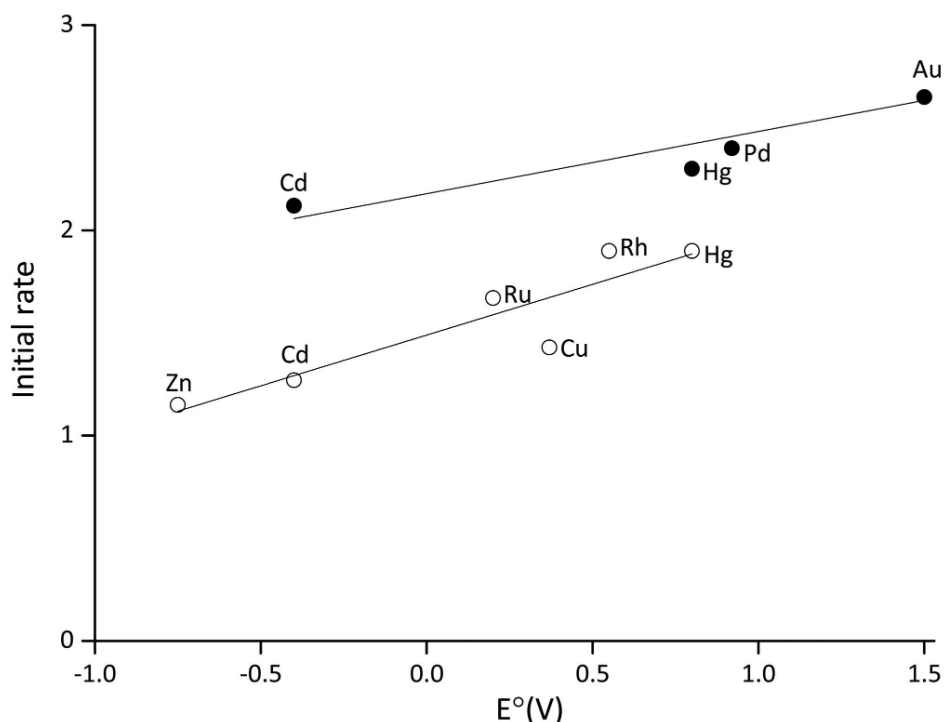


Figure 8 - Correlation of the initial activity (mol of HCl converted per mol of metal per hour) with the standard electrode potential for the reaction $M^{2+} + 2e^- \rightarrow M$ ($M = Zn, Cd, Cu, Ru, Rh, Hg, Pd$) and for $Au^{3+} + 2e^- \rightarrow Au^0$. \circ 10^{-4} mol metal, \bullet 10^{-5} mol metal. Reaction conditions: $C_2H_2:HCl = 1:1.1$; reactor set point temperature = $180^\circ C$. Gas hourly space velocity (GHSV) = $1080 h^{-1}$, defined as the total volume of reactant gas passed per volume of catalyst per hour (data redrawn from ref [34])

Figure 8 confirms the correlation with the standard electrode potential. The data shown is based on the initial activity (determined as an integrated rate over the catalyst bed) this is because the other catalysts other than gold deactivate rapidly.

Previous studies have shown that the hydrochlorination reaction between Au(III) and acetylene in the acetylene hydrochlorination reaction occurs via the formation of a $C_2H_2/Au/HCl$ complex [35], [36] with an activation effect by HCl and a detrimental effect by C_2H_2 on the catalyst performance during on stream studies. The catalysts are also affected by a slow deactivation [37], and this was found to be due to the reduction of Au^{3+} to Au^0 during the reaction. On-stream studies have shown that it is possible to regenerate the catalyst by means of Cl_2 and NO [38], therefore increasing the catalyst effective useable life. However, it was also demonstrated that an off-line treatment which involved boiling the catalyst in aqua regia was highly effective as a regeneration method [39], and at present it appears that aqua regia is also the best solvent for the preparation of this catalyst.

1.9 Acid Washing of HOPG and its Effect on the Deposition of Au Metal Nanoparticles

Carbon materials such as graphite have been regularly used in heterogeneous catalysis as a low cost, high surface area support. Carbon also has the additional advantage that precious metals can be reclaimed from the surface at the end of the catalyst's lifetime with relative ease.[40]

The effectiveness of carbon catalysts can be determined both by the topography and surface chemistry which can be studied effectively through AFM and XPS analysis. In the case of activated carbons the topography can be chosen with different proportions of micro, meso or macropores.[41]

A lot of research has been done with metal deposition on graphite surfaces (Highly Ordered Pyrolytic Graphite) under vacuum conditions where the surface functionality has been removed. However, this ignores the interactions between the metal nanoparticles and these surface functionalities and their effect on the nucleation, stability and chemistry of the metal nanoparticles on the surface. [42]

It is well known that the interaction between the active phase and the support depends significantly on the preparation method, the pre-treatment and/or addition of promoters. This changes the surface functionalities which significantly changes the interactions between the support and the active species as well as their dispersion. As a result, the vast majority of carbon catalyst preparations involve washing the carbon support in either HCl, HNO₃ or aqua regia before adsorption of the active catalyst. The washing step also removes contaminants such as N, P, Si, Ca, Na, K, Al, Zn and Fe that can accumulate on the surface.[43]–[45]

A study of the effects of Ni catalyst supported on activated carbon found that the surface area and pore volume of carbon supports are generally enhanced upon acid treatment. The adsorption capacity of Ni²⁺ on the carbon supports was also shown to increase with a close correlation to the surface acidity. They attributed this to the formation of acidic functional groups and noted that HCl treatment produced a less stable catalyst than HNO₃ treated carbons.[45]

A separate study conducted by Wang and Zhu produced further information on the differences between HCl and HNO₃ treated carbon, using adsorption of dye molecules and studying it using temperature programmed desorption (TPD) and x-ray photoelectron spectroscopy (XPS). Studies by TPD observed differences in the evolution of CO and CO₂ from HCl and HNO₃ treated carbon. HNO₃ treatment resulted in the desorption of more CO₂ at lower temperatures. The author's suggest that HNO₃ treatment produced carboxylic acid, anhydride, lactone and phenol groups.

Work done by the Cardiff Catalysis Institute looked at the functional groups on acid treated HOPG through the selective derivatisation of HNO₃ and HCl treated carbon functional groups and

subsequent XPS characterization. This was done through reacting the functional groups on the surface with fluorinated compounds that selectively react with certain oxygen groups in a 1:1 stoichiometric ratio. Three different fluorinated compounds were used separately, each one targeted to a different oxygen functionality on the surface (hydroxyl, ketone and carboxylic acid), the presence of fluorine, as seen by XPS, showed bonding of the fluorinated compound to its subsequent oxygen group. This method showed that both nitric acid treatment and hydrochloric acid treatment of graphite generates almost solely hydroxyl groups. [46], [47] In the case of HCl treated graphite the hydroxyl groups were shown to get converted to ketone and ether functionalities with heating of the sample.[47]

Further work by Cardiff University looked at how HNO_3 treatment of graphite surfaces affects the deposition of gold nanoparticles from chloroauric acid. A graphite surface was treated for 30 minutes with $0.5 \text{ mol dm}^{-3} \text{ HNO}_3$, blow dried with helium and then treated with a $2 \times 10^{-6} \text{ mol dm}^{-3}$ solution of chloroauric acid for 30 minutes before being blow dried with helium again. It was discovered that gold nanoparticles showed a better dispersion on the hydroxylated surface compared to surfaces that were clean or contained ketone and ether groups. XPS results also showed that gold adsorbed onto hydroxylated surfaces was completely reduced to Au^0 whereas gold adsorbed onto ketone and ether functionalized carbon contained a small component attributed to Au^{3+} .

The acid used in the treatment of carbon for Au/C catalysts for hydrochlorination of acetylene is aqua regia, however there is very little work done on looking at how aqua regia effects the gold deposition. This study looks at how different concentrations of aqua regia effects the deposition of Au(III) and how this compares to samples treated with only nitric acid. Whilst previous studies have shed some light onto the effect of $0.5 \text{ mol dm}^{-3} \text{ HNO}_3$ on graphite and the subsequent effect the acid activation has on the deposition of gold nanoparticles, no work has been done yet on how the graphite surface changes or how the deposition of gold nanoparticles differs when the surface is treated with varying concentrations of HNO_3 . As such this paper looks at the effect of varying concentrations of HNO_3 and Aqua Regia on the surface of graphite and its effect on gold nanoparticle deposition in a bid to further understand the mechanism. These samples were studied with XPS and AFM.

1.10 Atomic Force Microscopy (AFM)

1.11 Introduction to AFM Theory

Atomic force microscopy is a type of scanning probe microscopy that is capable of investigating surfaces of conductors and insulators at near atomic scale. The atomic force microscope is a combination of the principles of both the scanning tunnelling microscope and the stylus profilometer and was developed from the scanning tunnelling microscope by G. Binnig, C. F. Quate and C. Gerber in 1986.[48]

AFM is used when conventional optical microscopes cannot reach the levels of magnification required to study the topography of the surface as a result of the visible light wavelengths (~300-700nm). AFM has advantages when compared to other nano-imaging techniques due to the fact that it can be conducted in ambient conditions without the need for ultra-high vacuum conditions. It is also capable of imaging soft surfaces without damaging them which makes it particularly useful for imaging biological samples.

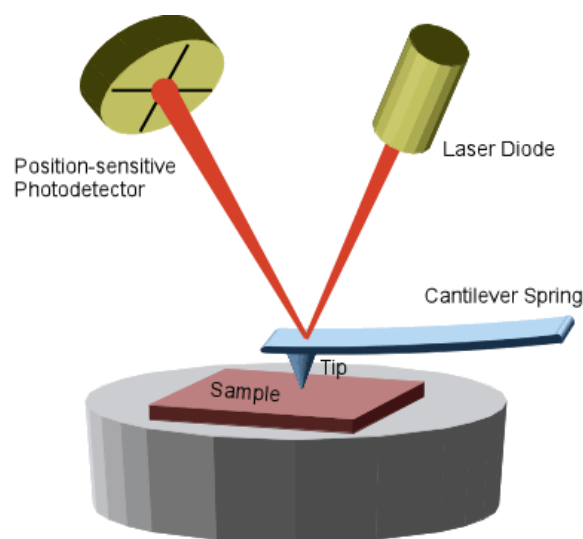


Figure 9: A schematic representation of an atomic force microscope

Figure 9 shows a diagram of the operation of an atomic force microscope. A sample is mounted onto an XYZ stage below the scanning probe which can be moved accurately in two dimensions. The tip of the probe is extremely fine, typically between 1-20nm and was once made from diamond but is now more commonly made from either silicon or silicon nitride.[49], [50]

The probe is brought into close proximity to the samples surface. At a certain distance from the surface, atomic forces such as Van-der Waals or Pauli exclusion forces between the tip and the surface become significant and causes the cantilever to deflect according to Hooke's law.

$$F = -kx$$

Equation 1: Hooke's Law

F = Force of the cantilever extension

k = Spring/stiffness constant of the cantilever

x = Distance of cantilever deflection

A laser beam is focused onto the top of the cantilever which is coated with a thin reflective film. The laser deflects the beam into a four quadrant photo detector. As the tip is moved across the samples surface, the cantilever experiences deflection due to the atomic forces between the tip and the surface. This cantilever deflection changes the angle at which the laser reflects into different areas of the split 4 quadrant photodiode detector. Processing of the detected information by computer software leads to a production of a topological image alongside a deflection image of the area being scanned. The sample holder moves along the x and y dimensions, moving the sample beneath the tip as opposed to the tip across the sample. The laser deflection from the cantilever then gives the z component. This z component is another big advantage in using AFM over other nano-imaging techniques as it allows the build-up of a three dimensional model of the surface.

1.12 AFM Scanning Modes

1.12.1 Contact Mode

Contact mode AFM is a static mode of operation where the tip remains in close contact with the sample and is deflected as the sample moves in the x and y direction beneath the tip. Despite the name, contact mode AFM does not actually touch the surface as this would damage both the tip and the surface. Instead contact mode utilizes the intermolecular forces between the tip and sample. However the close contact (a few angstroms) between tip and sample causes a large lateral repulsive force on the surface as the tip scans across the surface. Attractive forces occur from changes in potential as electrons overlap with chemical bonds. Repulsive forces are a result of nuclear and Pauli repulsions as the tip is brought very close to surface atoms.

There are two methods for using contact mode AFM, these work by maintaining either constant height or constant force between tip and surface. Constant deflection is achieved by employing a piezoelectric element for movement in the z direction and using a feedback loop of the repulsive

regime of the inter-molecular force curve for maintaining the height of the tip over the sample as the sample's topography changes. Contact mode is most commonly used for imaging hard and very hard samples due to the fact that the large lateral repulsive forces caused by the tips close proximity to the surface can damage softer surfaces.

1.12.2 Non-contact Mode

Non-contact mode is another commonly used AFM imaging technique. In this mode the cantilever is oscillated at its resonant frequency using a piezoelectric device and moves between 50 and 150 Å above the sample's surface. This mode of AFM relies on long range intermolecular forces such as van der Waals forces and electrostatic forces which are capable of interacting with the tip at this height and consequently decreasing the resonance frequency of the cantilever. The constant oscillation amplitude or frequency is maintained using a feedback loop. As the interactions between tip and surface changes the resonance frequency, the amplitude is kept constant by changing the distance between the tip and the surface. This tip-to-sample distance at each x, y coordinate is measured and used to determine the topography of the surface which results in the production of an AFM image when used in combination with appropriate software.

Two different dynamic mode operations can be used in non-contact mode AFM. In frequency modulation mode the frequency of the cantilever can be measured with very high sensitivity. This is usually achieved using very stiff cantilevers as it allows the tip to approach closer to the surface whilst maintaining its stability. Atomic resolution can be obtained using this modulation technique if performed in ultra-high vacuum conditions.

The second dynamic mode of operation is the amplitude modulation mode which uses feedback signals from the changes in oscillation amplitude to investigate and characterize different materials on the sample surface. This mode is also capable of using very stiff cantilevers and therefore can be used to achieve atomic resolutions.

Due to non-contact modes use of attractive, long range and weak intermolecular forces, this method of AFM imaging normally produces lower resolution images than either contact mode or tapping mode AFM in its normal use in ambient conditions. Its advantage over contact mode AFM is that it can be used on surfaces that are easily damaged such as biological surfaces, organic thin films or any other soft materials without causing surface degradation.

1.12.3 Tapping Mode

Tapping mode AFM is another dynamic mode of operation and is capable of producing high resolution topographical images for surfaces that are easily damaged, loosely held to their substrate or difficult to image through other techniques due to being insulating. It has the advantage of overcoming many of the issues faced with other AFM imaging techniques such as friction, adhesion or electrostatic forces.

This mode of operation works by setting the height of the tip at the point of maximum deflection of the cantilever. The probe tip gets close enough to the surface for a fraction of its oscillation period so that short range forces become detectable such as in contact mode AFM. But unlike contact mode AFM the tip is then lifted before the tip can be stuck to the sample and drag across the surface.

As the tip approaches the surface van der Waals forces, dipole interactions, electrostatic forces and other intermolecular forces interact with the cantilever resulting in the momentary decrease in oscillation frequency or amplitude in accordance with Hooke's law. The AFM image is therefore obtained by measuring the tips deflection in the z direction at each x, y coordinate as a result of the forces between tip and surface. Because of the lifting of the tip between coordinates the lateral forces are massively reduced allowing softer samples to be imaged at higher resolutions than can normally be obtained in non-contact mode under ambient conditions. This change is significant enough that adsorbed single molecules can be imaged without introducing changes to the surface.

1.13 AFM Images

AFM images can be obtained in multiple ways depending on the information required. Surface topography and deflection images are the common ones used in this project.

1.13.1 Surface Topography

Surface topography images give direct representation of the height of areas in an image. The data required to create these images is the deflection of the cantilever in the z direction and is directly obtained from contact, non-contact and tapping mode AFM imaging techniques. The differences in height are shown through colour mapping where the highest areas are typically represented with lighter colours and the lower areas represented with darker colours.

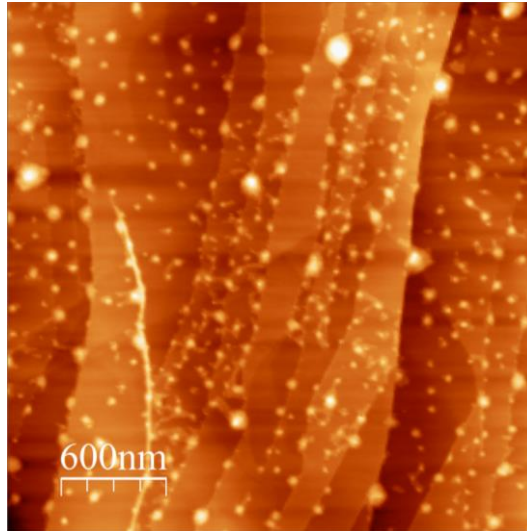


Figure 10: Surface topography AFM image showing an example of colour mapping.

Figure 10 shows an example of a topographical image where colour mapping has been applied to show a contrast between high areas, which appear almost white in colour, and low areas that are darker orange. Since these images are comprised from direct height and distance information line profiles can be taken that provide information on the height and width of particle islands on the surface, or the height of step edges.

1.13.2 Deflection Images

These images are obtained at the same time as the topographical images. Deflection images are the other type of image used in this project. Deflection images are a representation of the first derivatives of the deflection that are directly measured. This type of imaging gives a greater contrast of the surface topography as the derivation of the deflection enhances the gradient on the surface therefore generating more resolved images than those in standard surface topography. This results in clearer and more resolved images than those obtained using standard surface topography. As such deflection images are most commonly used in surface representation. The main disadvantage of this image is that the first derivative of the actual information is being used and therefore line profiles do not provide accurate height and width information.

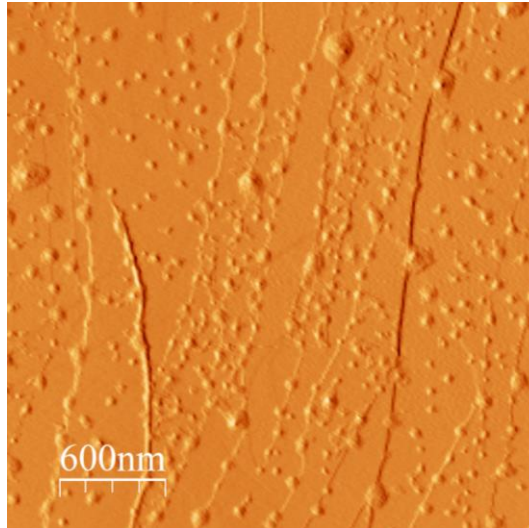


Figure 11: Deflection AFM image obtained with tapping mode AFM

Figure 11 shows the deflection image of the same area as in Figure 10. The shapes of the different features on the surface are more distinguishable and as such a much easier evaluation of the surface can be made.

1.14 X-ray Photoelectron Spectroscopy (XPS)

1.15 Introduction to XPS Theory

X-ray photoelectron spectroscopy (XPS) was first developed in the 1950's & 1960's by Kai Siegbahn and his research group under the name Electron Spectroscopy for Chemical Analysis (ESCA).[31] This is a widely used surface sensitive technique to investigate the identities and quantities of chemicals on a surface. This technique can give a lot of information including the elemental composition, chemical and oxidation state, and electronic state of the elements present in the first 10-12 nm of the surface.

1.15.1 Photoelectric Effect

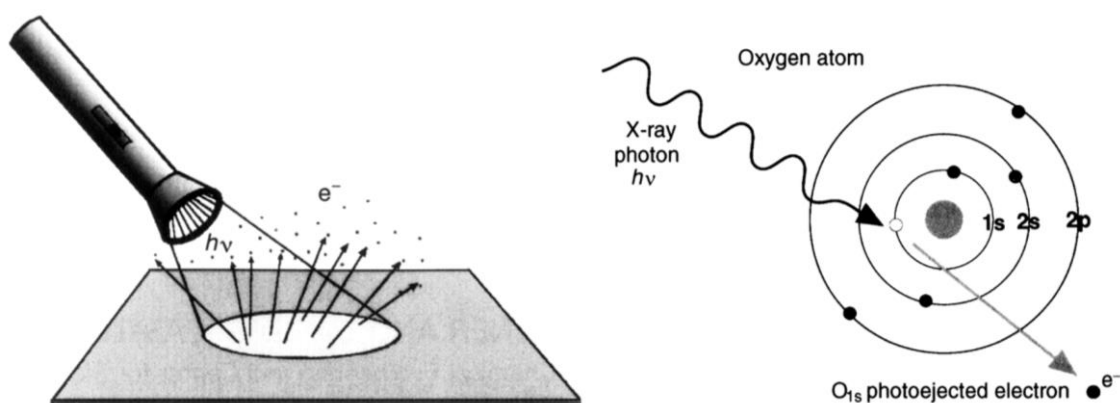


Figure 12 – Schematic representation of the photoelectric effect, where a light source on a surface causes the ejection of an electron from a core electron in an atom, in this case of oxygen.

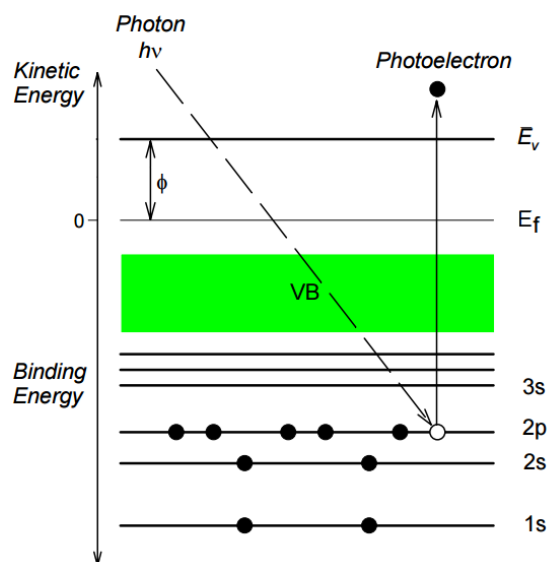


Figure 13: Energy level diagram of the photoemission of a core electron by excitation with $h\nu$.

Figure 13 is a diagram showing the photoelectric effect which is utilized in XPS. The photoelectric effect involves the irradiation of a sample with x-rays and the subsequent excitation and ejection of electrons that have the same energy as the x-ray photons. These high energy photons are aimed at exciting core electrons in XPS and the ejected electrons called photoelectrons. The photoelectrons kinetic energy is dependent on the energy of the x-ray photons and the binding energy of the element from which the electron came from. From measuring this kinetic energy the elements binding energy can be determined using the Einstein's photoelectric equation (Equation 2). This binding energy is specific to the atom involved and allows the determination of the exact element that the electron came from by comparison to known binding energies.

$$E_k = h\nu - (E_b + \phi)$$

E_k = kinetic energy of the photoelectrons

h = Plank constant

ν = frequency of the incident x-ray photons

E_b = binding energy of the photoelectron

ϕ = the work function of the material

1.15.2 Electron Mean Free Path

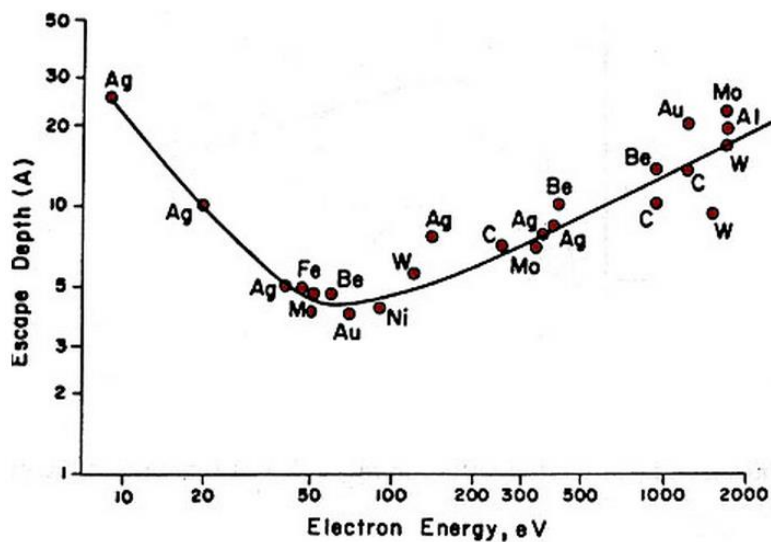


Figure 14: Graph showing the mean free paths for different elemental electrons[51]

XPS is a very sensitive technique and only investigates the top 3 – 5 nm of a sample. This is because although the incident x-rays penetrate deep into the sample, the electrons emitted have a very short mean free path, usually between 5 and 10 Å, and therefore only the very top most layers have electrons emitted that do not get reabsorbed by the bulk sample. This is shown in Figure 14 where different elements are shown to have different mean free paths based on the identity of the atoms being analysed.

1.15.3 Koopmans' Theorem

Koopmans' theorem states that in closed-shell Hartree-Fock theory, the first ionization energy of a molecular system is equal to the negative of the orbital energy of the highest occupied molecular orbital (HOMO). This theorem was published in 1934 and named after its discoverer Tjalling Koopmans who later became a Nobel laureate in 1975 in economics.[52]

According to Koopmans' theorem, the binding energy of an electron that has undergone photoemission is equal in energy to the orbital from which the electron was ejected. This makes the assumption that the ejected photoelectron does not interact in anyway with the cloud of the remaining electrons in the atom and atoms surrounding, within the timescale of photoemission i.e. that within the timescale of photoemissions, the distribution of the electrons is unchanged.

1.15.4 XPS Instrument

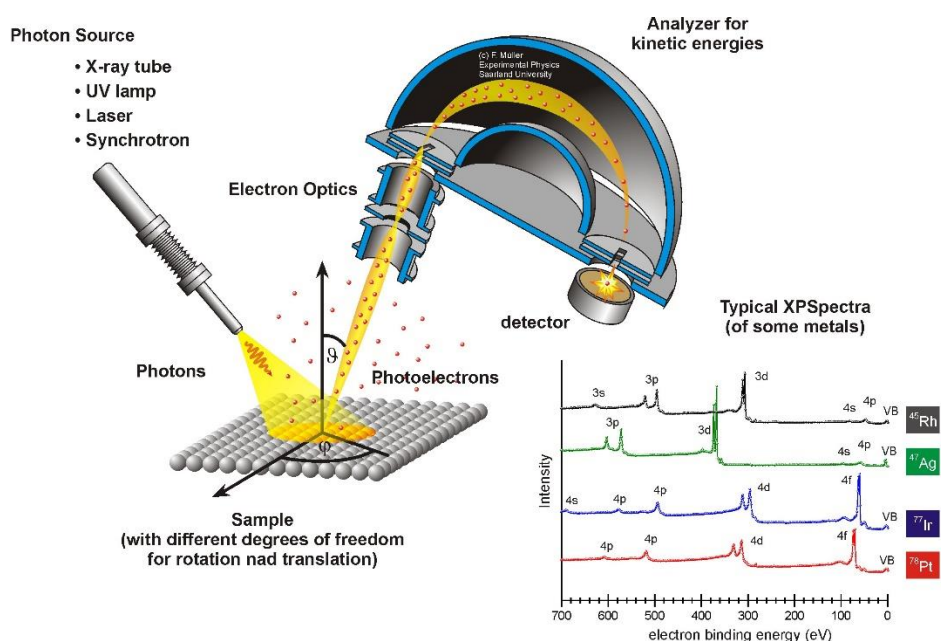


Figure 15: Schematic of an X-ray Photoelectron Spectrometer

Figure 15 shows the schematic of an x-ray photoelectron spectrometer. The spectrometer consists of several key components: an x-ray source (modern x-ray sources are all monochromatic using Mg K_{α} and Al K_{α} sources most commonly which provide photon energies of 1486 eV and 1258 eV respectively); a low voltage electron flood gun, commonly used in non-conducting samples to prevent a build-up in positive charge on the sample as electrons are ejected. This is important as charge build-up has a significant effect on the kinetic energies of electrons ejected (the electron flood gun is not present in the schematic shown). Finally there is an electron analyser which is used to determine photoelectron kinetic energies. Emitted photoelectrons are focused through a lens system into the

electron analyser and the kinetic energies of the photoelectrons are determined. These are then fed into an electron multiplier and detector used to determine the relative intensities of different energy photoelectrons. This provides quantitative information about the different elements on the surface. The intensity (number) of electrons detected with a specific binding energy is recorded in counts per second (CPS) to create a graph of CPS against binding energies as shown in Figure 16.

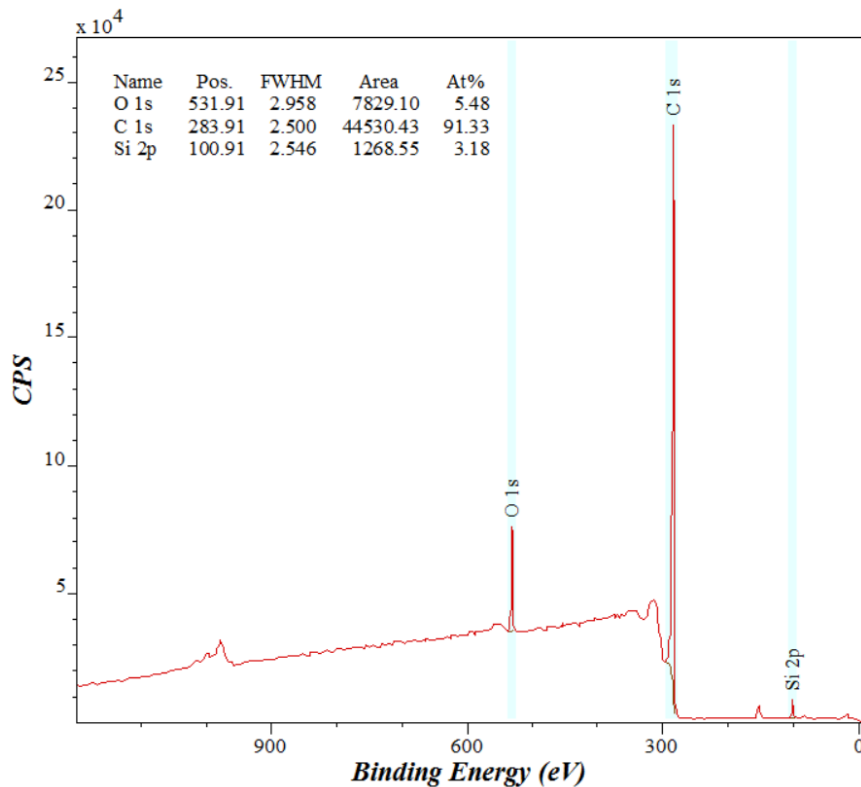


Figure 16: Wide scan XPS spectra of an untreated graphite surface.

XPS spectrometers require ultra-high vacuum (UHV) corresponding to pressures of 1.3×10^{-9} mbar which is achieved through a combination of rotary, turbo and ion pumps. This is required to remove any gases as electrons cannot travel through a gaseous medium. The pumps also remove any interference that could be caused through contamination. Sometimes the XPS chamber will also be heated whilst being evacuated to desorb and remove any contaminants that have become impregnated into the chamber walls, this further reduces the contamination risk. UHV is also required to ensure electrons have a long enough mean free path from the surface of the samples to the analyser to be detected without losing energy through interactions with other molecules in the system.

1.16 Initial and Final State Effects on XPS Spectra

A number of different factors can influence the position and shape of XPS peaks and need to be taken into account. These include the chemical environment of the elements of interest, the charging of the substrate and spin-orbit coupling.[53] The results describe only effects seen in this thesis.

1.16.1 Chemical Environment, Oxidation States and Chemical Bonds

Different chemical environments can change the effective nuclear charge of an atom. A higher oxidation state in an atom increases the binding energy of the core electrons resulting in a slight shift of the peak. This is useful in establishing the different oxidation states present and their relative quantities.

Different chemical bonds also shift peak positions but not normally to the same extent as different oxidation states. As such the presence of certain chemical bonds can be determined but quantities are often impossible to distinguish if more than one type of bonding to an element is present due to strong peak overlap.

1.16.2 Surface Charging

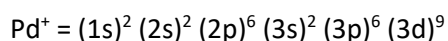
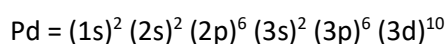
Surface charging is another effect that can change XPS spectra, but unlike with different chemical environments this effect needs to be minimized as it provides no useful information about the elements on the surface. This can make reading the spectra much more difficult or often impossible. As electrons are emitted from the sample surface, a build-up of positive charge occurs, this can cause the following photoelectrons to lose kinetic energy due to attraction to the sample after emission resulting in a greater observed binding energy of the electron and a shifting of the spectra in the x direction. Modern XPS instruments use low energy electron flood guns that flood the sample surface with low energy electrons that neutralise the surface.

Differential charging is a phenomenon that can occur on varying samples where certain areas contain different elements to others. This can lead to charge build up on the surface that isn't uniform. The result of this is broadening of the spectrum and the appearance of multiple peaks. This problem is also solved using low energy electron flood guns.

1.16.3 Spin-Orbit Coupling

Close inspection of an XPS spectrum shows that emission from all levels except s levels (most obviously 3p and 3d) gives rise to a closely spaced doublets. When $l > 0$ the magnetic coupling between the spin of an unpaired core electron with its angular momentum induces splitting known as spin-orbit coupling.

Spin-orbit splitting arises from an element obtaining a new electronic configuration following photoionisation. An unpaired electron is left which has a spin vector ($s = \pm 1/2$) where the spin is either parallel or anti-parallel to its orbital angular momentum vector (l). An example of this is with palladium, where the initial electronic configuration of Pd is:



The removal of an electron from the 3d sub-shell by photoionization leads to a $(3d^9)$ configuration for its final electron state. This $3d^9$ configuration gives rise to two states (ignoring any coupling with valence levels) which differ slightly in their energy and in their degeneracy.

For a one-hole configuration the degenerate hole state resolves into two components e.g. for Cu(2p), $l=1$ and $s=1/2$, this gives rise to two components labelled Cu ($2p_{3/2}$) for the antiparallel configuration and Cu ($2p_{1/2}$) for the parallel configuration. The respective intensities of these two final states are given by $(2J+1)$ resulting in a Cu($2p_{3/2}$):Cu($2p_{1/2}$) intensity ratio of 2:1.

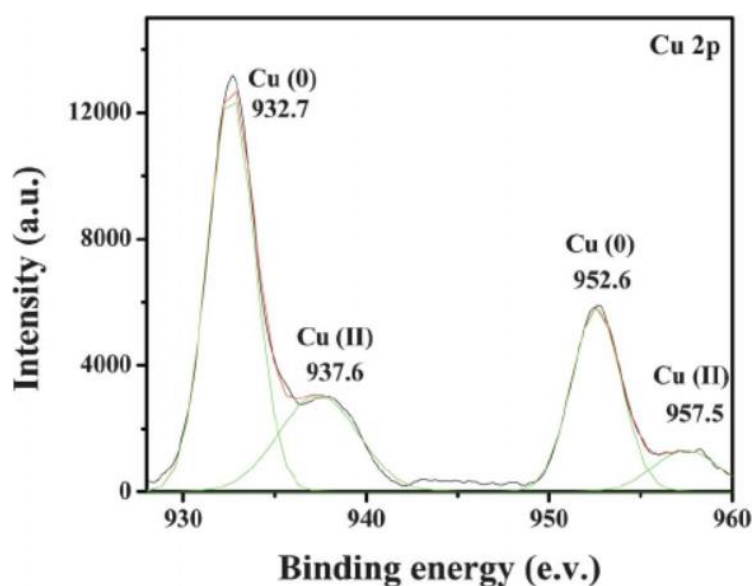


Figure 17 - Illustration of Cu 2p peaks for Cu(0) and Cu(II) where peaks at 932.7 eV and 932.6 eV refer to Cu $2p_{3/2}$ and peaks at 952.6 eV and 957.5 eV refer to Cu $2p_{1/2}$. [51], [54]

1.17 XPS – Quantitative Analyses

1.17.1 Determining Surface Concentration of Adsorbed Species

Relative Intensities of the XPS peak areas of adsorbent to substrate can be used to determine the surface concentrations of the adsorbent. The measured peak area is dependent on the following variables.

- The photo-emission cross section (probability of photo-emission occurring from a specific core level.)
- The inelastic mean free path (IMFP) of the photo-emitted electron.
- The instrument response efficiency, the efficiency with which the spectrometer detects electrons as a function of kinetic energy.

To determine the area under a peak, a point at the base of the peak on both sides is selected, and the peak area measured by the XPS analysis software.[55] Points are selected carefully to ensure an accurate curve fitting and peak area. Curve fitting is most important when peaks overlap.

The background in XPS spectra is caused by the loss of energy of electrons during emission at binding energies higher than the peak energy. The background is continuous because the energy loss processes of electrons are random and multiple. This background is removed before peak measurements using a Shirley background subtraction calculated using CasaXPS software.

The equation below was developed by Carley and Roberts[56] and was used to determine the surface concentration of the surface species. This equation was developed from the original work by Madey[57] where the equation developed was modified to include the photo-ionisation cross section & the probability of electrons photo-emitted from a particular atomic orbital of a specific element. This value is dependent on the size and shape of the orbital and the ionising photon energy.

$$\sigma_a = \frac{A_a}{A_s} \times \frac{KE_a}{KE_s} \times \frac{\mu_s}{\mu_a} \times \frac{(N_A \lambda_s \rho_s)}{M_s} \cos\phi$$

σ_a (atom/cm²) = surface concentration of the adsorbate.

A_a & A_s = Peak area of adsorbate & substrate respectively.

KE_a & KE_s = Photoelectron kinetic energy of the adsorbate and substrate material respectively.

N_A (mol⁻¹) = Avogadro's constant.

λ_s (cm) = Inelastic mean free path of the surface substrate.

ρ_s (gcm⁻³) = Density of the surface substrate.

μ_a & μ_s = Photo-ionisation cross section of the adsorbate and substrate respectively.

ϕ = Angle at which photo-electrons are collected with respect to the surface normal.

$M_s(\text{gmol}^{-1})$ = Relative molecular mass of the substrate.

The photo ionisation cross section μ' of C and Au are calculated using the equation below to account for the angle between the source and analyser. This is done by including the angular distribution asymmetry parameter, β , which is tabulated for different subshells at Z values up to 100 for Al K_α (1486.6 eV) X-rays incident on atoms.[58]

$$\mu' = \mu \left(1 - \frac{\beta}{2} \left(\frac{3 \cos^2 \theta - 1}{2} \right) \right)$$

μ' = Photo-ionisation cross section of C and Au.

μ = Photo-ionisation cross section at a source analyser angle of 90°. Values are tabulated from

β = Angular distribution asymmetry parameter.

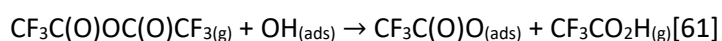
θ = Angle between source and analyser.

1.18 Selective Derivatization for Determination of Oxygen Functionalities

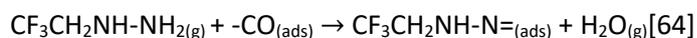
Because of the breadth and overlap of different oxygen peaks on the surface, it is often the case that an XPS narrow scan is unable to distinguish between the different components presence and relative concentrations of different oxygen groups on sample surfaces such as hydroxyl, ketone, carboxylic acid or ether groups.

Selective derivatization can be used to determine the identities and quantities of oxygen functionalities on the surface of samples. This works through reacting the functional groups on the surface with fluorinated compounds that selectively react with certain oxygen groups in a 1:1 stoichiometric ratio. Different fluorinated compounds can be used separately, each one targeted to a different oxygen functionality on the surface with high selectivity.

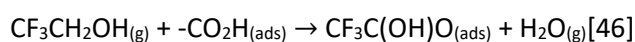
Identifying hydroxyl groups on the carbon surface. Trifluoroacetic anhydride (TFAA, $\text{CF}_3\text{C}(\text{O})\text{OC}(\text{O})\text{CF}_3$) reacts selectively with hydroxyl groups with a 1 : 1 stoichiometric ratio creating an adsorbed fluoroacetate and an acetic acid that desorbs or reacts with other hydroxyl groups to generate the same product.[59], [60]



Identifying ketone groups at carbon surfaces. Trifluoroethyl hydrazine (TFH, $\text{CF}_3\text{CH}_2\text{NH-NH}_2$) reacts selectively with ketone groups on the carbon surface with a 1 : 1 stoichiometric ratio through a condensation reaction, eliminating water as a product.[59], [62], [63]



Identifying carboxylic acid groups on the carbon surfaces. Trifluoroethanol (TFE, $\text{CF}_3\text{CH}_2\text{OH}$) in the presence of DTBC) reacts selectively with carboxylic acid groups on the carbon surface with a 1 : 1 stoichiometric ratio through a condensation reaction, eliminating water as a product.[59], [62], [63]



After reaction of a surface with one of these fluorinating agents, XPS analysis can be performed where the presence of fluorine on the surface shows the presence of the corresponding oxygen group. Knowing the stoichiometric ratio of the reaction between oxygen groups and the fluorinating compound the exact quantity of the oxygen group on the surface can be determined as well making this a powerful analytical tool.

The aims of this thesis is to determine how acid washing of carbon surfaces effects the topography of the carbon surface and the quantity and identity of the functional groups introduced. Gold is then deposited from aqueous solution to determine how the change in topography and functionalization effects the deposition of gold, including the ionisation states, sizes and dispersion of nanoparticles. This is to provide an understanding of how to manipulate gold on carbon for use in catalysis in such systems as the hydrochlorination of acetylene.

2 Experimental

2.1 Graphite Samples

All experiments were conducted on Highly Oriented Pyrolytic Graphite (HOPG). Each HOPG crystal had dimensions 10.0 x 10.0 x 2.0 mm³, a mosaic spread of 0.8 – 1.2 degrees and a thickness dispersion of ± 0.2 mm. These were ZYB quality and supplied by NT-MDT Co.

HOPG samples were chosen as the model carbon support for catalysis as it provides an atomically flat surface which provides a featureless flat surface without carbon functionalization which only provides a carbon elemental signature. This allows the introduction of specific functional groups for further study.

Before each new experiment the HOPG crystal was cleaned using adhesive tape to remove the first few layers from the top of the working side of the crystal. This ensures a clean and flat surface for functionalization.

2.2 Nitric Acid, Aqua Regia, Sulphuric Acid, Chloroauric Acid & Mixed Solutions

Since the use of deionized water has previously shown to leave surface contaminants of sodium and calcium deposits. As such ultra-pure water (UPW) was used in all experiments in this project and used to dilute all solutions.[43]

All nitric acid solutions were made using a stock solution of 70% nitric acid (1.42 g/ml purchased from Fischer Scientific). This was then diluted using UPW to create five different nitric acid solutions of 0.25, 0.5, 1.0, 2.0 and 5.0 moldm⁻³.

Aqua regia solutions were created using a mixture of 70% nitric acid (1.42 g/ml purchased from Fischer Scientific) and 37% hydrochloric acid (1.2g/ml purchased from Sigma Aldrich) diluted with UPW to create 0.25, 0.5, 1.0, 2.0 and 5.0 moldm⁻³ solutions where the concentration refers to the concentration of hydronium ions in solution assuming full dissociation of acid in UPW.

Sulfuric acid solutions were created using 99.999% sulfuric acid purchased from Sigma Aldrich and diluted with UPW to create 0.1, 0.2 and 0.3 moldm⁻³ solutions.

Chloroauric acid solutions were created using solid H₂AuCl₄ which was purchased from Sigma Aldrich which was then dissolved in ultrapure water and diluted multiple times to create 2.0 x 10⁻⁶, 4.0 x 10⁻⁶, 6.0 x 10⁻⁶ and 2.0 x 10⁻⁵ moldm⁻³ solutions.

Five different chloroauric acid and nitric acid mixed solutions were created with each solution containing $2 \times 10^{-6} \text{ mol dm}^{-3}$ HAuCl_4 and different concentrations of nitric acid (0.25, 0.5, 1.0, 2.0 and 5.0 mol dm^{-3}).

2.3 UPW Treatment for Creating References

A $100 \mu\text{l}$ droplet of UPW was dropped onto a clean HOPG surface using a micropipette and left for 30 minutes before drying under a clean He stream for two minutes. The surface was then characterized using AFM and XPS.

2.4 Nitric Acid Treatment

A $100 \mu\text{l}$ droplet of five different HNO_3 concentrations were dropped on five different clean HOPG surfaces using a micropipette and left for 30 minutes. They were then dried under a clean He stream for two minutes. The surface was then characterized using AFM and XPS.

2.5 Gold Treatment

HAuCl_4 solutions of a specific concentration were created with UPW. $100 \mu\text{l}$ of the solution was dropped onto HOPG surfaces that have been treated with different concentrations of acid. Gold treatment was left for 30 minutes before being dried using a clean stream of He for 2 minutes. All samples were characterized using AFM and XPS.

2.6 Gold in Acid Treatment

Five mixed HAuCl_4 with nitric acid solutions were created using $2 \times 10^{-6} \text{ mol dm}^{-3}$ HAuCl_4 with different nitric acid concentrations (0.25, 0.5, 1.0, 2.0 and 5.0 mol dm^{-3}). $100 \mu\text{l}$ of each solution was placed on different clean HOPG surfaces using a micropipette and left for 30 minutes before being dried under a clean He stream for two minutes. These samples were then characterized using AFM.

2.7 Selective Derivatization of Oxygen Functionalities

Three different fluorinated compounds were used separately, each one targeted to a different oxygen functionality on the surface. Derivatization reagents include trifluoroacetic anhydride (TFAA, 99%), trifluoroethyl hydrazine (TFH, 70 wt% in water) and a mixture of trifluoroethyl hydrazine (TFE),

pyridine and N-N'-di-tert-butylcarbodiimide (DTBC, 99%) in a 9:4:8 ratio. These derivative agents react selectively with hydroxyl, ketone and carboxylic acid groups respectively. The presence of fluorine as seen by XPS shows bonding of the fluorinated compound to its subsequent oxygen group.

After acid treatment of the surface, the HOPG samples were placed in a glass crucible along with a glass beaker containing 5ml of the derivatization reagent solutions that had been frozen through the beakers exposure to liquid nitrogen. The glass crucible was then sealed and pumped down to vacuum using a rotary pump for 15 minutes. After which the pump was turned off and the crucible completely sealed to the outside environment. The frozen derivatization reagent was left to sublime and fill the chamber to react with surface oxygen groups for 24 hours before the chamber was exposed to atmosphere for sample collection.

3 Results and Discussion

3.1 Clean HOPG Treated with UPW

Clean HOPG was prepared and studied using AFM and XPS to provide a reference for further work and checking the purity of the surface.

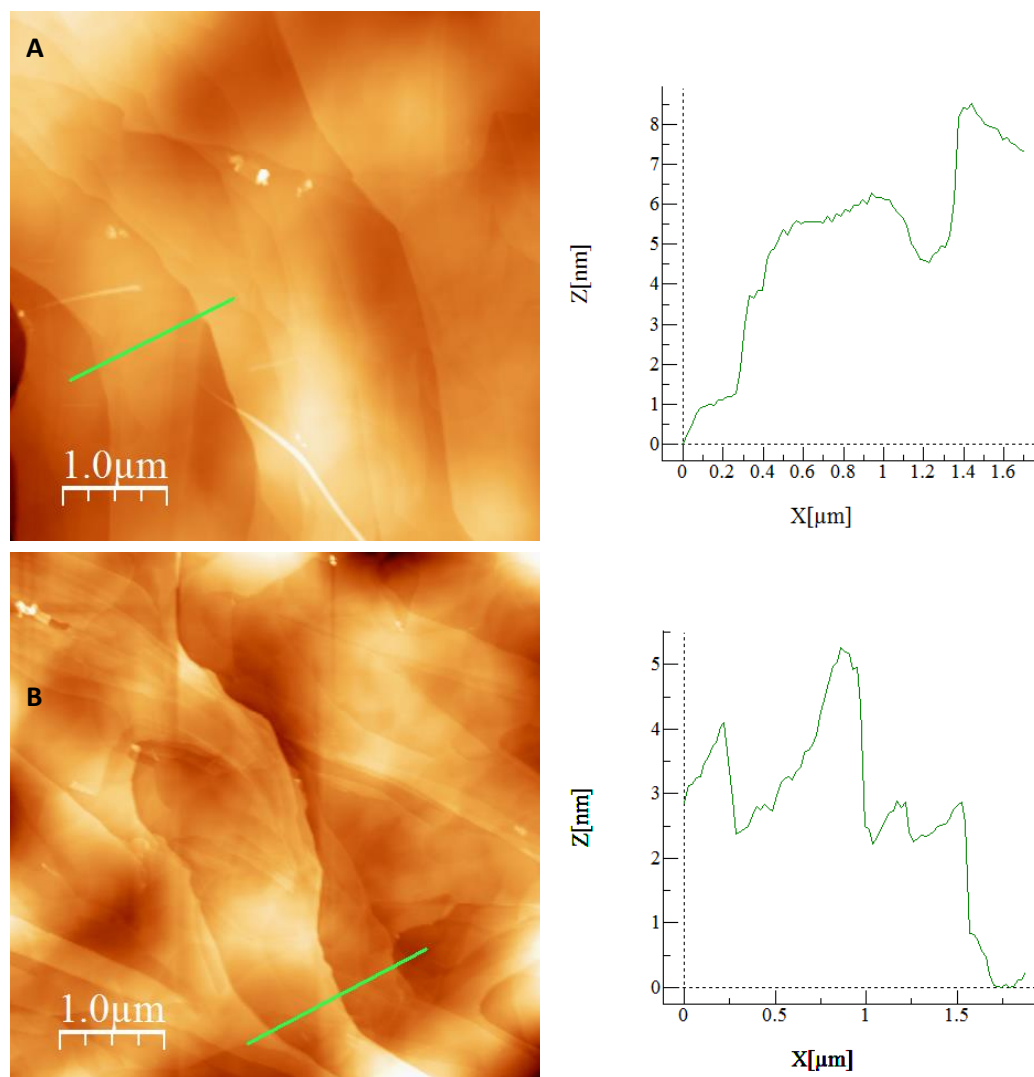


Figure 18 – 5.0x5.0 μm AFM images of a clean HOPG surface in two different locations with line profiles going from left to right showing step edge heights on different areas of the same sample.

Figure 18 shows how the graphite surface remains free of any visible impurities on the surface. The surface appears flat under a microscope but at high magnification AFM the surface is shown to comprise of flat areas divided by long step edges that vary between 1 and 3nm in height.

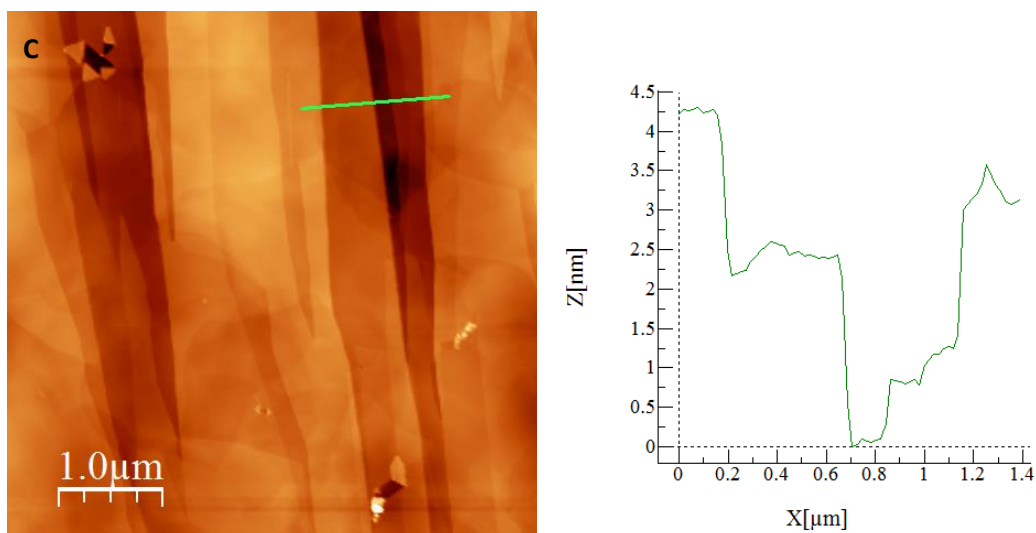


Figure 19 – 5.0x5.0 μm AFM images of a second clean HOPG surface with line profiles going from left to right showing step edge heights on a different sample

Figure 19 was taken to ensure that there was no obvious variance with different HOPG crystals used in sample preparation. Both samples show clean surfaces with no visible impurities at high AFM magnification, comprising flat terraces, divided by step edges of 1 – 3 nm height.

The step heights observed are particularly significant when considering the interplanar spacing of graphene sheets which is 0.335 nm[65]. Therefore, a step edge of 3 nm is equivalent to 9 graphene sheets giving a large area of high energy sites with uncoordinated carbon atoms. It is likely that these high energy sites are going to have a significant impact on the adsorption/reactivity of the surface to different chemical treatments. Step edges also provide the potential for greater coordination of adsorbed molecules compared to terraces. There are no clear adatoms or vacancies on the surfaces however these can be exceptionally small and therefore not show up at the AFM magnification that can be obtained.

Once calibrated the XPS wide scan shown in Figure 20 revealed the presence of two elements.

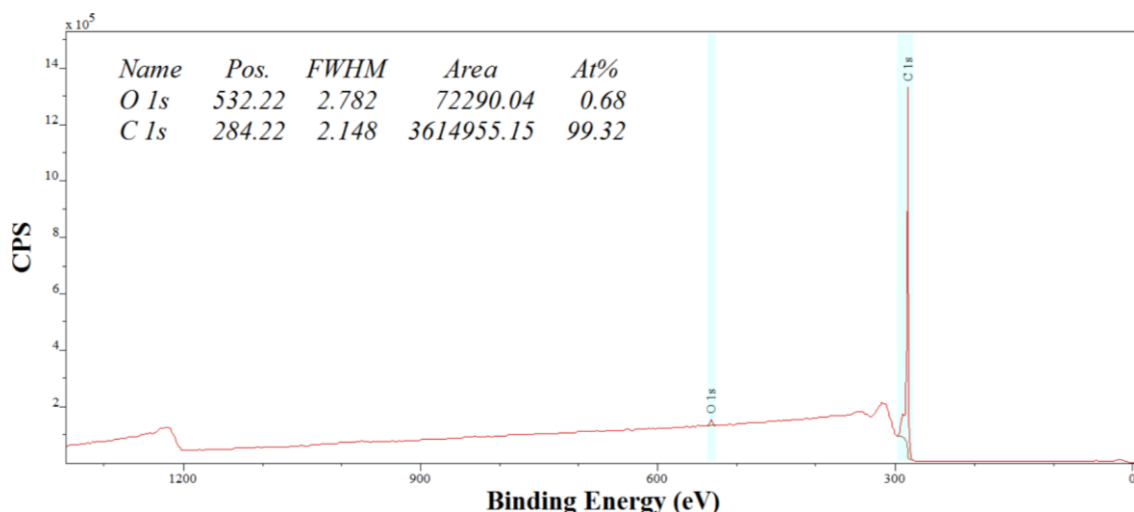


Figure 20 – XPS Spectra of a HOPG surface treated with UPW. Source accredited to Vaughn Roberts.

Figure 20 shows a strong carbon peak (1s, 284.2 eV) which is the referenced binding energy for C1s electrons for sp^2 hybridized carbons in graphite. The oxygen peak (1s, 532.5 eV) shows that a small amount of oxygen is present and is likely a result of oxidation of very high energy defects created after the surface top layer of graphene is stripped off with adhesive tape leaving a fresh surface with defects on the surface as a result of the harsh cleaning technique. No other elements were detected on the surface; this provides an important reference sample for all subsequent experimental data.

3.2 HNO₃ Treatment on HOPG

Samples treated with different concentrations of nitric acid were studied to determine how the surface topography and functionality changed. This was a necessary first step in determining the effects different concentrations of nitric acid have on the deposition of gold nanoparticles.

Concentrations of HNO₃ used were 0.25M, 0.5M, 1.0M, 2.0M and 5.0M.

3.2.1 0.25M HNO₃ Treated HOPG

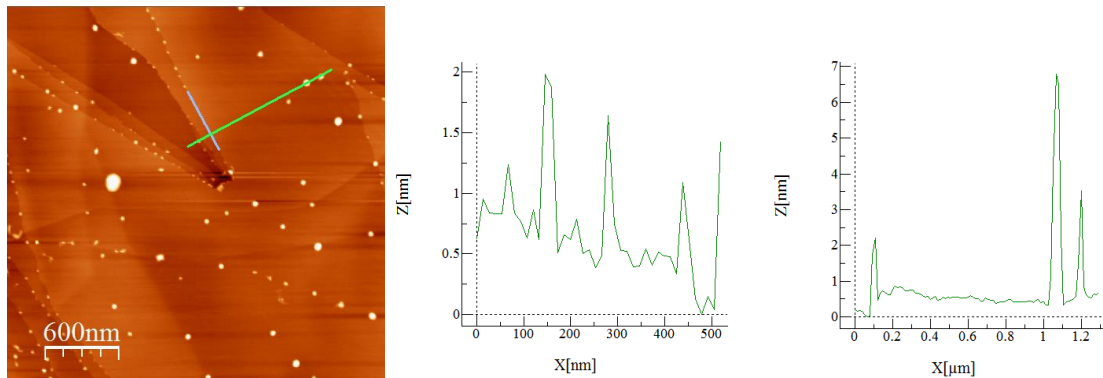


Figure 21 – 3.0x3.0μm AFM image of 0.25M HNO₃ treated HOPG with line profile going from left to right. The grey line refers to the left profile and the green line the right profile.

The AFM images shown in Figure 21 show raised features across the graphite surface. These vary in size where small islands are around 50 nm in width and 1 - 2 nm in height. Large features vary in width between 100 – 200 nm in width and 4 – 7 nm in height.

A lot of islands congregate along step edges as shown from the grey line profile in Figure 21. The islands are very small where $z = 1-2$ nm, however the step sizes in this image are all under 1 nm in height.

From flooding analysis of the image using WSxM software a percentage coverage can be estimated as 1.5%. WSxM is a freeware application that allows us to measure different plots on a fixed surface point.[66] Flooding works through applying a minimum height for the image where the image is removed where it doesn't exceed this minimum height. All parts of the image that exceed this minimum height (the islands) are calculated as a percentage of the overall image. This can only work accurately if the surface, excluding the islands, are completely flat. Therefore, flooding analysis can only provide a rough quantitative estimate of surface coverage.

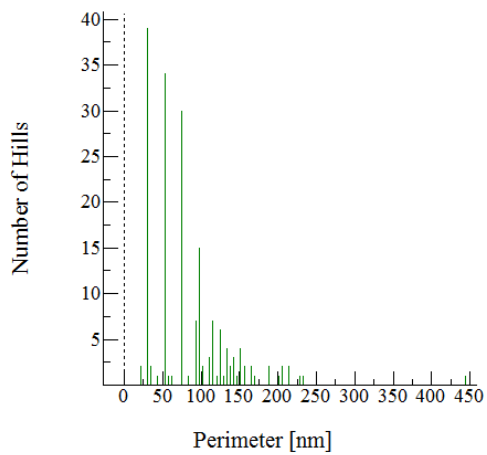


Figure 22 – Bar chart of the number of features of the same size in 0.25M HNO₃ treated HOPG.

3.2.2 0.5M HNO₃ Treated HOPG

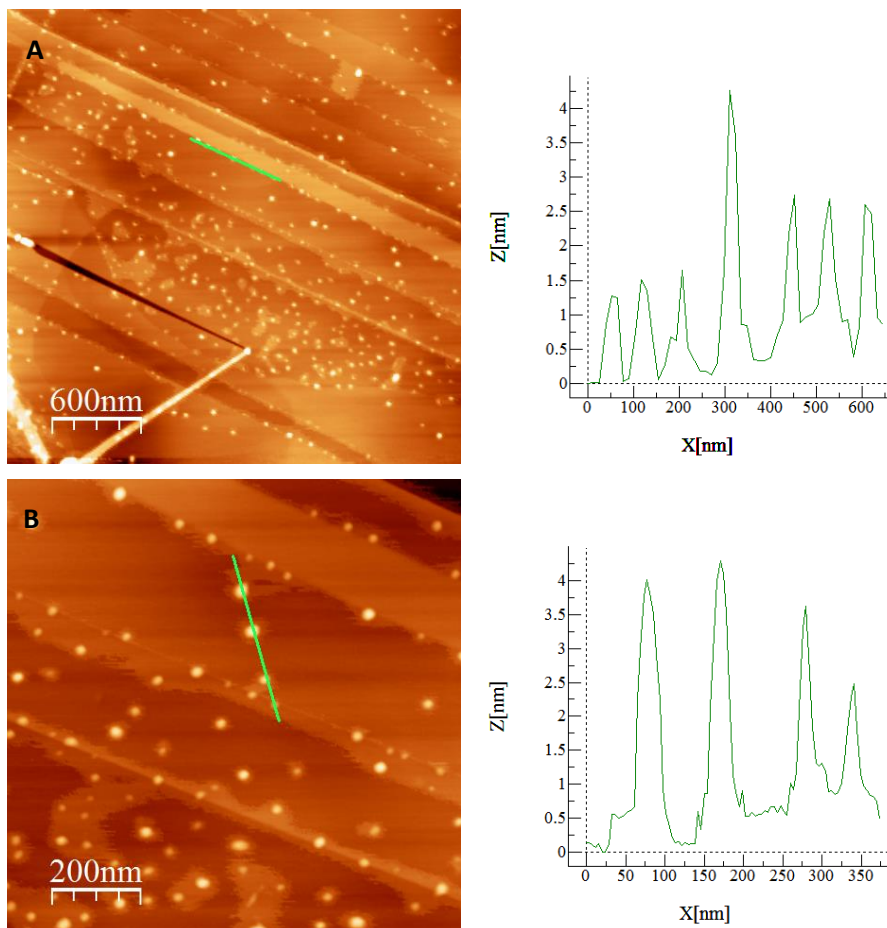


Figure 23 – (A) 3.0x3.0 μm AFM images of a 0.5M HNO₃ treated HOPG surface, (B) 1.0x1.0 μm AFM image showing a magnified section of the sample surface. Line profiles are shown on the image and go from left to right.

The AFM images shown in Figure 23 show raised features across the graphite surface. These lie across the entire surface with a slight preference for step edges over terraces determined qualitatively by appearance. Unlike 'HNO₃ (0.25M)' this surface contained much greater uniformity between island sizes. There was also a much greater number of islands present. However due to issues with the flattening of the surface an accurate histogram could not be obtained for this sample.

3.2.3 1.0M HNO₃ Treated HOPG

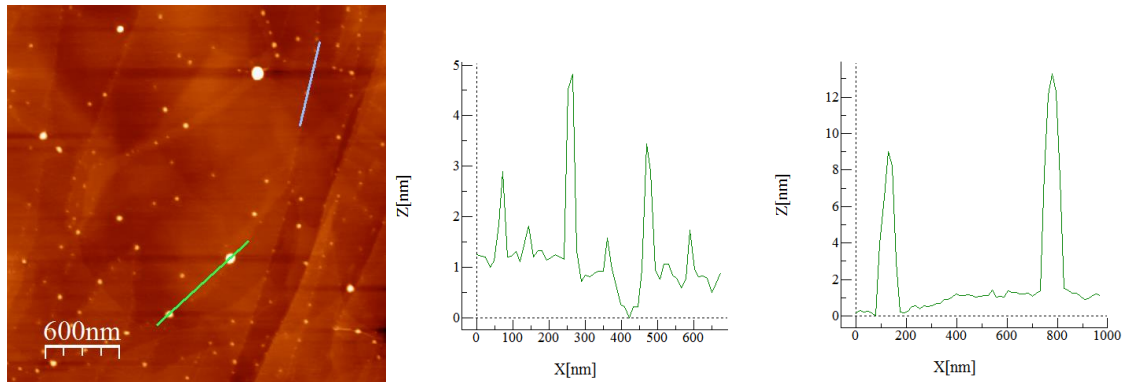


Figure 24 – 3.0x3.0μm AFM image of 1.0M HNO₃ treated HOPG with line profile going from bottom to top. The grey line refers to the left profile and the green line the right profile.

The AFM images shown in Figure 24 show raised features across the graphite surface. These lie across the entire surface with a slight preference for step edges and kinks over terraces. Island sizes vary significantly across the surface. A histogram of the perimeters of islands on the surface is shown in Figure 25 and shows great similarity between this sample and 'HNO₃ (0.25M)'. Surface coverage was calculated through flooding to be 1.45%.

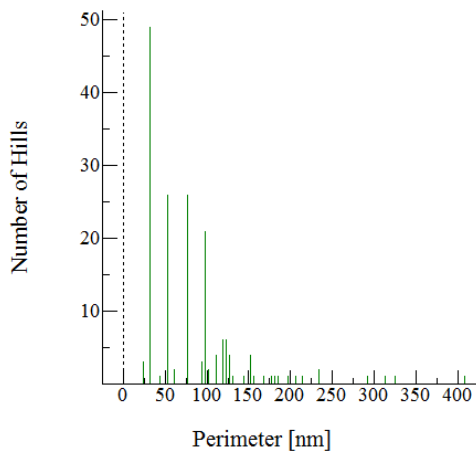


Figure 25 – Bar chart of the number of features of the same size in 1.0M HNO₃ treated HOPG.

3.2.4 2.0M HNO₃ Treated HOPG

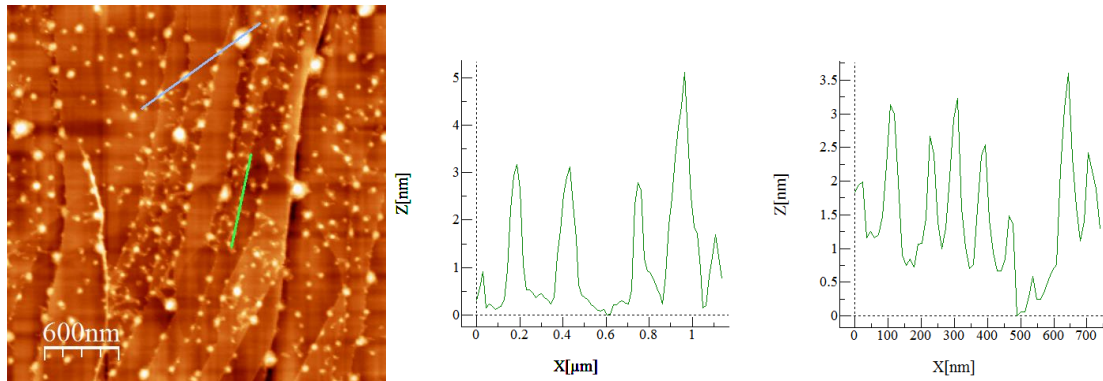


Figure 26 – 3.0x3.0µm AFM image of 2.0M HNO₃ treated HOPG with line profile going from bottom left to top right. The grey line refers to the left profile and the green line the right profile.

Whilst dilute nitric acid (0.25M, 0.5M and 1.0M) has had a large effect on the topography of the surface compared to surfaces treated with UPW, there has not been a massive difference between samples with different concentrations of HNO₃ used. However, upon treatment with more concentrated nitric acid the change in surface coverage of islands significantly increases. Flooding analysis shows an estimated surface coverage of 4.8% and a perimeter histogram shows a prevalence of both large and small islands. The increase in surface coverage is symptomatic of an increase in the number of islands and the increase in width of many of the islands.

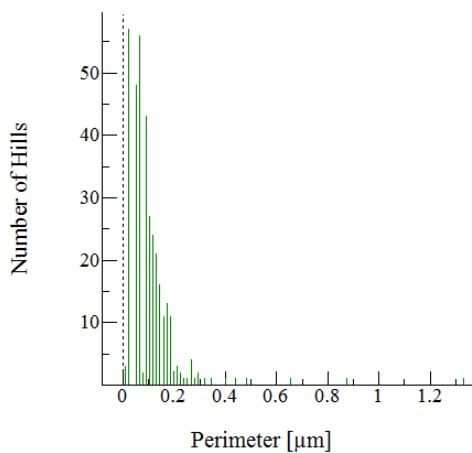


Figure 27 – Bar chart of the number of features of the same size in 2.0M HNO₃ treated HOPG.

3.2.5 5.0M HNO₃ Treated HOPG

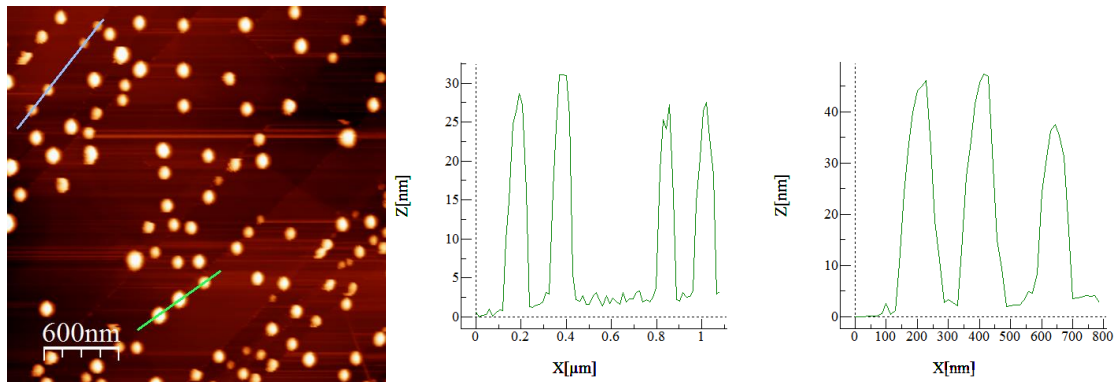


Figure 28 – 3.0x3.0μm AFM image of 5.0M HNO₃ treated HOPG with line profile going from left to right. The grey line refers to the left profile and the green line the right profile.

Figure 28 shows a large increase in the size of islands observed. Whilst a pattern of increasing surface coverage has so far been observed, a significant change in the heights of the islands has not been observed until now. Flooding analysis has shown the surface coverage to increase by roughly 11.5% and the perimeter histogram shown in Figure 29 shows an increase in the average perimeter of the islands

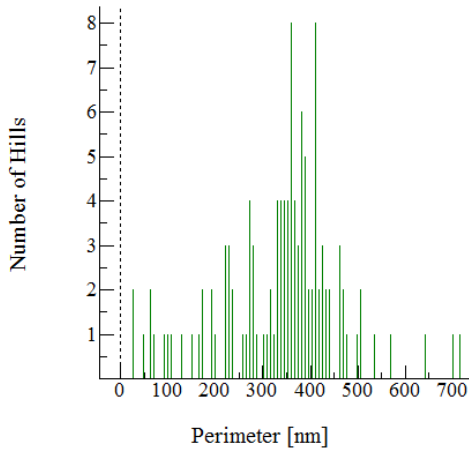


Figure 29 – Bar chart of the number of features of the same size in 2.0M HNO₃ treated HOPG.

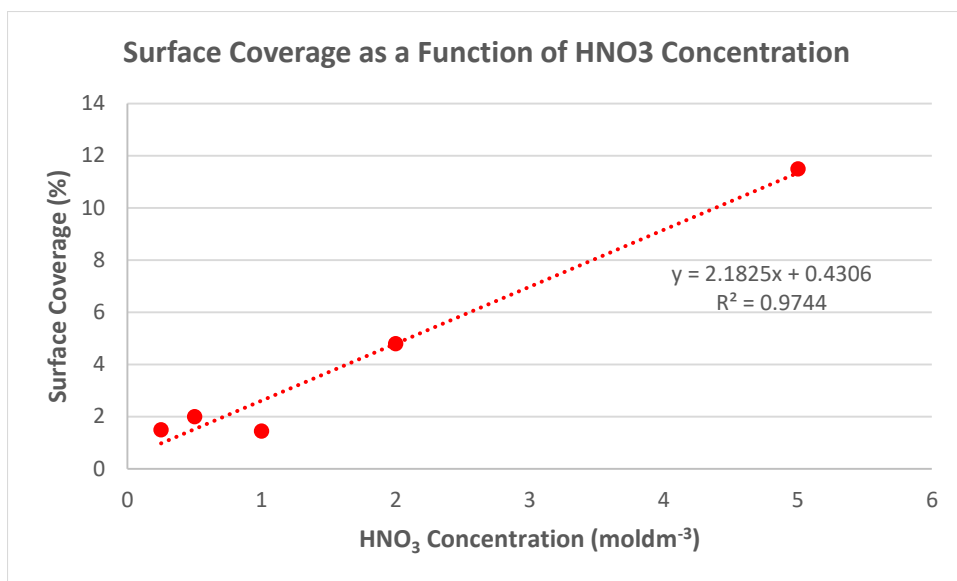


Figure 30 – Graph showing the island surface coverage as a function of HNO₃ Concentration

Figure 30 shows the increase in surface coverage of the islands with increasing HNO₃ concentration. This shows a roughly linear correlation however due to variables such as slight differences in the structure of the HOPG crystals used as a result of manufacturing, this difference is only visible when using higher concentrations of HNO₃.

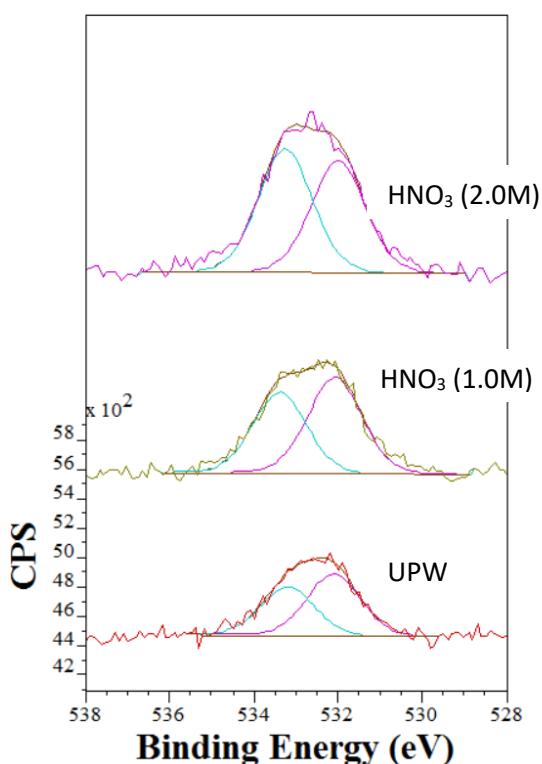


Figure 31 – Overlay narrow scan O1s XPS spectra of nitric acid treated HOPG.

	O1s(533eV)/C1s Peak Area Ratio	O1s(532eV)/C1s Peak Area Ratio
UPW	401/74195 = 0.005	678/74195 = 0.009
1.0M	882/70542 = 0.013	1060/70542 = 0.015
2.0M	1345/67325 = 0.020	1234/67325 = 0.018

Table 2 - Ratio of peak areas of different oxygen components and the peak area of the carbon component for different scans.

AFM images show that HOPG treated with nitric acid under ambient conditions results in surfaces covered with raised features that vary in size and density with changing nitric acid concentration as shown by Cardiff University[46]. Several images were taken across the surface to ensure that the surface was uniform. Control experiments used UPW for contrast, these showed flat HOPG surfaces with none of the hemispherical features mentioned. Wide scan XPS results have shown only the C1s peak present from the graphite substrate and an O1s peak from oxidised high energy sites on the surface. No other elements were detected. Previous studies done on 0.5 mol dm^{-3} nitric acid treated surfaces resulted in the theory that the blisters imaged by AFM are a result of local delamination between the top layers of graphite and the layers beneath them.[43] An illustration of this is shown in Figure 32.

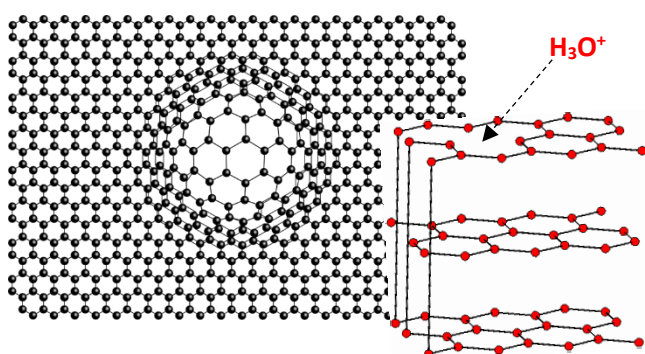


Figure 32 – Illustration of blisters created by hydronium ions penetrating the top layers of graphite through surface defects.

Due to the XPS results obtained in this work when comparing surfaces treated with differing concentrations of nitric acid, an alternative theory to the increasing blister sizes can be hypothesised. The alternative theory is that increasing nitric acid concentration results in an increase in the number of oxygen groups introduced to the surface. The subsequent rehybridization of planar sp^2 carbons to tetrahedral sp^3 carbons could result in the carbon losing attraction to the carbons in the layer beneath them causing local delamination. XPS results show an increase in the quantity of oxygen on the surface as shown in Figure 31. Survey scans shows no N introduced to the surface. As shown through peak fitting of the oxygen narrow scan, only one side of the O1s peak increases in size significantly. This suggests that one type of oxygen functionality remains constant whilst other oxygen functionalities increase in concentration. The binding energies (BE) of different oxygen functionalities deduced in reference [43] are as follows hydroxyl, 531.5 - 532 eV; ketone, 532 - 533 eV; Ether, 533.3 eV. Because of the two oxygens present in carboxylic acid groups, any O1s peak components present from carboxylic acid would span the breadth of the binding energies.[67] The XPS peak that increases in size with increasing concentrations of nitric acid in Figure 31 has a binding

energy of 532.8 eV. This suggests that the increasing oxygen concentration is due to the introduction of more hydroxyl groups.

Table 2 shows the ratio of the peak areas of the different oxygen components with their respective carbon peak areas, this allows determination of the relative change in oxygen concentration with increasing concentrations of nitric acid and shows a general increase in quantities of oxygen with increasing concentrations of nitric acid. Although both oxygen components peak areas increase with increasing nitric acid concentration, the higher binding energy oxygen component that corresponds with the binding energy of ketone groups increases a lot more suggesting a small increase in hydroxyl groups added to the surface and a large increase in ketone groups added to the surface with increasing nitric acid concentration.

3.3 HAuCl_4 ($2 \times 10^{-6} \text{ mol dm}^{-3}$) Treatment of HNO_3 Treated HOPG

HOPG samples were treated with 100 μl of different concentrations of HNO_3 solution for 30 minutes before being treated with 100 μl of HAuCl_4 ($2 \times 10^{-6} \text{ mol dm}^{-3}$) for a further 30 minutes. This was done to observe how HNO_3 treatment of HOPG affects the deposition of gold onto the surface. This includes the quantity of gold nanoparticles, their size, shape and the oxidation states of the gold atoms.

All samples were prepared in exactly the same way but with a change in the concentration of HNO_3 being used for the acid treatment of the HOPG. Samples are labelled as follows.

UPW – HAuCl_4 ($2 \times 10^{-6} \text{ M}$)

HNO_3 (0.25M) – HAuCl_4 ($2 \times 10^{-6} \text{ M}$)

HNO_3 (0.5M) – HAuCl_4 ($2 \times 10^{-6} \text{ M}$)

HNO_3 (1.0M) – HAuCl_4 ($2 \times 10^{-6} \text{ M}$)

HNO_3 (2.0M) – HAuCl_4 ($2 \times 10^{-6} \text{ M}$)

HNO_3 (5.0M) – HAuCl_4 ($2 \times 10^{-6} \text{ M}$)

3.3.1 Clean HOPG Treated with UPW before Treatment with HAuCl_4 ($2 \times 10^{-6} \text{M}$)

Clean HOPG was prepared and treated with UPW before treatment with HAuCl_4 ($2 \times 10^{-6} \text{M}$). These were then studied by AFM and XPS to provide a reference to further work. Any variance between this sample and the samples which have been treated with nitric acid is therefore a direct result of the nitric acid treatment.

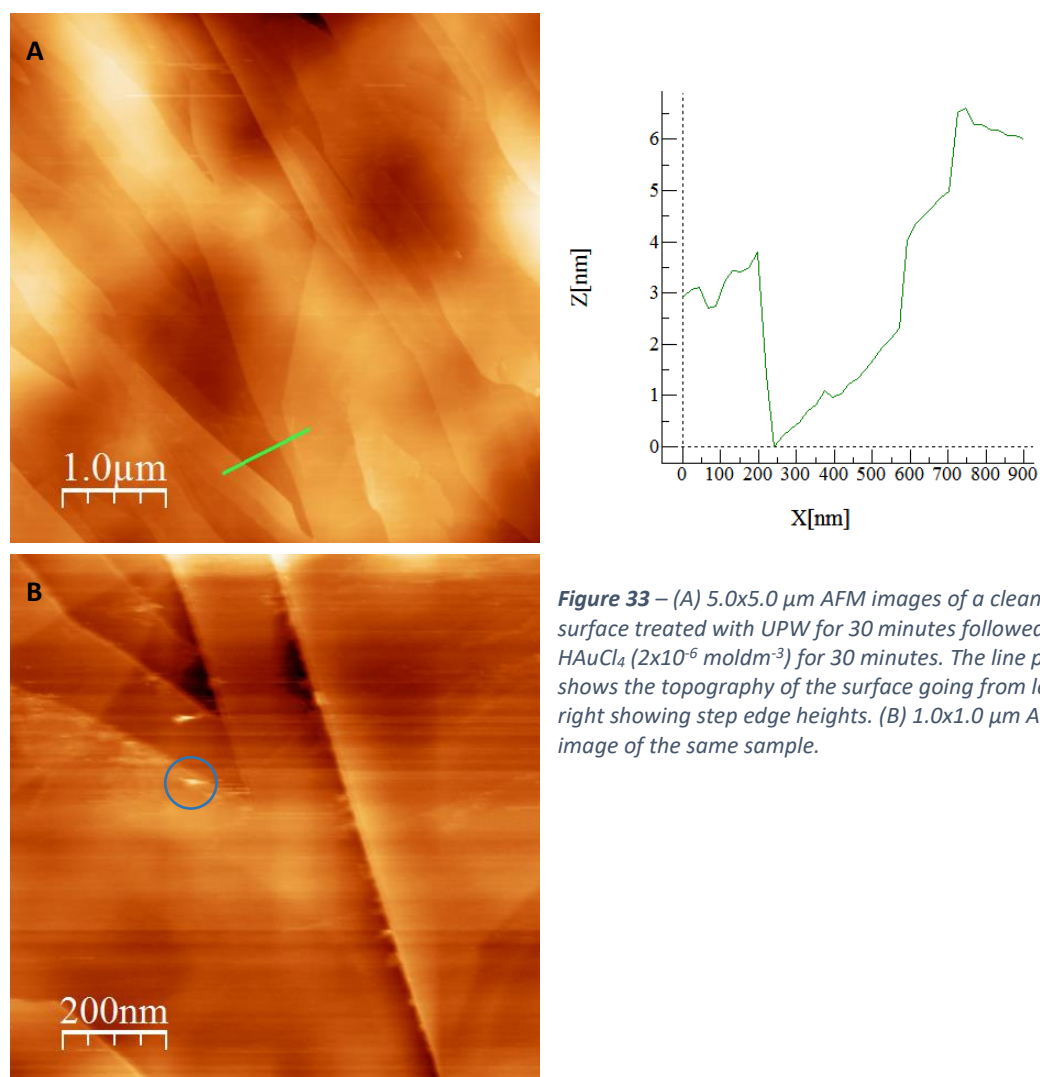


Figure 33 – (A) 5.0x5.0 μm AFM images of a clean HOPG surface treated with UPW for 30 minutes followed by HAuCl_4 ($2 \times 10^{-6} \text{mol dm}^{-3}$) for 30 minutes. The line profile shows the topography of the surface going from left to right showing step edge heights. (B) 1.0x1.0 μm AFM image of the same sample.

AFM images of 'UPW – HAuCl_4 ($2 \times 10^{-6} \text{M}$)' is shown in Figure 33 and shows very little change in the surface topography. Image A shows an enlarged portion of the surface and at this magnification shows no change from Figure 18 'Clean HOPG Treated with UPW' suggesting that without acid treatment there is almost no adherence of gold nanoparticles to the surface. Image B shows the same surface at a much greater magnification, step edges and kinks in the image appear to show very small features on the surface with very little defined shape or form. An example of this is shown

in the blue circle of image B. This could potentially be gold deposits that became trapped in these areas of the surface or simply some impurities. XPS data showed no gold deposited as shown in Figure 34.

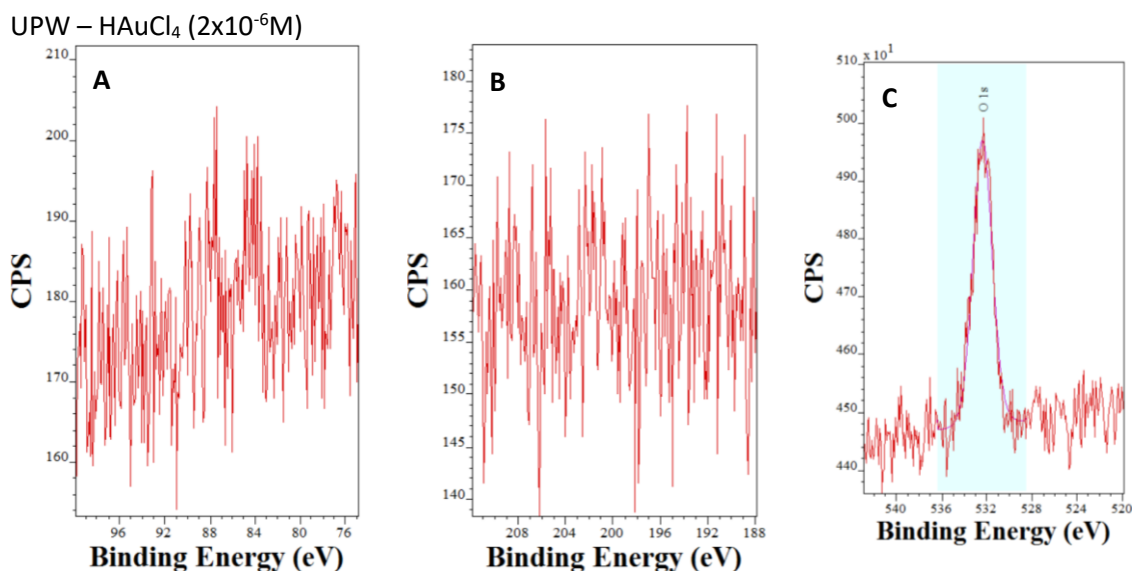


Figure 34 – Narrow scan XPS spectra of ‘UPW – HAuCl₄ (2x10⁻⁶M)’ where A is the Au^{4f} peak, B is the Cl^{2p} peak and C is the O^{1s} peak.

3.3.2 HNO₃ (0.25M) – HAuCl₄ (2x10⁻⁶M)

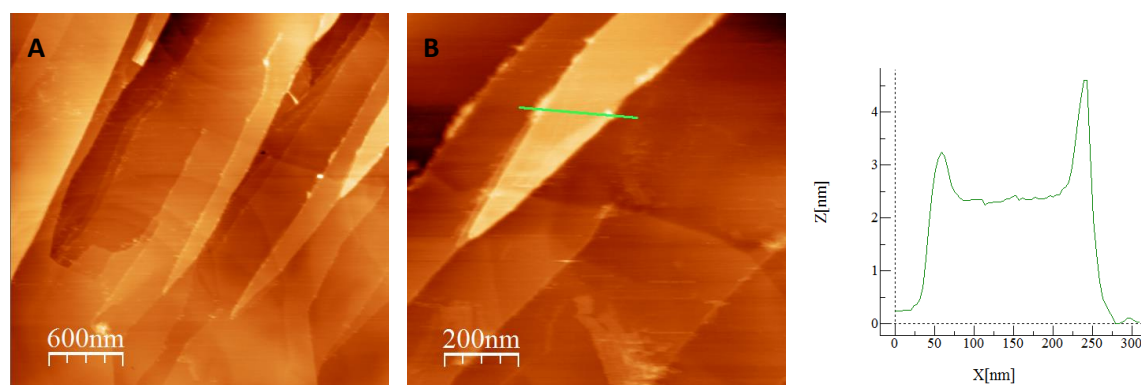


Figure 35 – (A) 3.0x3.0μm AFM image of HNO₃ (0.25M) – HAuCl₄ (2x10⁻⁶M), (B) 1.0x1.0μm AFM image of HNO₃ (0.25M) – HAuCl₄ (2x10⁻⁶M) with line profile going from left to right.

Figure 35 shows the presence of small amounts of deposits on the surface in step edges and kinks. Combined with XPS data these appear to be gold deposits which appear to be poorly defined due to their ill-defined shape. The two peaks in the line profile show how these deposits have created high ridges of 0.5 – 2 nm along step edges.

3.3.3 HNO_3 (0.5M) – HAuCl_4 ($2 \times 10^{-6}\text{M}$)

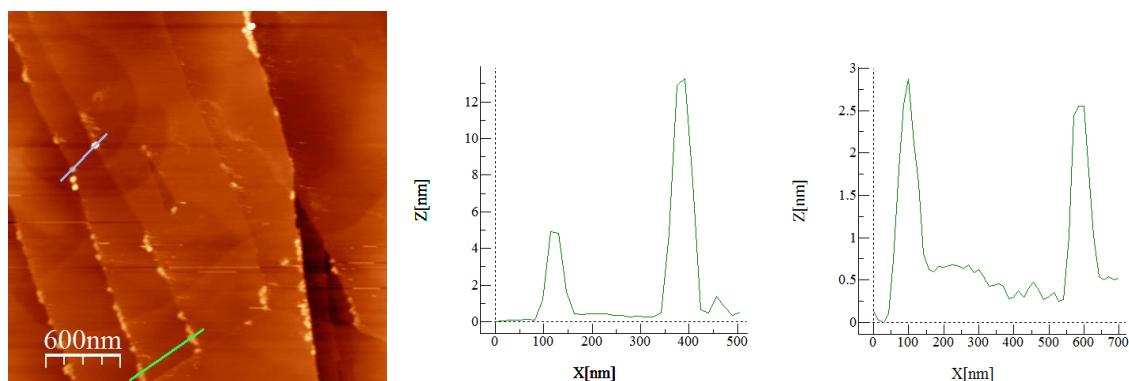


Figure 36 – $3.0 \times 3.0 \mu\text{m}$ AFM image of ' HNO_3 (0.5M) – HAuCl_4 ($2 \times 10^{-6}\text{M}$)' with line profile going from left to right. The grey line refers to the left profile and the green line the right profile.

AFM images of ' HNO_3 (0.5M) – HAuCl_4 ($2 \times 10^{-6}\text{M}$)' in Figure 36 shows an increase in the quantity of deposits on the surface. These still lie along step edges, the line profile shows no increase in the heights of the deposits however there is an increase in the quantity and thickness, with deposits stretching further onto terraces. Whilst most deposits still appear poorly defined in that there is no distinct shape, there are a few islands appearing with a more distinct well defined shape as shown in the grey line profile.

3.3.4 HNO_3 (1.0M) – HAuCl_4 ($2 \times 10^{-6}\text{M}$)

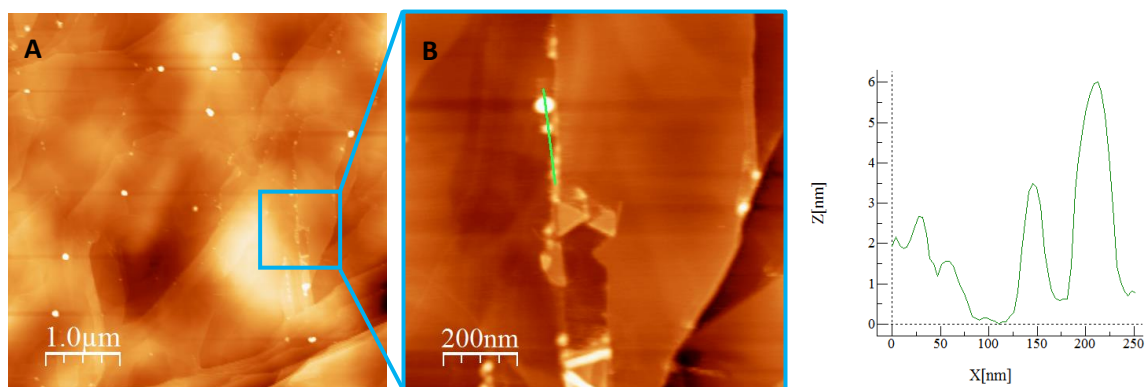


Figure 37 – (A) $5.0 \times 5.0 \mu\text{m}$ AFM image of ' HNO_3 (1.0M) – HAuCl_4 ($2 \times 10^{-6}\text{M}$)', (B) $1.0 \times 1.0 \mu\text{m}$ AFM image of ' HNO_3 (0.25M) – HAuCl_4 ($2 \times 10^{-6}\text{M}$)' with line profile going from bottom to top.

Figure 37(A) shows a uniform spread of large distinct islands across the surface. Several $5.0 \times 5.0 \mu\text{m}$ AFM images were taken to ensure this was the case and the best image chosen. Figure 37(B) shows a magnified AFM image showing how the shapes of the deposits are becoming more defined and hemispherical. The size of these features have also increased.

3.3.5 HNO_3 (2.0M) – HAuCl_4 ($2 \times 10^{-6}\text{M}$)

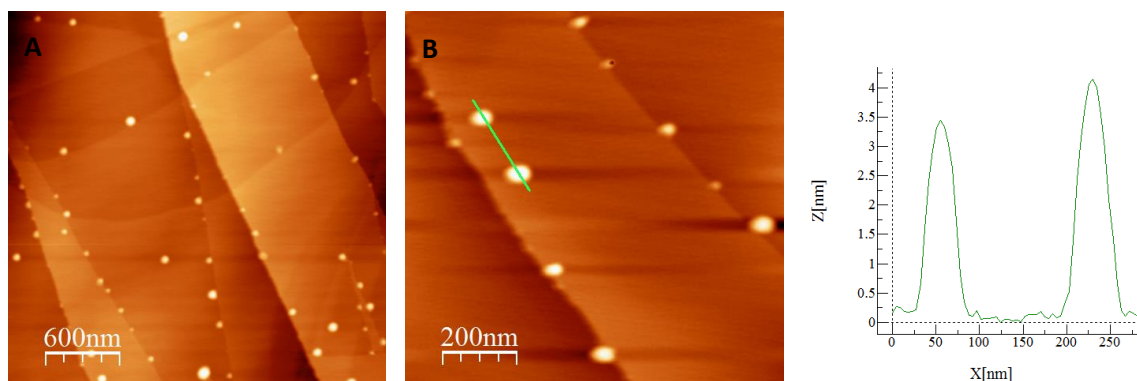


Figure 38 – (A) $3.0 \times 3.0 \mu\text{m}$ AFM image of ' HNO_3 (2.0M) – HAuCl_4 ($2 \times 10^{-6}\text{M}$)', (B) $1.0 \times 1.0 \mu\text{m}$ AFM image of HNO_3 (0.25M) – HAuCl_4 ($2 \times 10^{-6}\text{M}$) with line profile going from top to bottom.

Figure 38 shows how the deposits on the surface have become very well defined with close to zero islands appearing as amorphous. These islands are also becoming less constricted to step edges and kinks, however there is still a preference for the islands to appear along these areas.

3.3.6 HNO_3 (5.0M) – HAuCl_4 ($2 \times 10^{-6}\text{M}$)

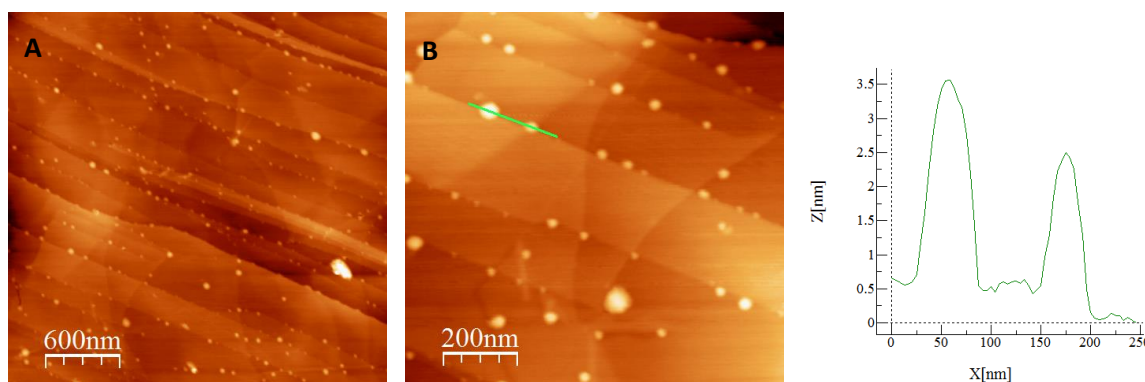


Figure 39 – (A) $3.0 \times 3.0 \mu\text{m}$ AFM image of ' HNO_3 (5.0M) – HAuCl_4 ($2 \times 10^{-6}\text{M}$)', (B) $1.0 \times 1.0 \mu\text{m}$ AFM image of HNO_3 (0.25M) – HAuCl_4 ($2 \times 10^{-6}\text{M}$) with line profile going from left to right.

Figure 39 shows a large quantity of islands present on the surface. From what can be seen with the line profile the medium sized islands do not change size much between ' HNO_3 (2.0M) – HAuCl_4 ($2 \times 10^{-6}\text{M}$)' and ' HNO_3 (5.0M) – HAuCl_4 ($2 \times 10^{-6}\text{M}$)'. However, it appears as though there are many more small islands. Flooding analysis of the surfaces was used to determine % island coverage.

HNO_3 (2.0M) – HAuCl_4 ($2 \times 10^{-6}\text{M}$) island coverage = 0.81%

HNO_3 (5.0M) – HAuCl_4 ($2 \times 10^{-6}\text{M}$) island coverage = 1.10%

All islands appear distinct in size and shape, the main difference between the sample treated with 5.0M and 2.0M HNO₃ is the increase in island coverage.

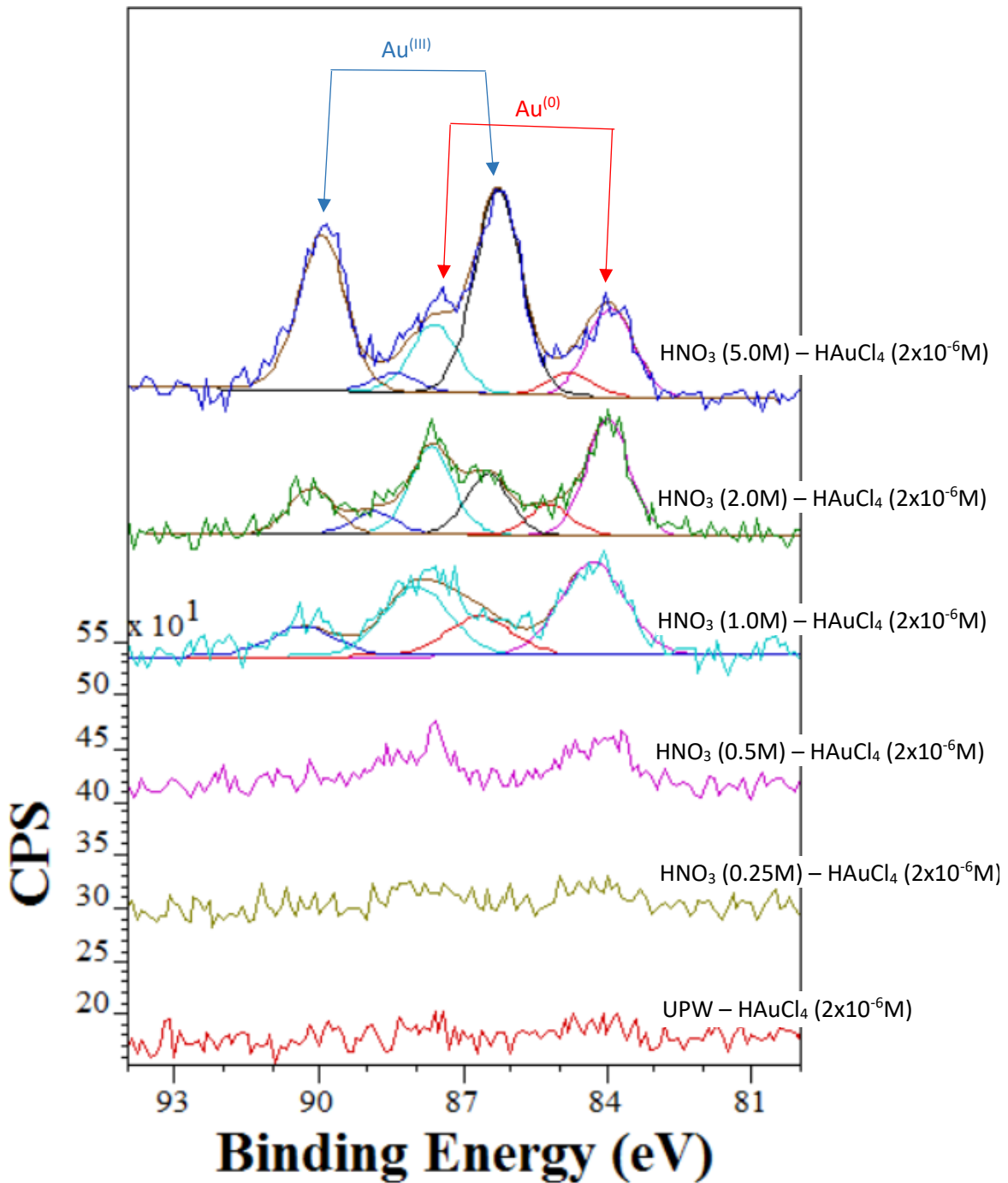


Figure 40 – Overlay narrow scan Au^{4f} XPS spectra of HOPG samples treated with HAuCl₄ (2x10⁻⁶ moldm⁻³) following treatment with HNO₃

Figure 40 shows that very little gold gets deposited on the surface of nitric acid activated HOPG when using low concentrations of nitric acid or no nitric acid. At nitric acid concentrations of 1.0M or higher there is a large increase in the quantities of gold on the surface. In particular Au(0) (84.0 eV), it is theorized that the hydroxyls found on the surface of HNO₃ treated surfaces cause a reduction of the gold from Au(III) (86.0 eV) to Au(0). At nitric acid concentrations of 1.0M to 5.0M the concentration of Au(III) increases significantly and Au(0) concentrations decreases. This supports the conclusions from Figure 31 'overlay narrow scan O1s XPS spectra of nitric acid treated HOPG,' which shows that at high concentrations of nitric acid treatment, the hydroxyls become oxidized further to ketone and ether groups as suggested by the increase in size of the oxygen 1s peak at high binding energies. These oxygen groups lack the reductive potential to reduce Au(III) to Au(0) and instead are likely to create an ion-dipole bond with the Au(III) ions showing the increase in the presence of Au(III) with increasing HNO₃ concentrations.

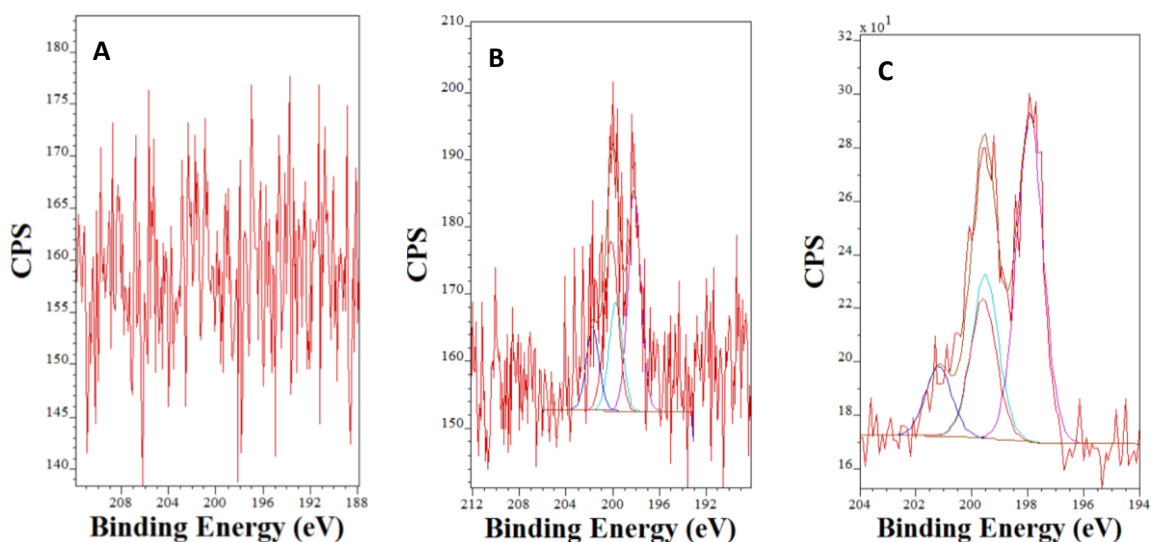


Figure 41 – Cl^{2p} narrow scan XPS spectra of HOPG samples treated with HAuCl₄ ($2 \times 10^{-6} \text{ mol dm}^{-3}$) following treatment with HNO₃. (A) UPW – HAuCl₄ ($2 \times 10^{-6} \text{ M}$), (B) HNO₃ (2.0M) – HAuCl₄ ($2 \times 10^{-6} \text{ M}$), (C) HNO₃ (5.0M) – HAuCl₄ ($2 \times 10^{-6} \text{ M}$).

XPS narrow scan analysis of Cl 2p peaks shows the presence of chlorine only in samples that contain Au(III) ions on the surface showing that Cl⁻ is being used to stabilise the Au on the surface. The presence of multiple Cl 2p peaks at high concentrations suggests multiple Cl environments. The peaks at higher binding energies belong to Cl that has bonded to the sample surface and the peaks at lower binding energies belong to Cl bonded to Au as shown in Figure 42. This is because bonding between Cl and Au is more ionic, the electrostatic shielding of the nuclear charge of the chlorine atom is reduced which results in a decrease in the core electrons binding energy.

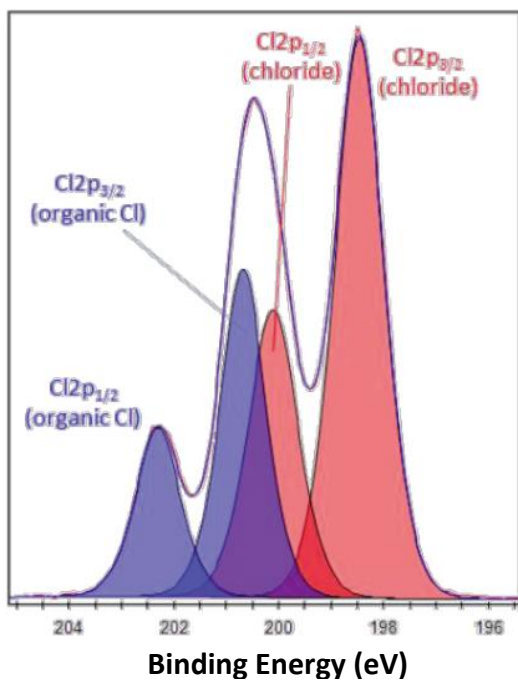


Figure 42 – Cl^{2p} narrow scan XPS spectra showing the locations of organic chloride and metal chloride peaks.

3.4 Aqua Regia (AR) Treatment of HOPG

Samples treated with different concentrations of aqua regia were studied to determine how the surface topography and functionality changed with treatment using different concentrations of AR. This was done in order to distinguish differences between samples treated with nitric acid and samples treated with aqua regia to determine why aqua regia is used in the acid washing step in the preparation of Au on carbon catalysts. This suggests a change in the chemistry when using the different acids through either the introduction of different functional groups or a change in the topography of the surface. [43] Concentrations of aqua regia used for surface treatment were 0.25M, 0.5M, 1.0M, 2.0M and 5.0M. These samples were labelled as followed respectively. The standard used for these samples is 'UPW – HAuCl₄ (2x10⁻⁶M)' whose AFM images are shown in Figure 33.

AR (0.25M)

AR (0.5M)

AR (1.0M)

AR (2.0M)

AR (5.0M)

3.4.1 0.25M AR Treated HOPG

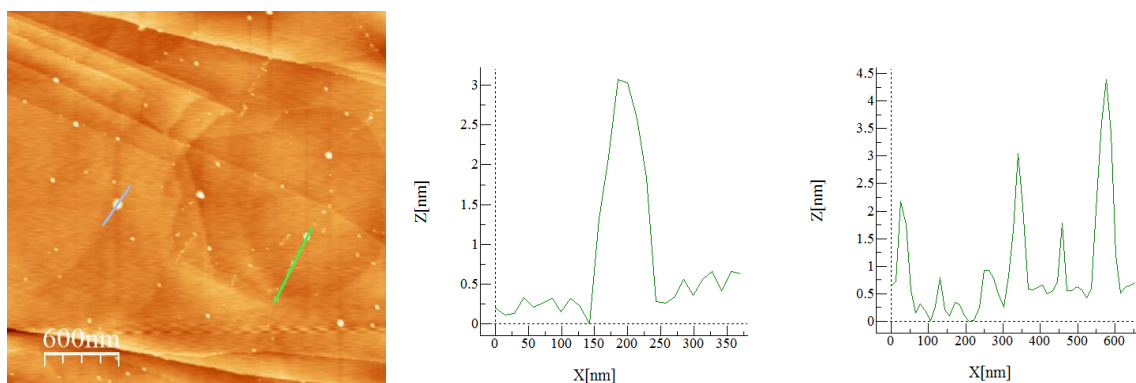
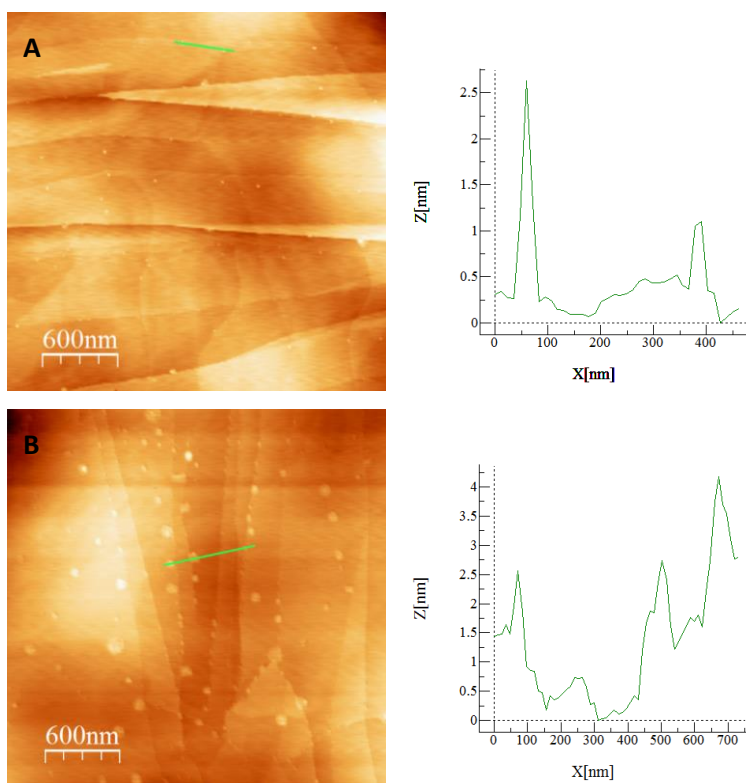


Figure 43 – 3.0x3.0 μ m AFM image of ‘AR (0.25M)’ with line profile going from left to right. The grey line refers to the left profile and the green line the right profile.

The 0.25M AR treatment of HOPG shows the introduction of a lot of new islands which vary in size between 1 and 3 nm in height and vary greatly in width. XPS data shows only the presence of the substrate and oxygen on the surface. No Cl or N from the acid anions have become incorporated into the sample suggesting that these islands are formed from the introduction of hydrophilic oxygen functional groups which appear very similar to nitric acid’s effect on the surface.

3.4.2 0.5M, 1.0M, 2.0M and 5.0M AR Treated HOPG



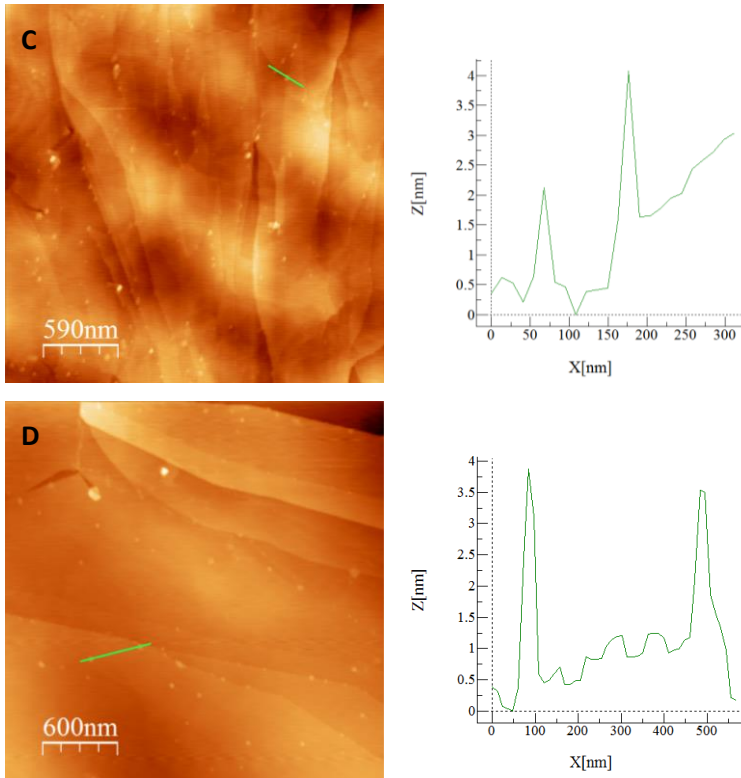


Figure 44 – $3.0 \times 3.0 \mu\text{m}$ AFM images of HOPG treated with different concentrations of AR with line profiles going from left to right. (A) AR (0.5M), (B) AR (1.0M), (C) AR (2.0M), (D) AR (5.0M)

Figure 43 and Figure 44 show very little change in the surface topography with changing concentration of AR used. XPS data is shown in Figure 45, a significant increase in oxygen concentration was detected compared to samples treated with UPW however there was no clear change in the oxygen concentration with changing AR concentration. Variances in the shape of the peak were also too small to determine any differences in the identity of the oxygen peaks, however the broad spectrum suggests multiple different oxygen functional groups are on the surface.

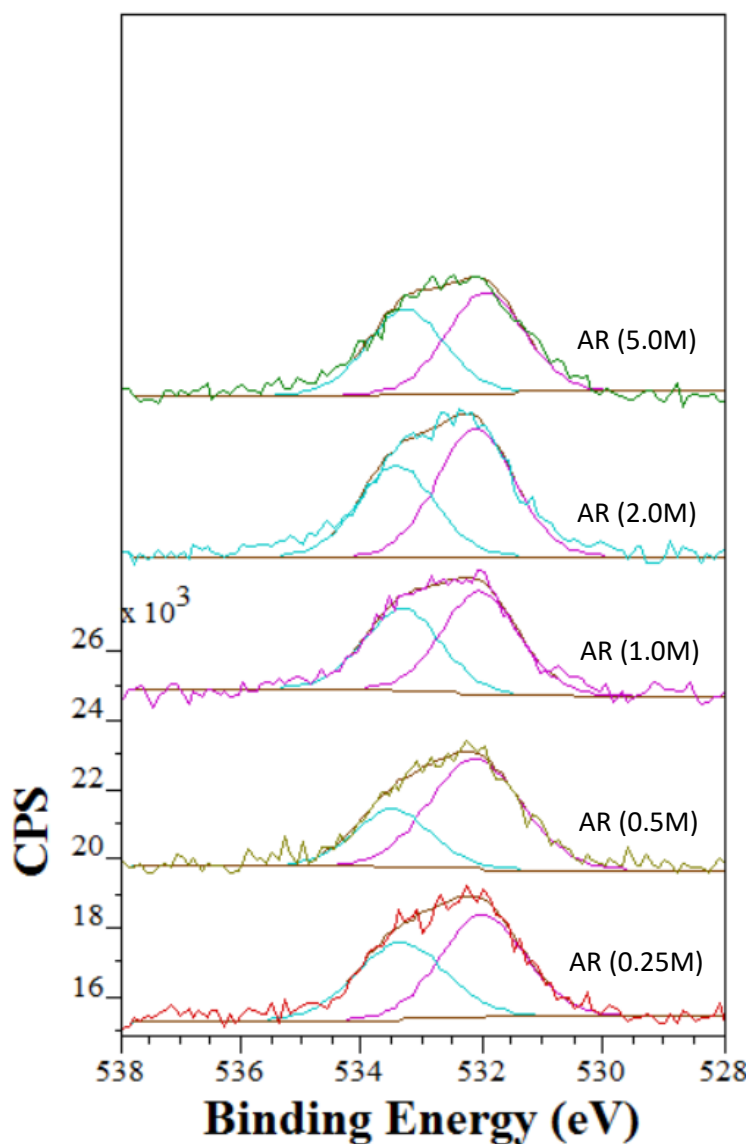


Figure 45 – Overlay narrow scan O 1s XPS spectra of HOPG samples treated with HNO₃

3.4.3 Fluorinating Hydrophilic Groups on AR Treated HOPG for Determination the Identity of the Oxygen Functionalities

From AFM and XPS results obtained, samples treated with aqua regia showed no clear change in the concentrations of oxygen on the surface or significant changes in surface topography. Because of this a more detailed study of the samples was conducted. This was aimed at the determination of the identity of the oxygen groups on the surface. Because of the breadth and overlap of different oxygen peaks, an XPS narrow scan is unable to distinguish between the different components to determine the presence and relative concentrations of different oxygen groups on the surface such as hydroxyl, ketone, carboxylic acid or ether groups.

Selective derivatization was used in the determination of the identities of the oxygen functionalities on the surface (refer to experimental section). This method showed that both nitric acid treatment

and hydrochloric acid treatment of graphite generates almost solely hydroxyl groups through binding with trifluoroacetic anhydride (TFAA, 99%). [46], [47] In the case of HCl treated graphite the hydroxyl groups were shown to get converted to ketone and ether functionalities with heating of the sample following acid treatment.[47]

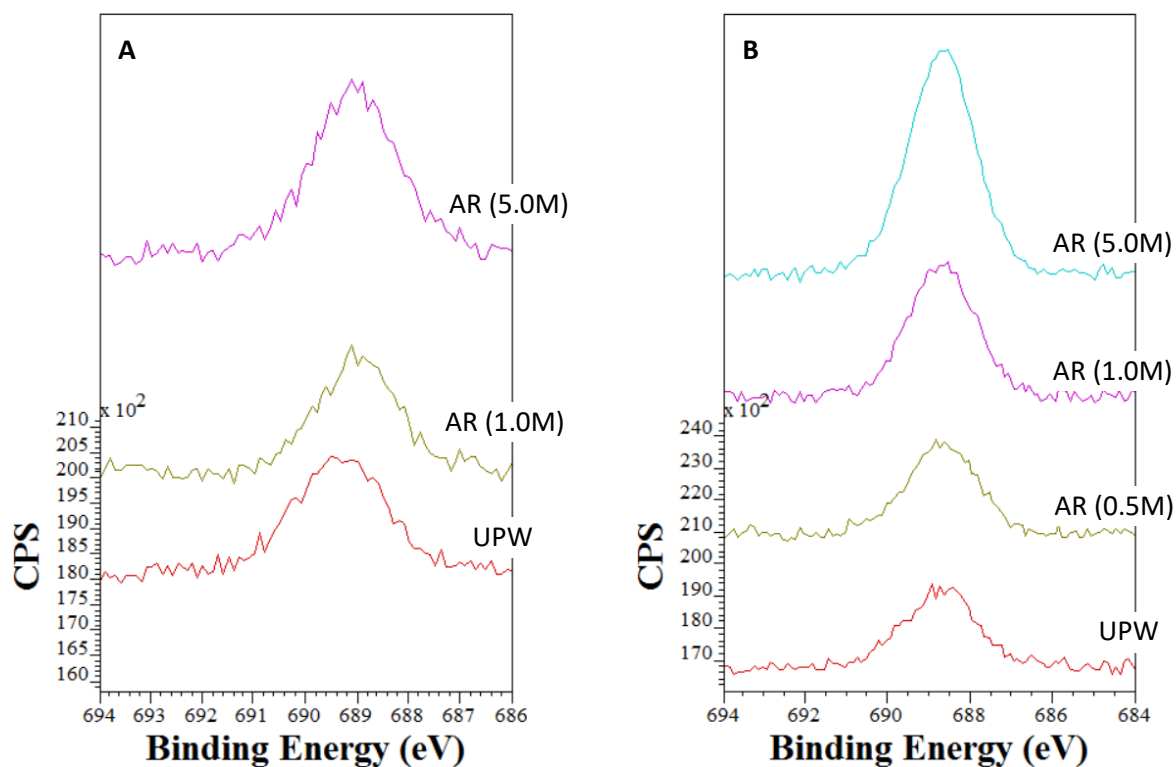


Figure 46 – Overlay of the narrow scan XPS spectra of F1s peaks in Aqua Regia Treated HOPG after selective derivatization. (A) Selective derivatization using TFAA for detection of hydroxyl groups. (B) Selective derivatization using TFH for detection of ketone.

XPS scans of aqua regia treated surfaces selectively derivativized using TFAA and TFH show the presence and concentration of hydroxyl and ketone groups respectively. Concentrations of these groups are directly proportional to the concentration of fluorine on the surface as detected by XPS. Quantities of OH groups as showed in Figure 46(A) show no clear change in concentration, however there is an obvious trend in the amount of ketone groups as shown in Figure 46(B) where higher concentrations of aqua regia results in a graphite surface covered with a higher concentration of ketone groups. Peak fitting of the narrow scan spectra in Figure 46 allowed determination of the area of the peak and therefore the relative concentrations of ketone groups on the surface. These areas are given in Table 3.

Sample ID	F1s/C1s Peak Area (AU)
UPW	5303/257718 = 0.021
AR(0.5M)-TFH	6267/257850 = 0.024
AR(1.0M)-TFH	8335/251169 = 0.033
AR(5.0M)-TFH	13927/250021 = 0.056

Table 3 – data showing the peak areas of the F1s peak in Aqua Regia treated HOPG after selective derivatization using TFH.

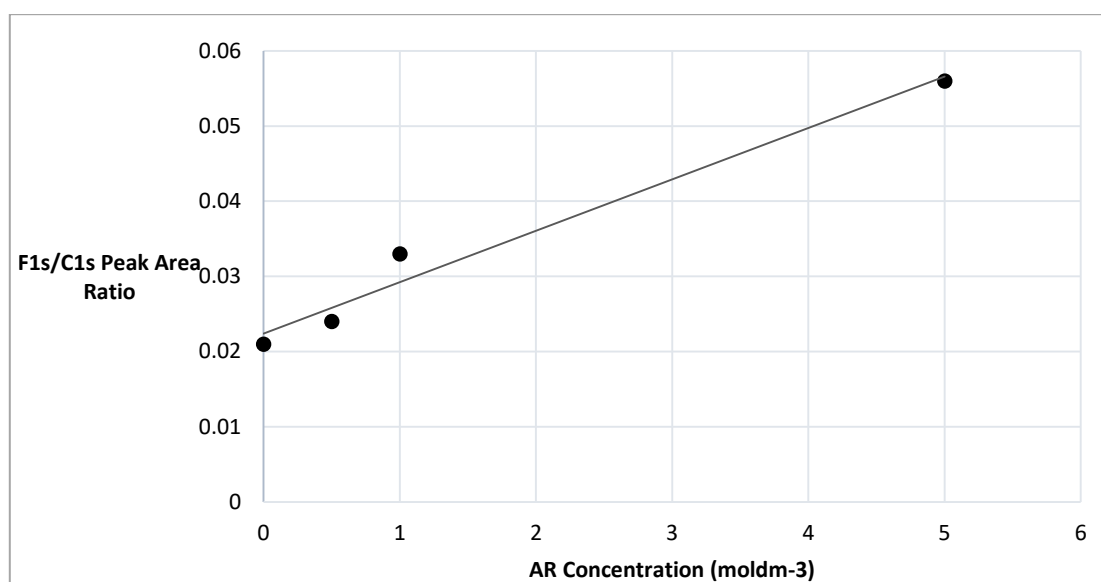


Figure 47 – Graph showing the concentrations of Fluorine in Aqua Regia treated HOPG after selective derivatization using TFH.

Figure 47 shows an approximately linear increase in the concentration of fluorine detected in the samples with increasing concentrations of aqua regia used. From the data a linear relationship was deduced, however further data points are needed to be confident of this pattern. The F1s peak area is directly proportional to the concentration of Fluorine on the sample, which in turn is directly proportional to the concentration of ketone groups on the surface. This is likely a result of the high oxidising ability of higher concentrations of aqua regia treatment. It also explains why AFM images shown in Figure 44 showed very little change in the topography of the surface, studies done on heated hydrochloric acid treated surfaces showed a decrease in the number of islands formed upon heating and an increase in the quantity of ketone groups observed through selective

derivatization.[47] This study supports the observation that increasing numbers of ketone groups result in a flattening of the surface.

3.5 HAuCl_4 ($2 \times 10^{-6} \text{ mol dm}^{-3}$) Treatment of AR Treated HOPG

HOPG samples were treated with $100 \mu\text{l}$ of different concentrations of AR solution for 30 minutes before being treated with $100 \mu\text{l}$ of HAuCl_4 ($2 \times 10^{-6} \text{ mol dm}^{-3}$) for a further 30 minutes. This was done to observe how AR treatment of HOPG effects the deposition of gold onto the surface due to the increasing quantities of ketone groups introduced to the surface. This includes how the ketone groups influence the quantity of gold nanoparticles, their size, shape and the oxidation states of the gold atoms.

All samples were prepared in exactly the same way but with a change in the concentration of aqua regia being used for the acid treatment of the HOPG. Samples are labelled as follows.

AR (0.25M) – HAuCl_4 ($2 \times 10^{-6} \text{ M}$)

AR (0.5M) – HAuCl_4 ($2 \times 10^{-6} \text{ M}$)

AR (1.0M) – HAuCl_4 ($2 \times 10^{-6} \text{ M}$)

AR (2.0M) – HAuCl_4 ($2 \times 10^{-6} \text{ M}$)

AR (5.0M) – HAuCl_4 ($2 \times 10^{-6} \text{ M}$)

Due to issues with the AFM apparatus images were unable to be obtained for samples 'AR (2.0M) – HAuCl_4 ($2 \times 10^{-6} \text{ M}$)' or 'AR (5.0M) – HAuCl_4 ($2 \times 10^{-6} \text{ M}$)'.

3.5.1 AR (0.25M) – HAuCl₄ (2x10⁻⁶M)

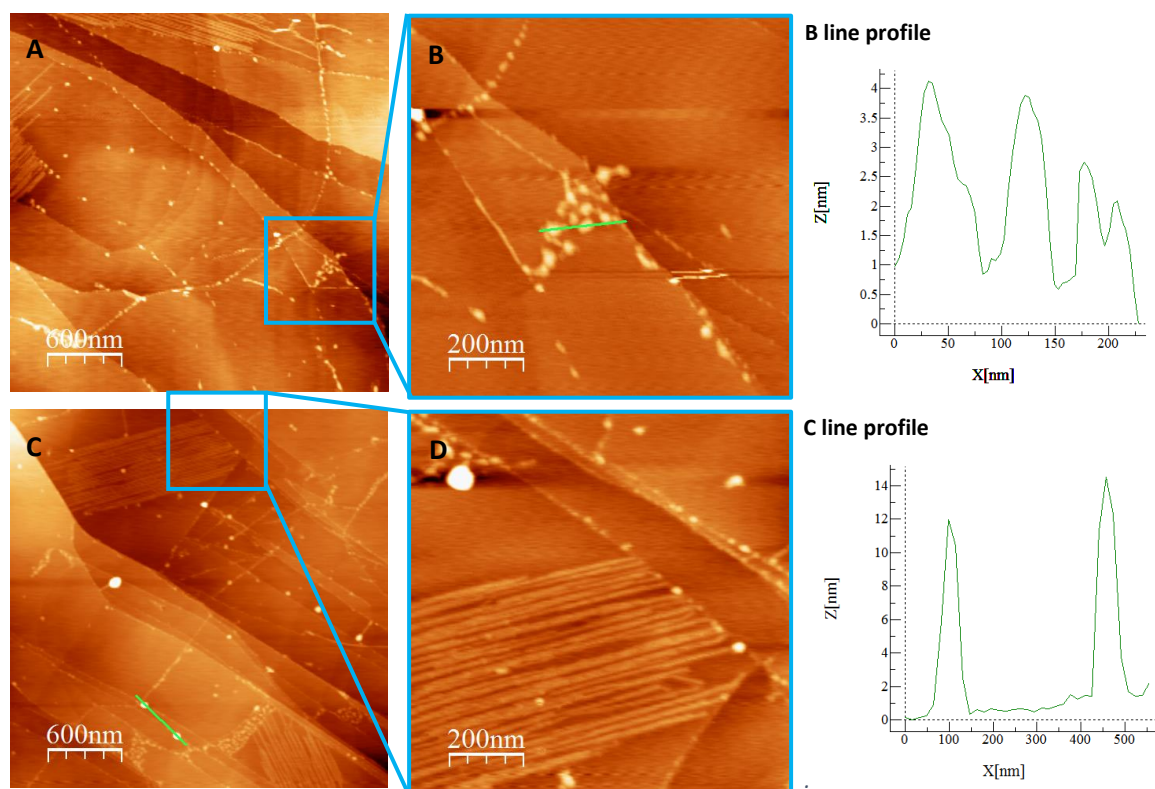


Figure 48 – AFM images of ‘AR (0.25M) – HAuCl₄ (2x10⁻⁶M)’ with a line profiles refer to the green line going from left to right. (A) 3.0x3.0 μm AFM image, (B) 1.0x1.0 μm, (C) 3.0x3.0 μm AFM image of the same sample in a different location, (D) 1.0x1.0 μm zoomed in AFM image.

The 0.25M AR treatment of HOPG shows the introduction of a lot of new islands, the majority of which vary in size between 1 and 4 nm in height and about 50 nm in width. Most islands are very small and are well defined in shape. Most islands have a prevalence for step edges, however an interesting development can be seen in images A and C where many areas of the surface are shown to have collections of islands which are shown in close view in image B. Image D shows the presence of streaked islands across the surface which has not been seen in any images thus far. Clean HOPG samples treated with UPW before treatment with HAuCl₄ (2x10⁻⁶M) was used as the standard for this sample and is shown in AFM images in Figure 33 and XPS data in Figure 34. The standard shows a very clean surface and samples treated solely with 0.25 moldm⁻³ aqua regia show very few islands on the surface suggesting that all islands viewed in Figure 48 are attributed to the presence of gold.

XPS data shows only the presence of the substrate carbon, as well as oxygen and gold on the surface. No Cl or N from the acid anions or chloroauric acid anions have become incorporated into the sample.

3.5.2 AR (0.5M) – H_{AuCl₄} (2x10⁻⁶M)

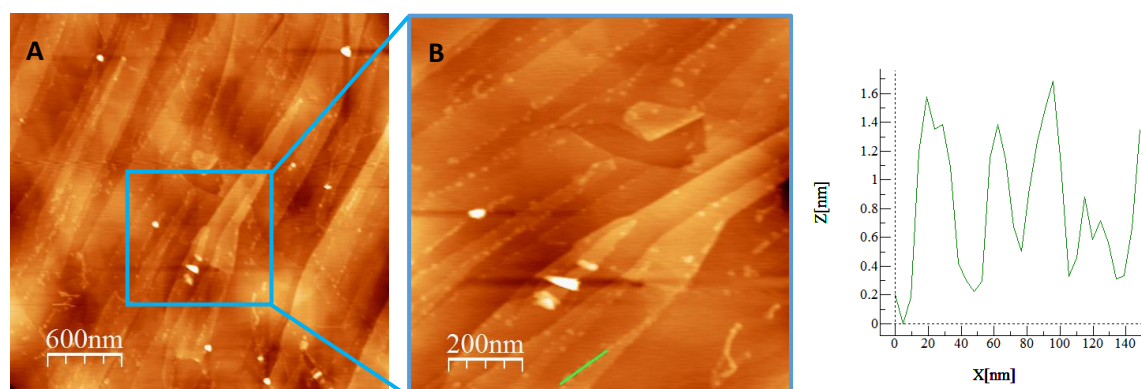


Figure 49 – (A) 3.0x3.0μm AFM image of 'HNO₃ (0.5M) – H_{AuCl₄} (2x10⁻⁶M)', (B) 1.0x1.0μm AFM image of HNO₃ (0.5M) – H_{AuCl₄} (2x10⁻⁶M) with line profile going from left to right.

Figure 49 shows an increase in the quantity of islands seen by AFM compared to AR (0.25M) – H_{AuCl₄} (2x10⁻⁶M), the islands that are present are smaller as shown from the line profile and the collection of islands do not appear to be present.

3.5.3 AR (1.0M) – H_{AuCl₄} (2x10⁻⁶M)

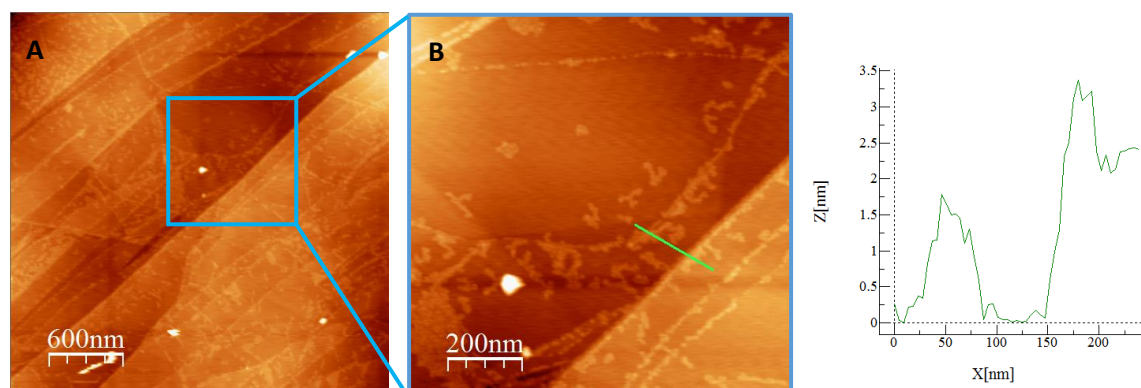


Figure 50 – (A) 3.0x3.0μm AFM image of 'HNO₃ (5.0M) – H_{AuCl₄} (2x10⁻⁶M)', (B) 1.0x1.0μm AFM image of HNO₃ (0.25M) – H_{AuCl₄} (2x10⁻⁶M) with line profile going from left to right.

The AFM images in Figure 50 shows a large increase in the surface coverage of islands and a clear coalescing of small islands into indistinct shapes. These have a preference for step edges but also branch out into the terraces. This image seems to show the start of less crystalline and more amorphous gold island formations.

AFM images of HOPG treated with aqua regia followed by gold treatment show an increasing surface coverage of gold islands with increasing aqua regia concentration. In all samples gold islands show a preference to appear along step edges as opposed to the terraces. With increasing aqua regia

concentration the islands also lose their hemispherical shaping and become smaller and more amorphous, by 1.0 M aqua regia many of the gold islands have coalesced to form small networks.

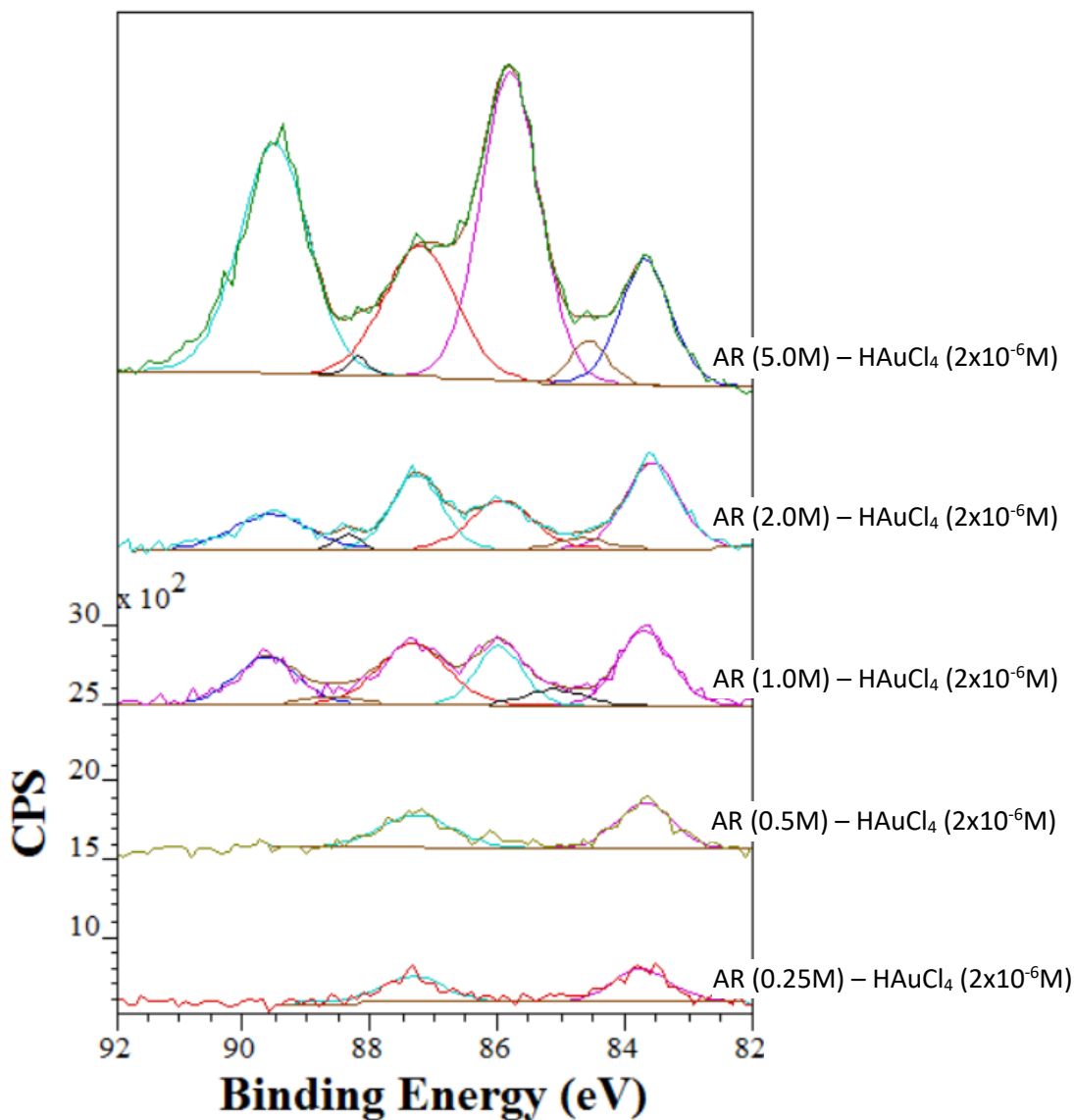


Figure 51 – Overlay narrow scan Au^{4f} XPS spectra of HOPG samples treated with HAuCl₄ ($2 \times 10^{-6} \text{ moldm}^{-3}$) following treatment with AR

Figure 51 – Overlay narrow scan Au^{4f} XPS spectra of HOPG samples treated with HAuCl₄ ($2 \times 10^{-6} \text{ moldm}^{-3}$) following treatment with AR Figure 51 shows the increasing quantities of gold present on the surface when treating the surface with different concentrations of aqua regia. There is a large component attributed to Au(0) suggesting that the hydroxyls found on the surface of HNO₃ treated surfaces cause a reduction of the gold from Au(III) (86.0 eV) to Au(0) (84.0 eV). At aqua regia concentrations of 1.0M to 5.0M the concentration of Au(III) increases significantly with only slight increases in the quantities of Au(0). Fluorine derivatisation using TFAA as shown in Figure 46 suggest

that samples treated with different concentrations of aqua regia show a similar quantity of hydroxyl groups. This combined with the similar quantities of Au(0) present in all H_{AuCl}₄ treatment of AR treated surfaces shown in Figure 51, provides further evidence that the mechanism for Au(0) formation involves the oxidation of hydroxyl groups.

At aqua regia concentrations of 1.0M to 5.0M the main component to the increasing gold concentration is attributed to the significant increase in Au(III). This supports the conclusions from the selective derivatization study of aqua regia treated studies using TFH, which shows an increase in the quantities of ketone groups on the surface when using higher concentrations of aqua regia. These ketone groups lack the reductive potential to reduce Au(III) to Au(0) and instead are likely to create an ion-dipole bond with the Au(III) ions showing the increase in the presence of Au(III) with increasing aqua regia concentrations.

3.6 Comparison of H_{AuCl}₄ Treated HNO₃ Activated HOPG with H_{AuCl}₄ Treated AR Activated HOPG

The XPS data collected for H_{AuCl}₄ treatment of AR treated surfaces shows a very familiar pattern in changes in the ratios of Au(0) to Au(III) between different samples when compared to H_{AuCl}₄ treatment of HNO₃ treated surfaces. This suggests that the different acids effects on the functionalisation of the surface with oxygen groups does not change in a significant way to change the relative ionisation states of Au on the surface. However, when comparing XPS data of H_{AuCl}₄ treatment of AR treated surfaces to H_{AuCl}₄ treatment of HNO₃ treated surfaces, there is a massive change in the quantities of gold deposited. Whilst the pattern of increasing quantities of gold with increasing acid concentration and the relative ratios of Au(0) to Au(III) appear very similar there is a very noticeable difference in the overall quantity of Au deposited where aqua regia results in much greater quantities. This is visually represented in Figure 52 where the differences in quantities of gold between H_{AuCl}₄ treatments of AR treated samples to H_{AuCl}₄ treatment of HNO₃ treated samples can be seen in the scale along the y-axis.

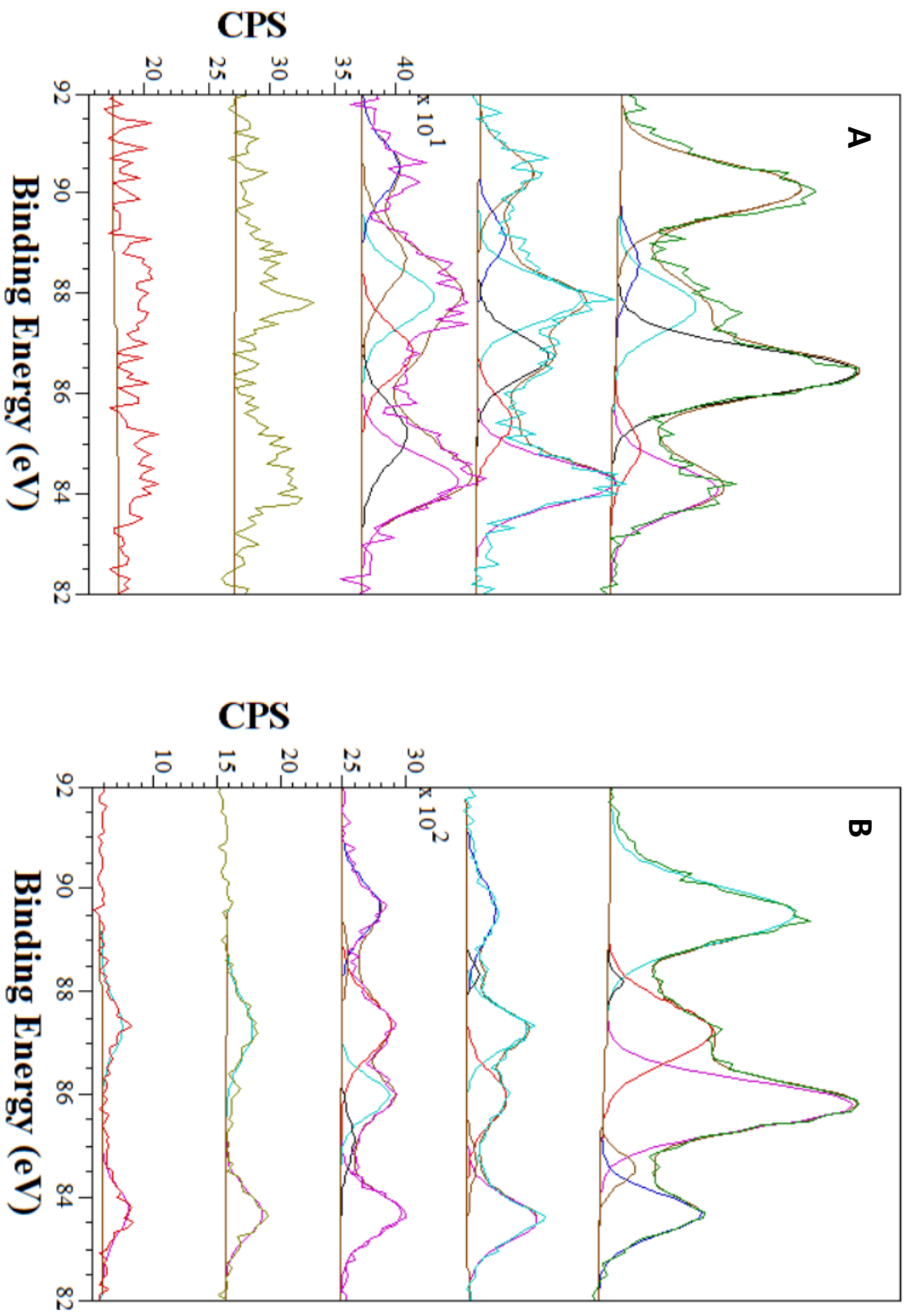


Figure 52 - Overlay narrow scan Au4f XPS spectra of HOPG samples treated with HAuCl₄ (2×10^{-6} mol dm⁻³) following treatment with different acids, (A) HAuCl₄ treatment of HNO₃ treated surfaces, (B) HAuCl₄ treatment of AR treated surfaces.

Concentration of HNO ₃ /AR (mol dm ⁻³)	HAuCl ₄ on HNO ₃ Treated Surfaces.	HAuCl ₄ on AR Treated Surfaces.
0.25M		$\sigma_{Au(0)} = 4.32 \times 10^{13} \text{ atoms/cm}^2$
0.5M		$\sigma_{Au(0)} = 6.30 \times 10^{13} \text{ atoms/cm}^2$
1.0M	$\sigma_{Au(0)} = 6.10 \times 10^{13} \text{ atoms/cm}^2$ $\sigma_{Au(I)} = 2.51 \times 10^{13} \text{ atoms/cm}^2$ $\sigma_{Au(III)} = 1.88 \times 10^{13} \text{ atoms/cm}^2$ $\sigma_{Au \text{ total}} = 1.05 \times 10^{14} \text{ atoms/cm}^2$ $Au^{III}: Au^0 = 1 : 3.24$	$\sigma_{Au(0)} = 1.03 \times 10^{14} \text{ atoms/cm}^2$ $\sigma_{Au(I)} = 2.41 \times 10^{13} \text{ atoms/cm}^2$ $\sigma_{Au(III)} = 7.04 \times 10^{13} \text{ atoms/cm}^2$ $\sigma_{Au \text{ total}} = 1.98 \times 10^{14} \text{ atoms/cm}^2$ $Au^{III}: Au^0 = 1 : 1.46$
2.0M	$\sigma_{Au(0)} = 7.53 \times 10^{13} \text{ atoms/cm}^2$ $\sigma_{Au(I)} = 1.90 \times 10^{13} \text{ atoms/cm}^2$ $\sigma_{Au(III)} = 3.87 \times 10^{13} \text{ atoms/cm}^2$ $\sigma_{Au \text{ total}} = 1.33 \times 10^{14} \text{ atoms/cm}^2$ $Au^{III}: Au^0 = 1 : 1.95$	$\sigma_{Au(0)} = 1.05 \times 10^{14} \text{ atoms/cm}^2$ $\sigma_{Au(I)} = 1.10 \times 10^{13} \text{ atoms/cm}^2$ $\sigma_{Au(III)} = 6.86 \times 10^{13} \text{ atoms/cm}^2$ $\sigma_{Au \text{ total}} = 1.85 \times 10^{14} \text{ atoms/cm}^2$ $Au^{III}: Au^0 = 1 : 1.53$
5.0M	$\sigma_{Au(0)} = 5.95 \times 10^{13} \text{ atoms/cm}^2$ $\sigma_{Au(I)} = 1.53 \times 10^{13} \text{ atoms/cm}^2$ $\sigma_{Au(III)} = 1.35 \times 10^{14} \text{ atoms/cm}^2$ $\sigma_{Au \text{ total}} = 2.10 \times 10^{14} \text{ atoms/cm}^2$ $Au^{III}: Au^0 = 1 : 0.44$	$\sigma_{Au(0)} = 1.55 \times 10^{14} \text{ atoms/cm}^2$ $\sigma_{Au(I)} = 3.94 \times 10^{13} \text{ atoms/cm}^2$ $\sigma_{Au(III)} = 4.32 \times 10^{14} \text{ atoms/cm}^2$ $\sigma_{Au \text{ total}} = 6.24 \times 10^{14} \text{ atoms/cm}^2$ $Au^{III}: Au^0 = 2.79 : 1$

Table 4 – data showing the coverage of gold on the surface of HOPG determined using the peak areas of the different synthetic components of the Au4f peaks in aqua regia and nitric acid treated HOPG.

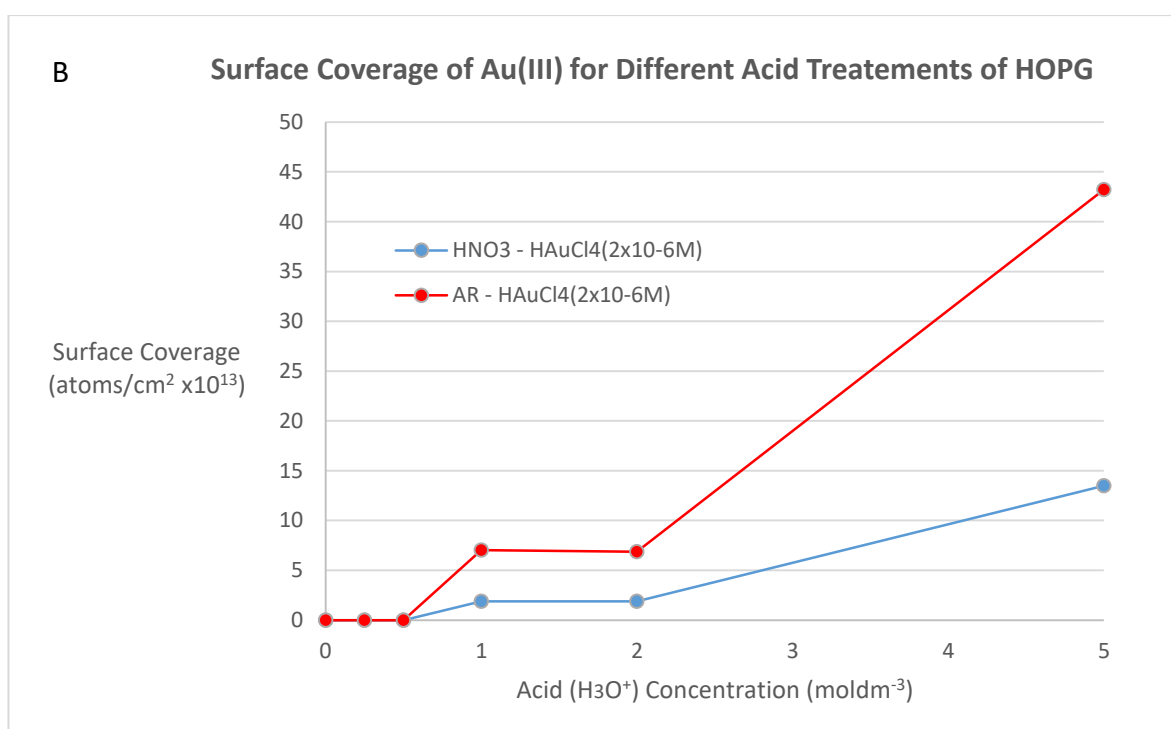
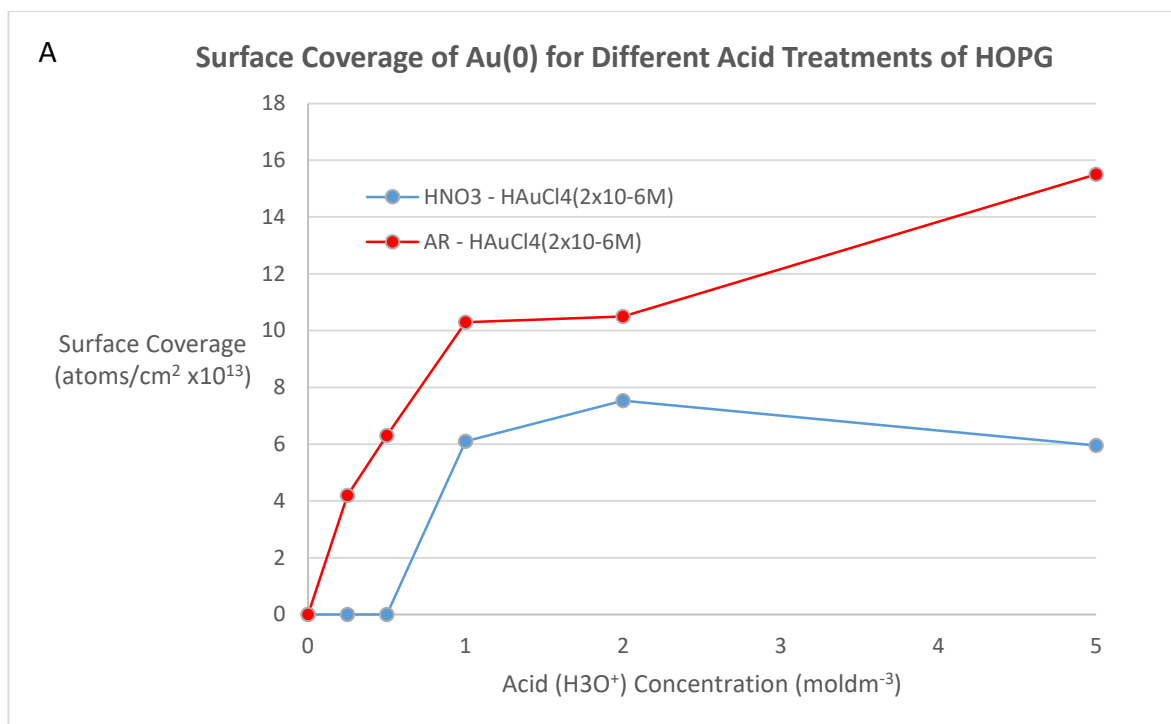


Figure 53 – (A) Graph showing the differing surface coverage of Au(0) on HOPG upon treatment with HNO₃ or AR followed by treatment with HAuCl₄ (2x10⁻⁶M). (B) Graph showing the differing surface coverage of Au(III) on HOPG upon treatment with HNO₃ or AR followed by treatment with HAuCl₄ (2x10⁻⁶M).

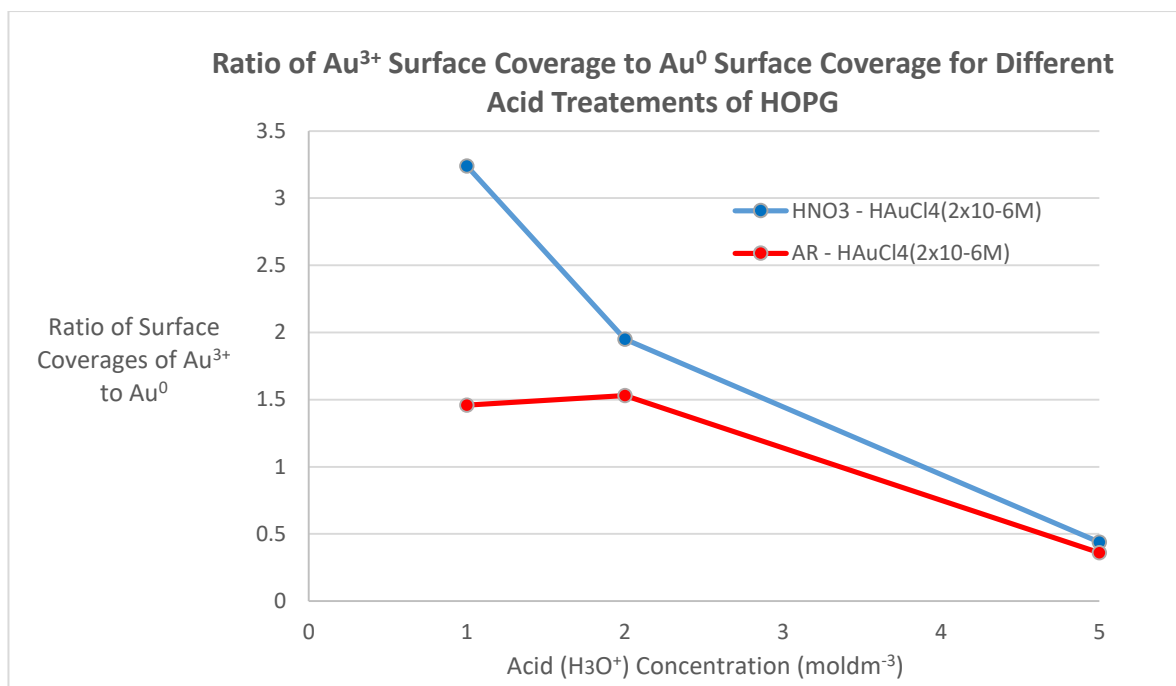


Figure 54 – (A) Graph showing the ratio of Au^{III} : Au⁰ on HOPG upon treatment with HNO₃ or AR followed by treatment with HAuCl₄ (2x10⁻⁶M). (B) Graph showing the differing surface coverage of Au(III) on HOPG upon treatment with HNO₃ or AR followed by treatment with HAuCl₄ (2x10⁻⁶M).

Figure 53 shows the pattern of increasing surface coverage of Au(0) and Au(III) with increasing nitric acid and aqua regia concentrations of samples treated with HAuCl₄ (2x10⁻⁶M) following treatment with nitric acid or aqua regia. The pattern of increasing gold surface coverage is very similar for both aqua regia and nitric acid treated surfaces. This is especially clear in Figure 53(B) showing the increase in Au(III).

These graphs and the XPS data obtained in Figure 52 show that when using aqua regia for activating the surface instead of nitric acid a lot of similarities can be seen. At low concentrations of acid Au(0) is all that is present and shows a steady increase until about 2 mol dm⁻³ is used at which point the concentration of Au(0) plateaus. Au(III), which is determined to be the active gold ion[68], is only present when using acid concentrations of 1 mol dm⁻³ or above with a dramatic increase in concentration of Au(III) between 2 mol dm⁻³ and 5 mol dm⁻³ in both nitric acid and aqua regia treated surfaces.

Whilst the ratios and patterns of increasing quantities of both Au(0) and Au(III) remained the same for both aqua regia and nitric acid activated surfaces, one of the main differences involved the quantity of Au(0) and Au(III) showing a doubling of the quantities of both Au(0) and Au(III) on the surface when using aqua regia.

3.7 Heat Treatment of AR Activated HOPG and Its Effect on the Deposition of H_{AuCl₄}

UPW – Heat (473K) – H_{AuCl₄} (2x10⁻⁶M)

AR (0.25M) – Heat (473K) – H_{AuCl₄} (2x10⁻⁶M)

AR (0.5M) – Heat (473K) – H_{AuCl₄} (2x10⁻⁶M)

AR (1.0M) – Heat (473K) – H_{AuCl₄} (2x10⁻⁶M)

AR (2.0M) – Heat (473K) – H_{AuCl₄} (2x10⁻⁶M)

AR (5.0M) – Heat (473K) – H_{AuCl₄} (2x10⁻⁶M)

3.7.1 UPW – Heat (473K) – H_{AuCl₄} (2x10⁻⁶M)

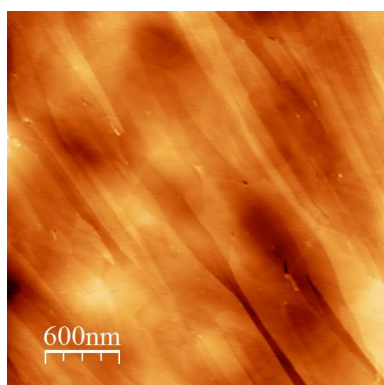


Figure 55 – 3.0x3.0μm AFM image of 'UPW – H_{AuCl₄} (2x10⁻⁶M)', (B) 1.0x1.0μm AFM image of HNO₃ (0.25M) – H_{AuCl₄} (2x10⁻⁶M) with line profile going from left to right.

Figure 55 is the AFM image being used as the standard by which the following AFM images can be compared.

3.7.2 AR (xM) – Heat (473K) – HAuCl_4 ($2 \times 10^{-6}M$)

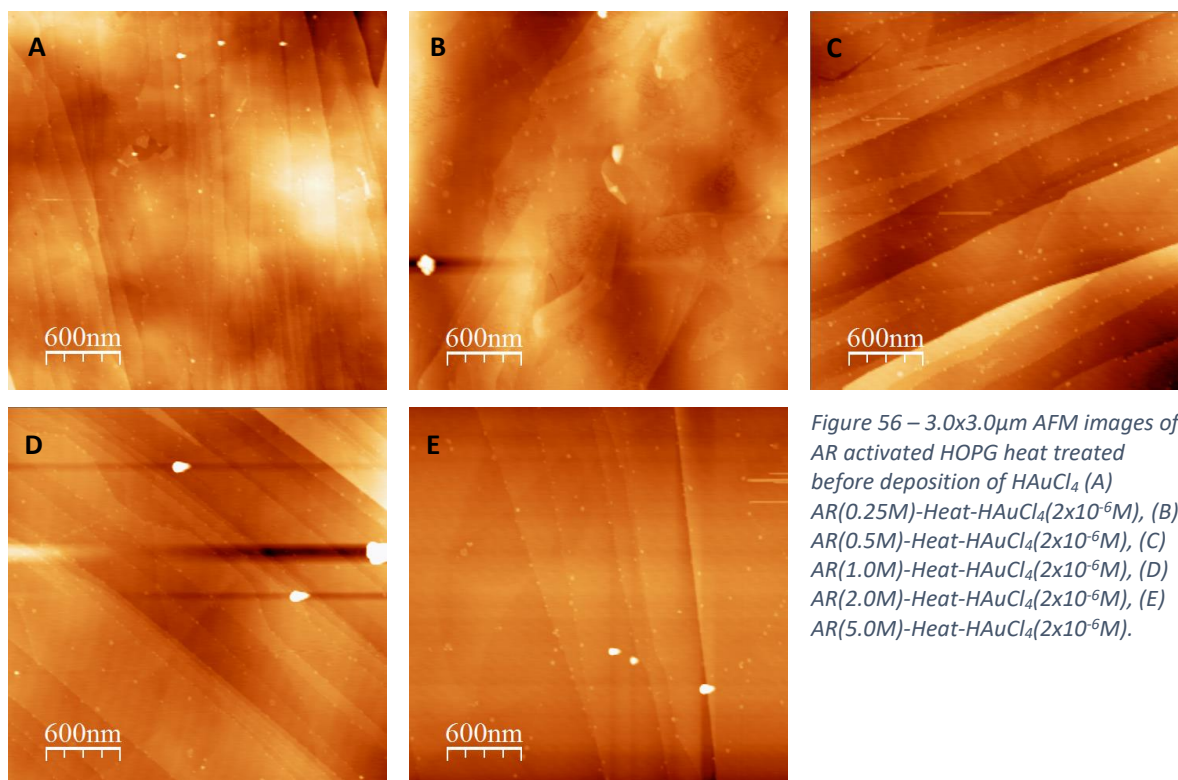
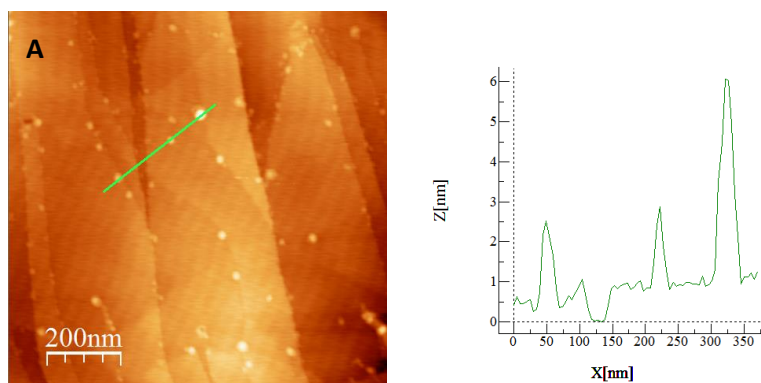


Figure 56 – $3.0 \times 3.0 \mu\text{m}$ AFM images of AR activated HOPG heat treated before deposition of HAuCl_4 (A) AR(0.25M)-Heat- HAuCl_4 ($2 \times 10^{-6}M$), (B) AR(0.5M)-Heat- HAuCl_4 ($2 \times 10^{-6}M$), (C) AR(1.0M)-Heat- HAuCl_4 ($2 \times 10^{-6}M$), (D) AR(2.0M)-Heat- HAuCl_4 ($2 \times 10^{-6}M$), (E) AR(5.0M)-Heat- HAuCl_4 ($2 \times 10^{-6}M$).

$3.0 \times 3.0 \mu\text{m}$ AFM images of AR activated HOPG heat treated before deposition of HAuCl_4 is shown in Figure 56 and shows huge similarity across the surface in all images. This is in stark contrast to AR activated surfaces treated with HAuCl_4 as shown in Figure 48 - Figure 50 which shows increasing concentrations of Au with increasing concentrations of aqua regia used.

The differences between samples which have been heat treated before gold deposition and samples that have not, suggests that the heating may affect the functionalisation groups on the surfaces of the AR treated HOPG's in such a way as to convert all functional groups to the same identity. Or that the heating removes some of the functional groups on the surfaces with greater deactivation occurring on the more activated samples treated with higher concentrations of aqua regia.



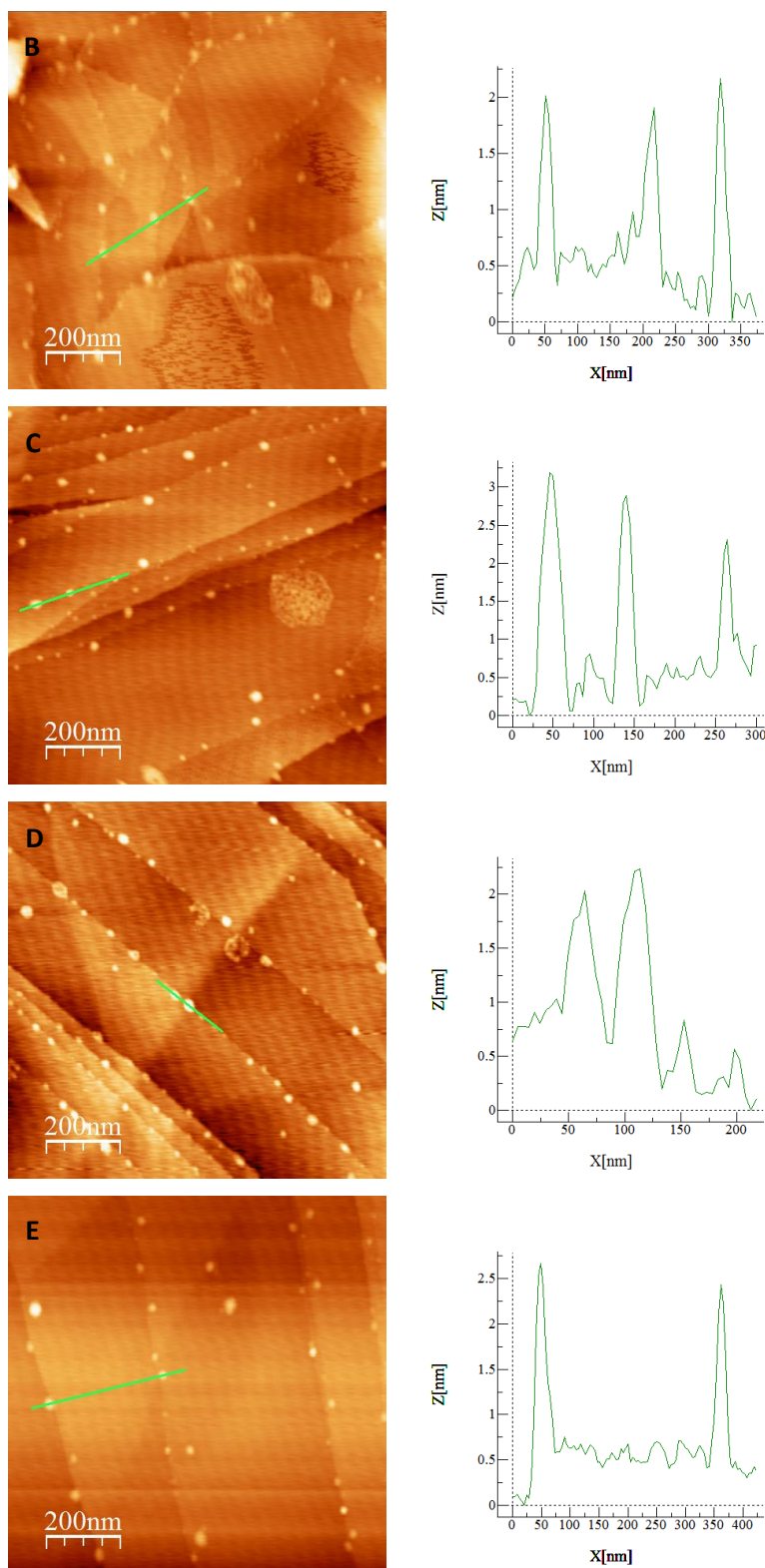


Figure 57 – 1.0x1.0 μ m AFM images of AR activated HOPG heat treated before deposition of HAuCl₄. Line profiles are shown by the green line going from left to right. (A) AR(0.25M)-Heat-HAuCl₄(2x10⁻⁶M), (B) AR(0.5M)-Heat-HAuCl₄(2x10⁻⁶M), (C) AR(1.0M)-Heat-HAuCl₄(2x10⁻⁶M), (D) AR(2.0M)-Heat-HAuCl₄(2x10⁻⁶M), (E) AR(5.0M)-Heat-HAuCl₄(2x10⁻⁶M).

The line profiles shown in Figure 57 show how little the islands vary in height or length with very few islands exceeding 3nm in height or 50nm in width. Percentage surface coverage appears very

uniform across each sample however because of the small sizes of the islands, flooding analysis was not possible.

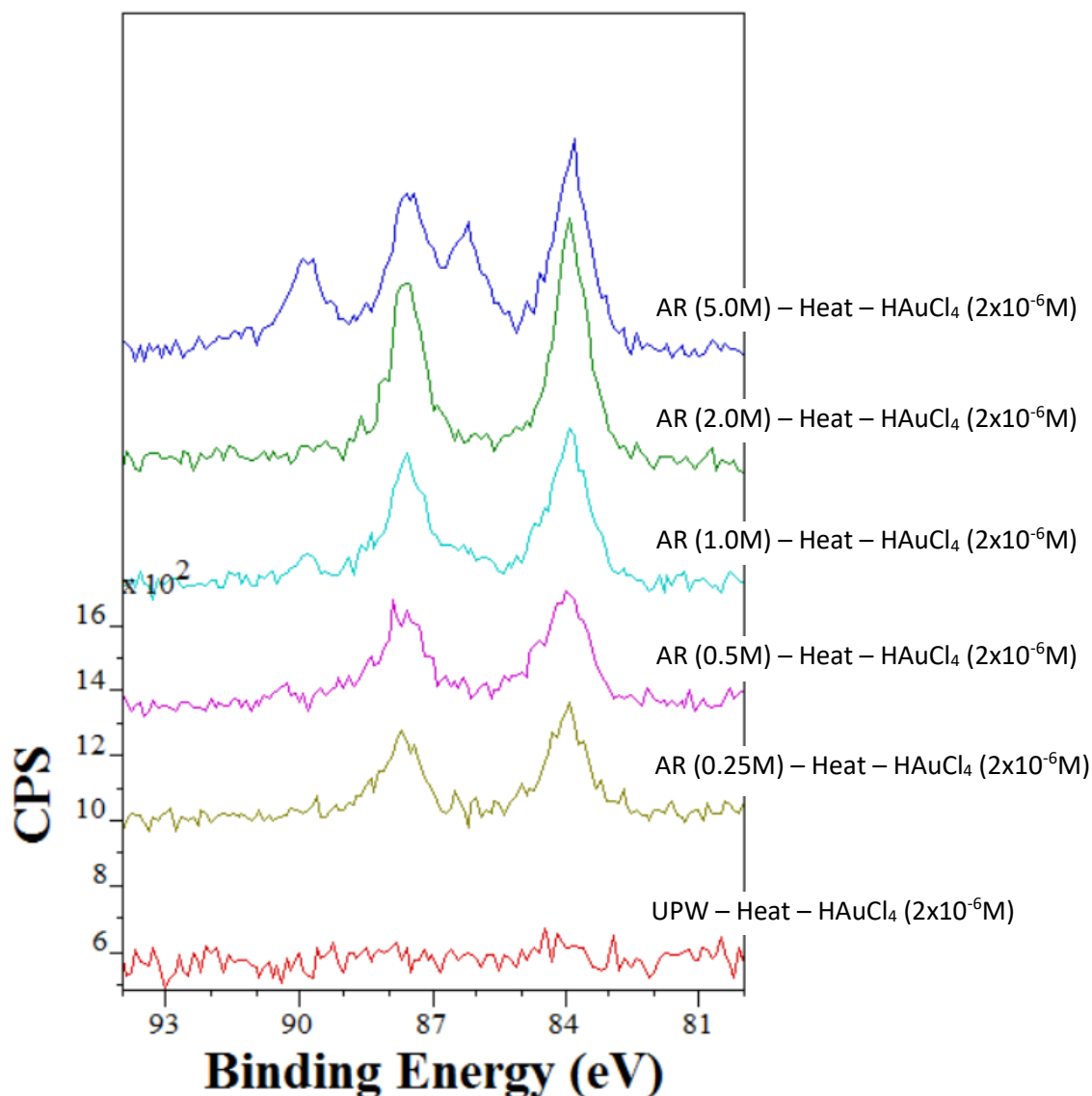


Figure 58 – Overlay narrow scan Au^{4f} XPS spectra of HOPG samples activated with aqua regia before heat treatment and deposition with HAuCl₄ (2×10^{-6} moldm⁻³).

XPS data shown in Figure 58 shows a very gradual increase in concentration of Au(0) with increasing concentrations of AR used. Similarly to AR treated surfaces without heating, Au(III) was shown to appear only when using higher concentrations of AR but Au(0) was still dominate.

The main difference in the XPS of AR-Heat-HAuCl₄ compared with the XPS of AR-HAuCl₄ is the decrease in the amount of Au seen and the smaller increases in the concentration of Au on the surface with increasing concentrations of AR. This suggests that the numbers of functional groups introduced on the surface may have decreased upon heating possibly due to thermal decomposition

or delamination of the surface layers on the graphite. With a disproportionate amount of deactivation occurring to the more heavily activated samples (higher aqua regia treated samples).

3.8 H₂SO₄ Treatment on HOPG

HOPG samples were treated with 100µl of different concentrations of H₂SO₄ in UPW for 30 minutes. This was done to observe how sulfuric acid treatment of graphite compares to surfaces treated with HNO₃ or Aqua Regia. This includes the size of blisters or the introduction of different functional groups.

All samples were prepared in exactly the same way but with a change in the concentration of H₂SO₄ being used for acid treatment of the HOPG. Samples are labelled as follows.

H₂SO₄ (0.1M)

H₂SO₄ (0.2M)

H₂SO₄ (0.3M)

The treatment with H₂SO₄ resulted in a massive surface deformation in all samples which was visible under a microscope. At a microscopic level this created areas with islands that were too large for the sensitivity of the AFM probe. As such areas that were flatter were studied.

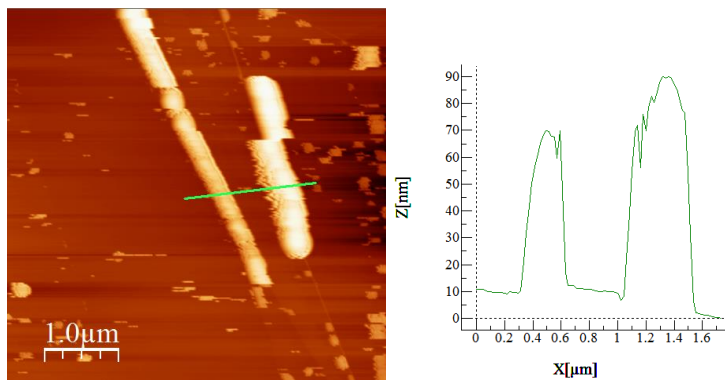


Figure 59 – 5.0x5.0µm AFM image of 0.3M H₂SO₄ treated HOPG. Line profile is shown by the green line going from left to right.

3.8.1 0.1M H₂SO₄ Treated HOPG

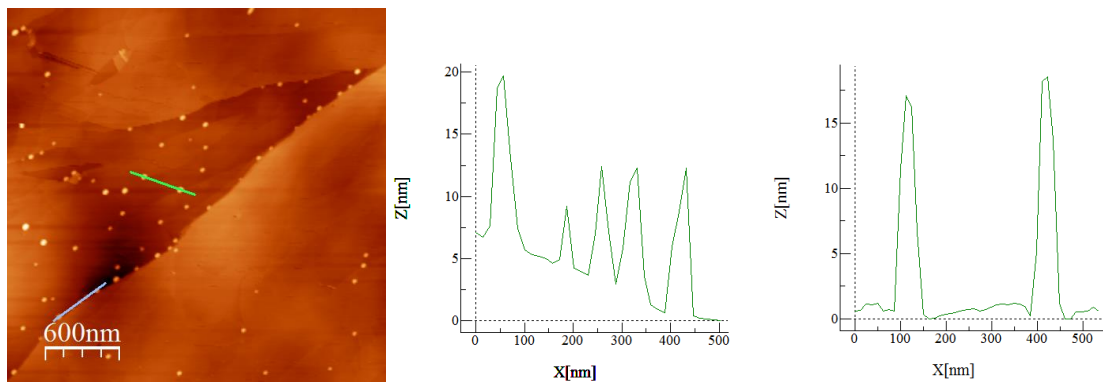


Figure 60 – 3.0x3.0 μm AFM image of 0.1M H₂SO₄ treated HOPG with line profile going from left to right. The grey line refers to the left profile and the green line the right profile.

The islands seen in Figure 60 are fairly large and show a slight preference for step edges. A closer 1.0x1.0 μm scan on an apparently flat area of the surface can divulge if any small blisters are apparent.

Small Islands (X = 25 – 50 nm, Z = 5 – 10 nm)

Large Islands (X = 100 – 150 nm, Z = 15 – 20 nm)

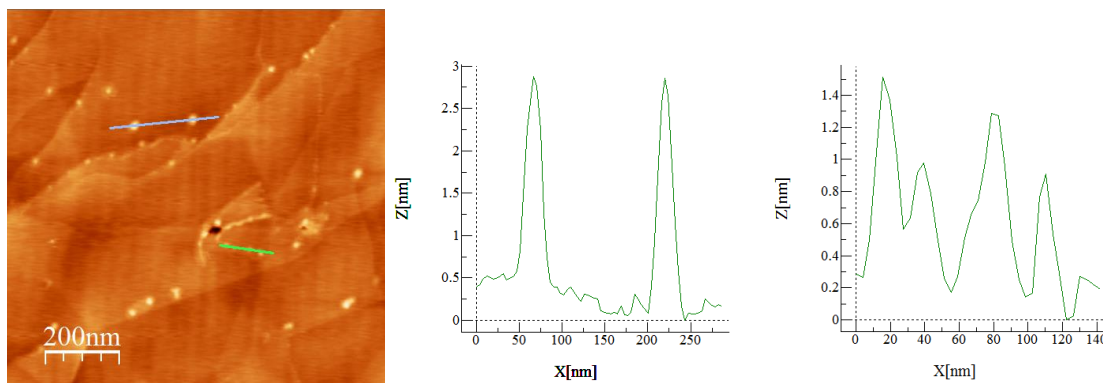


Figure 61 – 1.0x1.0 μm AFM image of 0.1M H₂SO₄ treated HOPG with line profile going from left to right. The grey line refers to the left profile and the green line the right profile.

Small islands are seen across the surface at smaller scan sizes such as those in Figure 61, these islands have a slight preference to appear along step edges and have a slight variance in size.

Small Islands (X = 20 – 50 nm, Z = 0.5 – 3 nm)

Large Islands (X = 50 – 70 nm, Z = 5 – 20 nm)

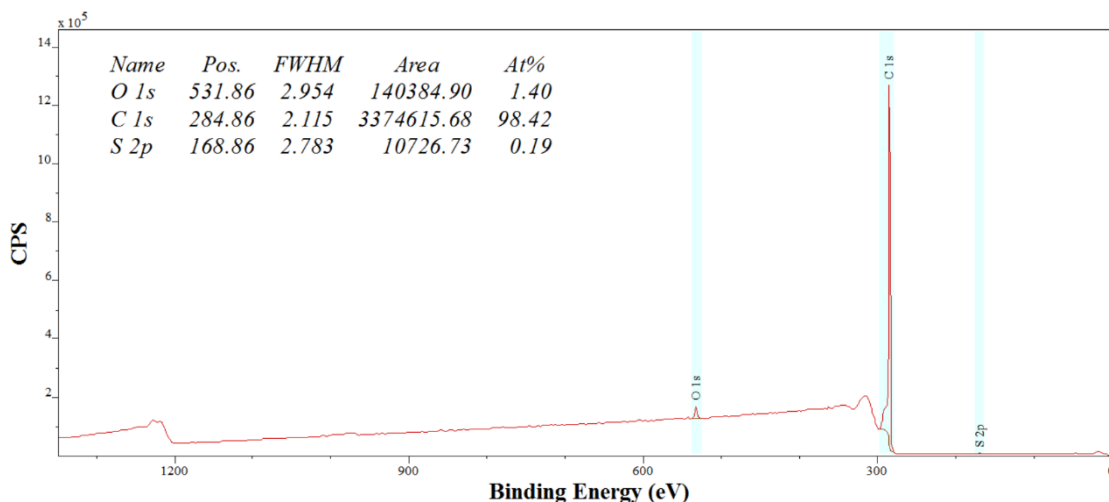


Figure 62 – Wide scan XPS spectra of 'H₂SO₄ (0.1M) – HAuCl₄ (2x10⁻⁶M)'

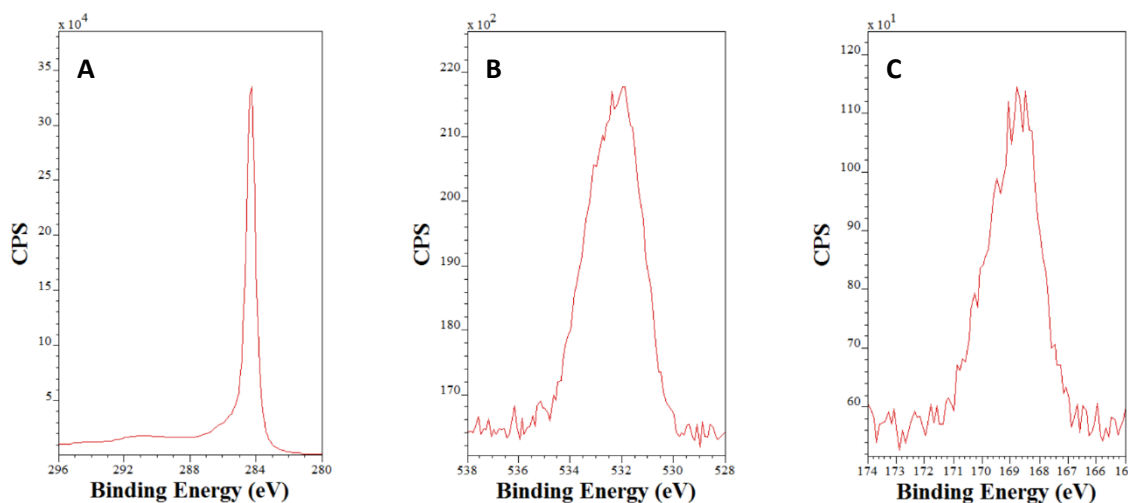


Figure 63 – Narrow scan XPS spectra of 'H₂SO₄ (0.1M), (A) C^{1s} narrow scan XPS spectra, (B) O^{1s} narrow scan XPS spectra, (C) S^{2p} narrow scan XPS spectra.

Figure 63 shows an incorporation of sulfur into the sample surface. This is very different from the samples treated with HNO₃ or HCl which showed no nitrogen or chlorine incorporated suggesting a very different mechanism for surface activation and shows that the sulfuric acid anions are involved in the final product state of the reaction and not only used in the intermediate steps.

3.8.2 0.2M H₂SO₄ Treated HOPG

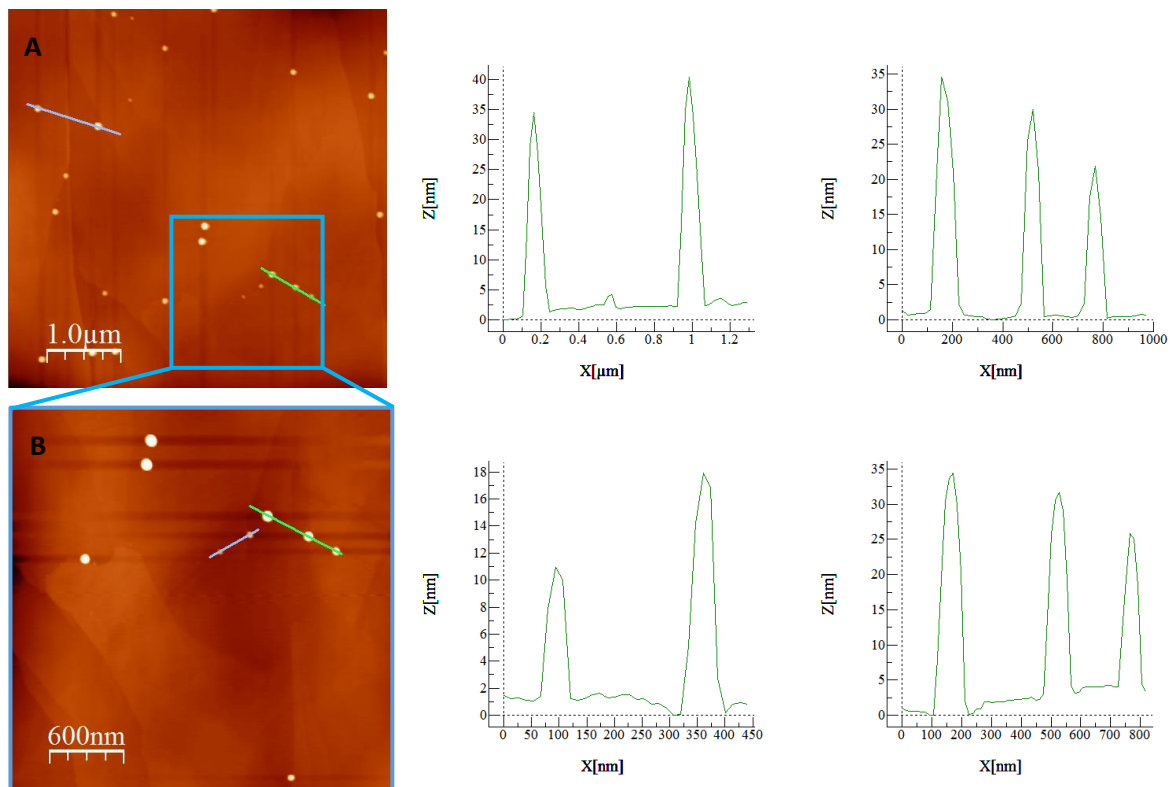


Figure 64 – (A) 5.0x5.0 μm AFM image of 0.2M H₂SO₄ treated HOPG. (B) 1.0x1.0 μm AFM image of 0.2M H₂SO₄ treated HOPG. Line profiles go from left to right. The grey lines refer to the left profile and the green lines the right profile.

AFM images of '0.2M H₂SO₄ Treated HOPG', shown in Figure 64 show a decrease in the quantity of islands present on the surface when compared to '0.1M H₂SO₄ Treated HOPG' as shown in Figure 60, however the individual size of islands are shown to almost double in size with heights of up to 40 nm. To determine whether or not any smaller islands were present a smaller scan size was taken and are shown in Figure 64(B).

Small Islands (X = 25 – 50 nm, Z = 10 – 15 nm)

Large Islands (X = 100 – 150 nm, Z = 30 – 50 nm)

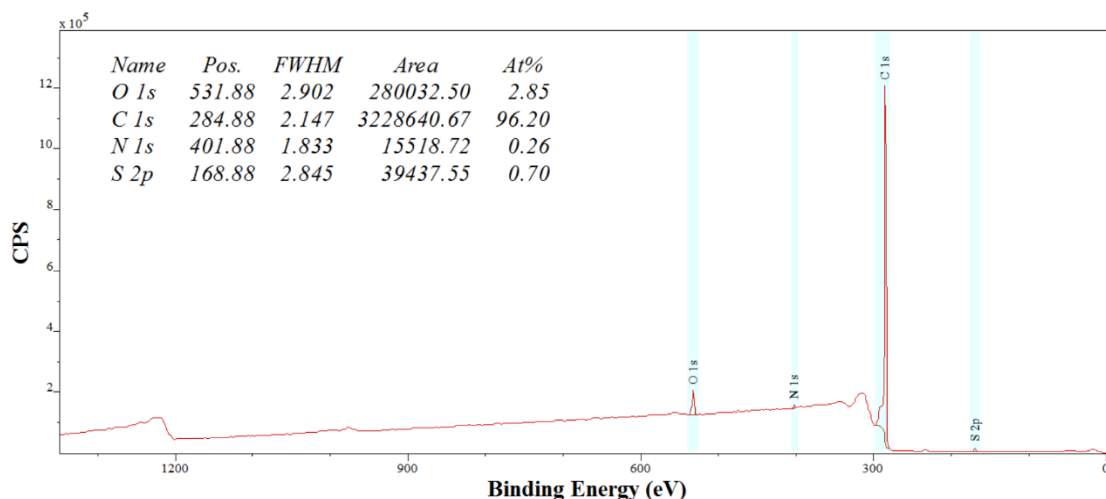


Figure 65 – Wide scan XPS spectra of 'H₂SO₄ (0.2M) – H_{Au}Cl₄ (2x10⁻⁶M)'

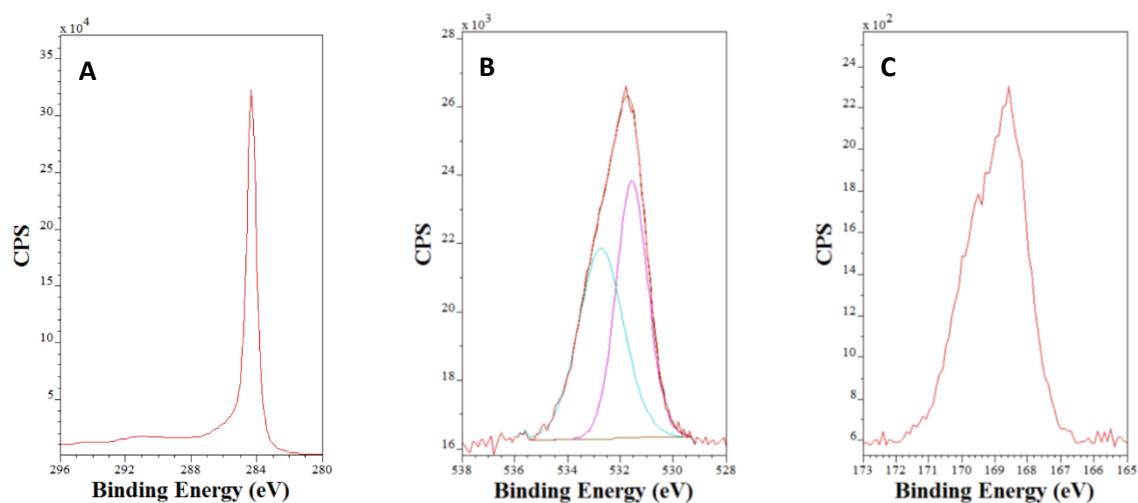


Figure 66 – Narrow scan XPS spectra of 'H₂SO₄ (0.2M), (A) C^{1s} narrow scan XPS spectra, (B) O^{1s} narrow scan XPS spectra, (C) S^{2p} narrow scan XPS spectra.

The oxygen peak shows a longer side at higher binding energies suggesting that a second oxygen peak exists there elongating it. The broad oxygen peak suggests that the sulfur exists on the surface as a sulfur oxide.

3.8.3 0.3M H₂SO₄ Treated HOPG

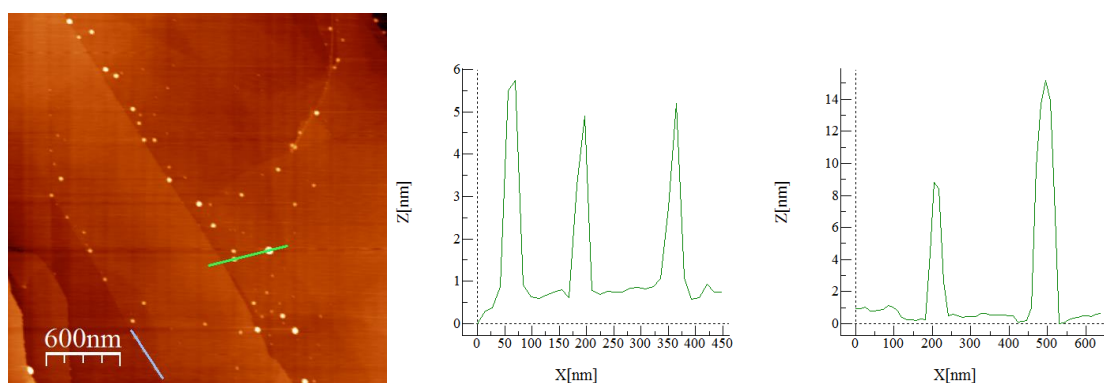


Figure 67 – 3.0x3.0 μm AFM image of 0.3M H₂SO₄ treated HOPG with line profile going from left to right. The grey line refers to the left profile and the green line the right profile.

The islands seen in the 3.0x3.0 μm image are fairly large and show a slight preference for step edges. This appears very similar to the 3.0x3.0 μm image of H₂SO₄ (0.1M), a closer 1.0x1.0 μm scan was not possible due to issues with the AFM apparatus.

Small Islands (X = 20 – 50 nm, Z = 2 – 10 nm)

Large Islands (X = 50 – 100 nm, Z = 10 – 15 nm)

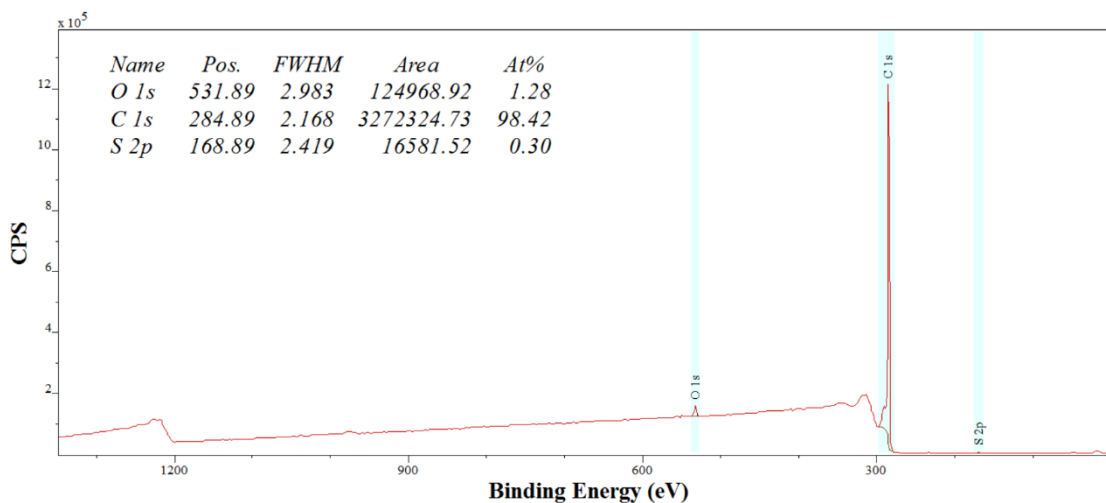


Figure 68 – Wide scan XPS spectra of 'H₂SO₄ (0.3M) – HAuCl₄ (2x10⁻⁶M)'

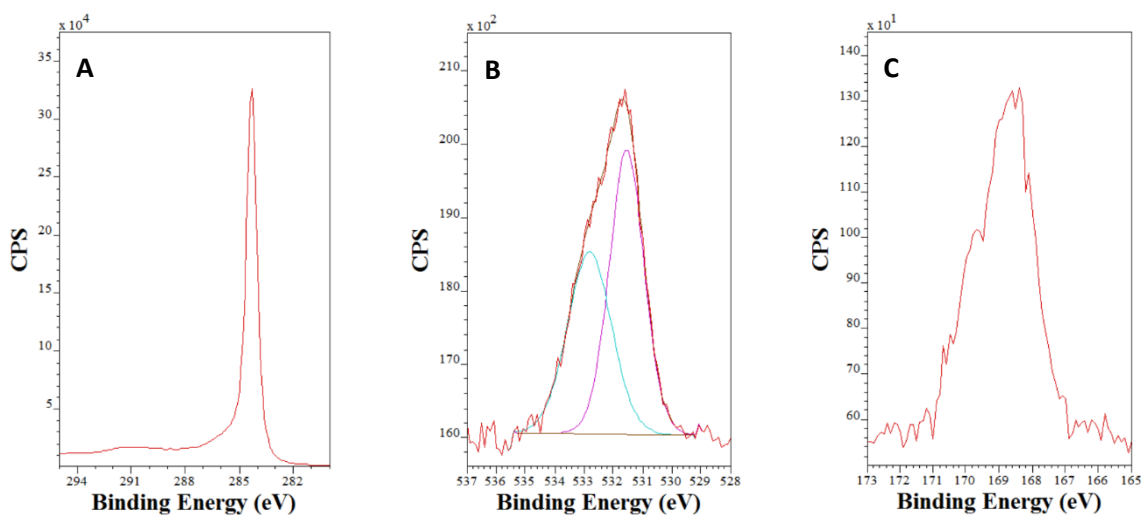


Figure 69 – Narrow scan XPS spectra of 'H₂SO₄ (0.3M), (A) C^{1s} narrow scan XPS spectra,' (B) O^{1s} narrow scan XPS spectra, (C) S^{2p} narrow scan XPS spectra.

XPS data shows a variation in the quantity of sulfur on the surface. The concentration of which does not correlate with increasing concentrations of H₂SO₄ used as shown in Figure 70. The narrow scan of the oxygen peaks suggest that two oxygen identities are present, this is clear from the elongated side of the Gaussian peak at higher energy. The two peaks shown in Figure 69(B) is a result of orbit splitting.

The identity of sulfur on the surface is very interesting as treatment of HOPG with nitric acid or hydrochloric acid does not incorporate detectable nitrogen or chlorine into the graphite structure.

Another major difference between samples treated with sulfuric acid in comparison to hydrochloric acid, nitric acid or aqua regia is the massive surface deformation that was visible under a microscope.

AFM images of H₂SO₄ treated HOPG shows very similar islands present in H₂SO₄ (0.1M) and H₂SO₄ (0.3M). This correlates with the nearly identical XPS data obtained for both samples. H₂SO₄ (0.2M) is the only sample that shows a deviation from this behaviour. AFM images show much larger islands present but a much lower island density seen. This difference in topology may explain the much larger sulfur peak witnessed in Figure 84.

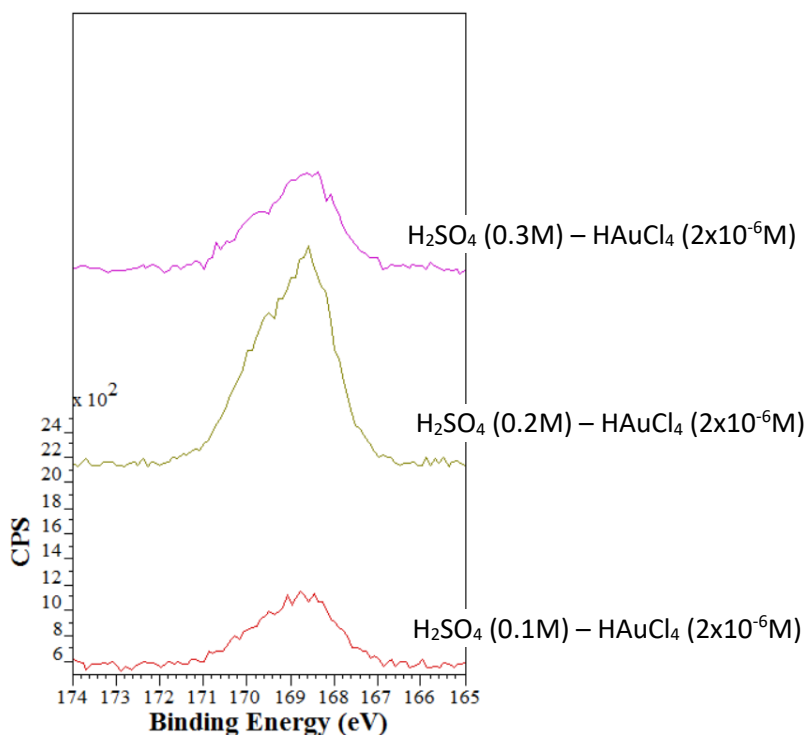


Figure 70 – Overlay of the narrow scan XPS spectra of S^{2p} peaks in H_2SO_4 Treated HOPG.

Sulfur was found present in all samples, this shows a very different mechanism for the reaction of HOPG through acid washing when using sulfuric acid as opposed to hydrochloric or nitric acid. Neither hydrochloric nor nitric acid treatment resulted in incorporation of the chloride or nitride anion. Sulfur peaks are broad suggesting two or more sulfur environments. These environments may possibly be due to the sulfate ion binding to the graphite through the sulfur atom in some instances and the oxygen atom in others.

H_2SO_4 Concentration	Ratio of O to S Atomic Percentages	Ratio of S to C Atomic Percentages
0.1M	7.4 : 1	0.0019
0.2M	4.1 : 1	0.007
0.3M	4.3 : 1	0.003

Table 5 - Ratio of O to S for different H_2SO_4 determined by atomic percentages in survey scans.

The data in **Error! Reference source not found.** shows that atomic percentages of O to S in 0.2M and 0.3M H_2SO_4 is close to 4:1 which fits with attachment of the sulphate anion SO_4^- being deposited on the surface, however from the ratio of S to C atomic percentages the amount of sulfur on the surface

decreases with increasing H_2SO_4 concentration showing that sulfuric acid treatment is not an effective way to introduce sulfur to the surface.

3.9 $H AuCl_4$ ($2 \times 10^{-6} \text{ mol dm}^{-3}$) Treatment of H_2SO_4 Treated HOPG

3.9.1 UPW – $H AuCl_4$ ($2 \times 10^{-6} M$)

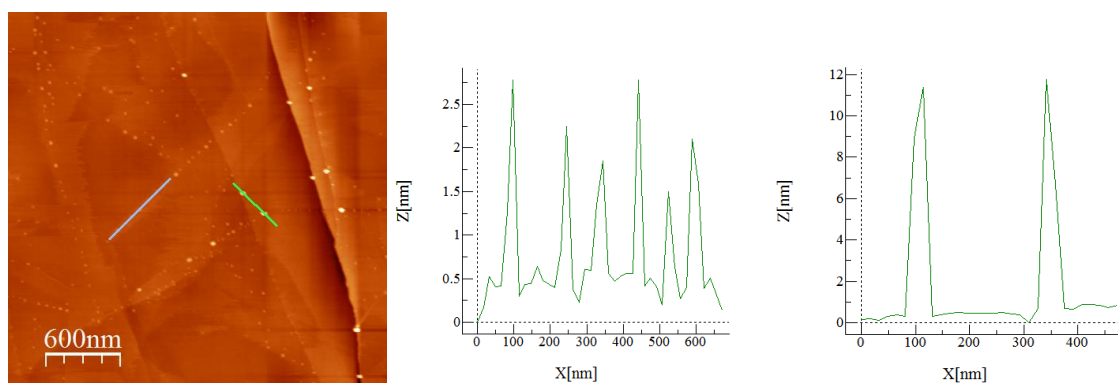


Figure 71 – $3.0 \times 3.0 \mu\text{m}$ AFM image of UPW – $H AuCl_4$ ($2 \times 10^{-6} M$) treated HOPG with line profile going from left to right. The grey line refers to the left line profile and the green line refers to the right profile.

As seen before, the AFM image of the standard UPW – $H AuCl_4$ shows small and numerous islands in a uniform distribution with a preference for step edges. The islands seen can be assumed to be gold aggregates as XPS indicates no strong signals for any other elements.

3.9.2 $2 \times 10^{-6} M H AuCl_4$ on $0.1 M H_2SO_4$ Treated HOPG

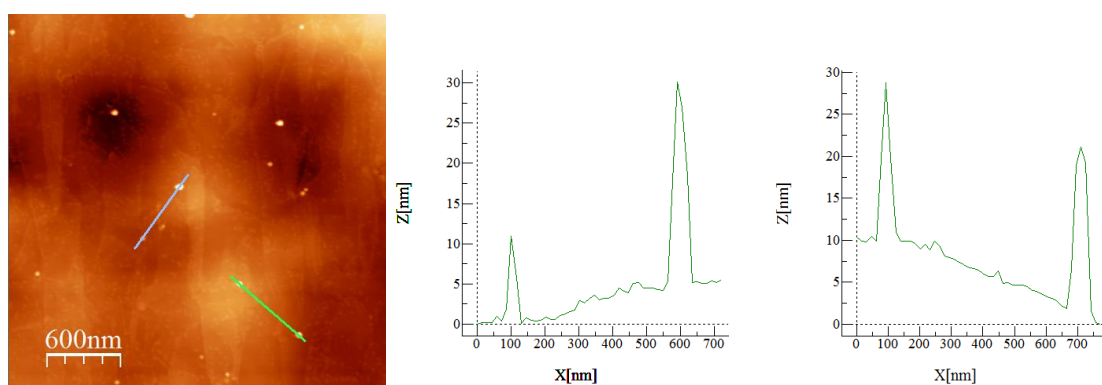


Figure 72 – $3.0 \times 3.0 \mu\text{m}$ AFM image of H_2SO_4 ($0.1 M$) – $H AuCl_4$ ($2 \times 10^{-6} M$) with line profile going from left to right. The grey line refers to the left profile and the green line the right profile.

Figure 21 shows a busy surface showing a significant change in the deposition of gold when using sulfuric acid to activate the graphite surface. A mixture of very large and very small islands can be seen in this image. Large islands look very similar in size and shape to HOPG samples treated solely

with H_2SO_4 and therefore are likely to be a graphite blister as opposed to gold aggregates. Gold aggregates are likely to be the very small islands that were not present in H_2SO_4 treated surfaces. These islands are too small to determine useful information at this scan size and therefore an image with a smaller scan size must be taken.

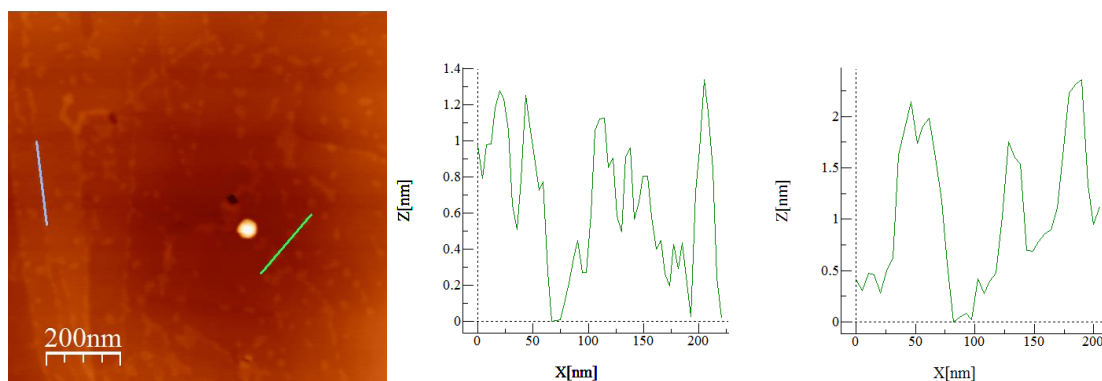


Figure 73 – $1.0 \times 1.0 \mu\text{m}$ AFM image of H_2SO_4 (0.1M) – HAuCl_4 ($2 \times 10^{-6}\text{M}$) with line profile going from left to right. The grey line refers to the left profile and goes from top left to bottom right and the green line refers to the right profile going from bottom left to top right.

The grey line in Figure 73 shows the gold aggregates along a step edge of the surface and the green line shows the gold aggregates across the bulk. Aggregates along step edges remain uniform in size and shape and are very small in size and appear to be some of the smallest gold islands imaged so far in this thesis. Islands across terraces appear to vary significantly in size and shape with few being hemispherical.

Small Islands ($X = 20 - 50 \text{ nm}$, $Z = 0.5 - 1.5 \text{ nm}$)

Large Islands ($X = 100 - 200 \text{ nm}$, $Z = 20 - 50 \text{ nm}$)

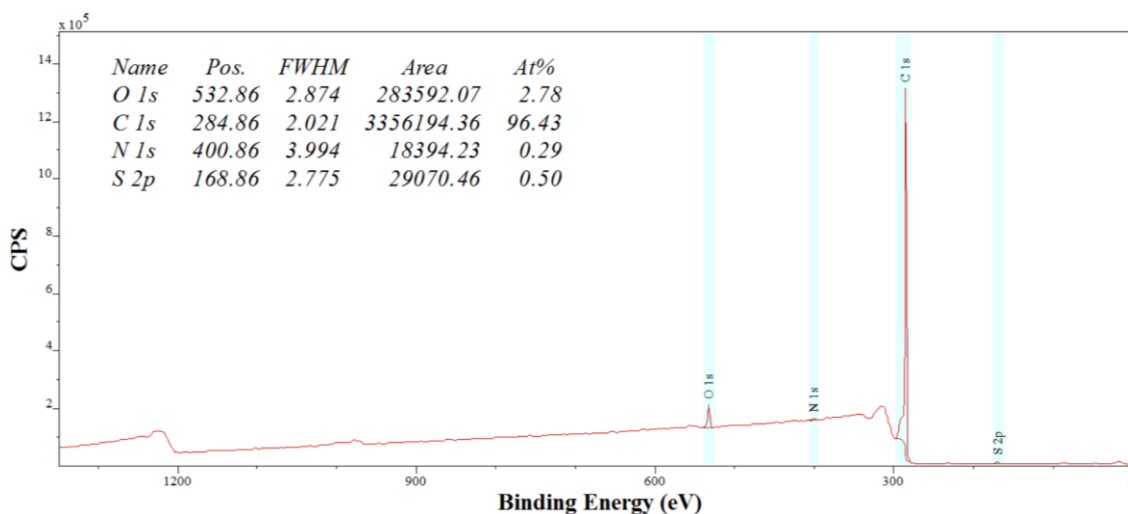


Figure 74 – Wide scan XPS spectra of ' H_2SO_4 (0.1M) – HAuCl_4 ($2 \times 10^{-6}\text{M}$)'

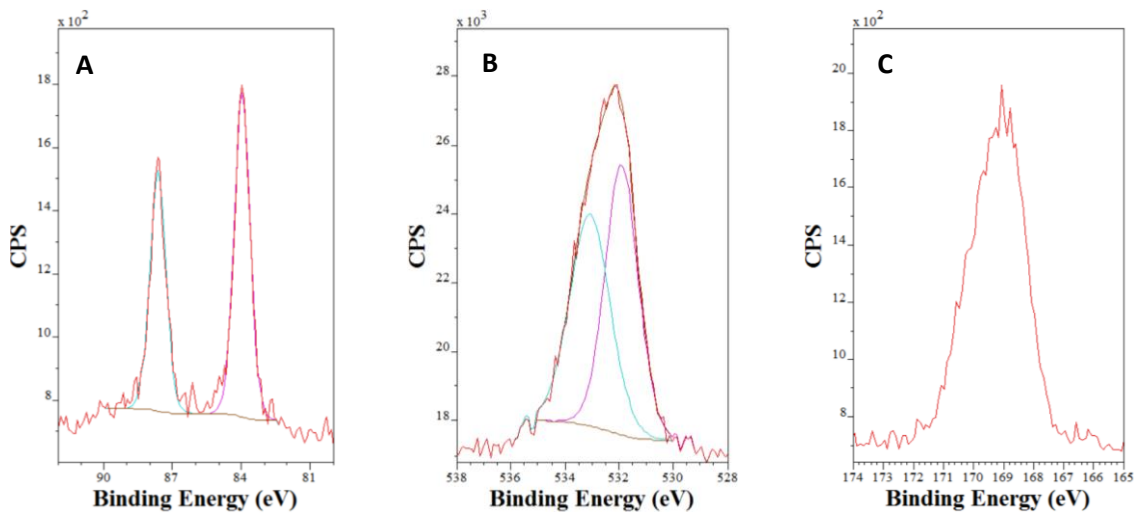


Figure 75 – Narrow scan XPS spectra of ‘H₂SO₄ (0.1M)’ where A is the Au^{4f} narrow scan, B is the O^{1s} narrow scan and C is the S^{2p} narrow scan.

3.9.3 2x10⁻⁶M HAuCl₄ on 0.2M H₂SO₄ Treated HOPG

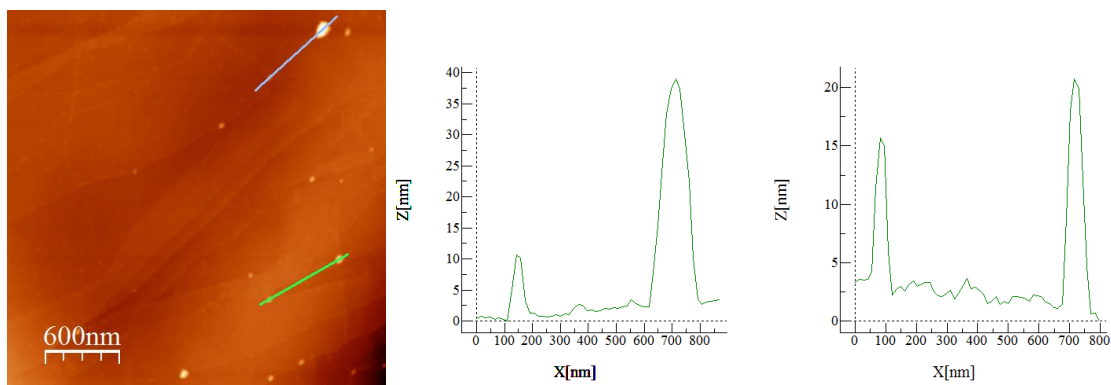


Figure 76 – 3.0x3.0μm AFM image of H₂SO₄ (0.2M) – HAuCl₄ (2x10⁻⁶M) with line profile going from bottom left to top right. The grey line refers to the left profile and the green line the right profile.

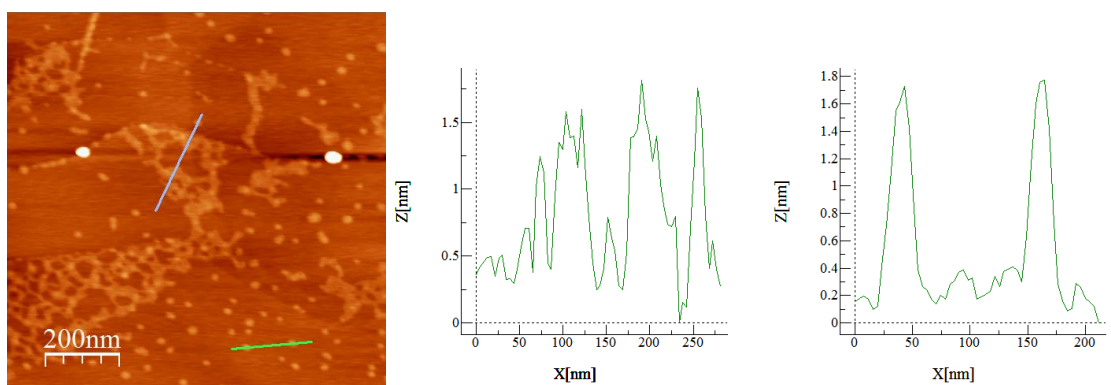


Figure 77 – 1.0x1.0μm AFM image of H₂SO₄ (0.2M) – HAuCl₄ (2x10⁻⁶M) with line profile going from bottom left to top right. The grey line refers to the left profile and the green line the right profile.

Figure 77 shows how the gold aggregates have coalesced into networks of gold islands. These networks often branch out from step edges onto terraces. Island shapes show poorly defined gold islands on the surface.

Small Islands (X = 30 – 50 nm, Z = 0.5 – 1.5 nm)

Large Islands (X = 50 – 70 nm, Z = 10 – 15 nm)

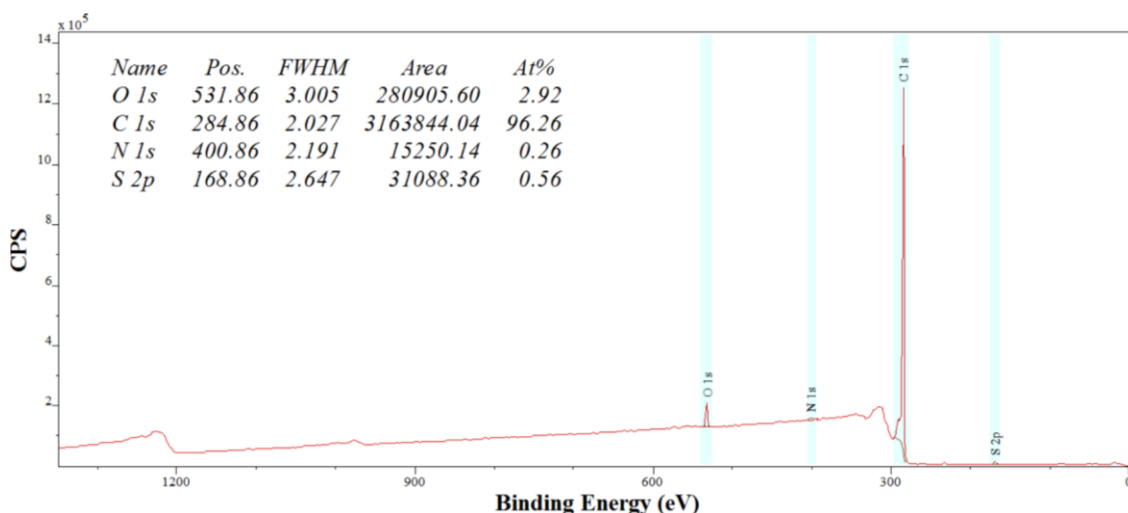


Figure 78 – Wide scan XPS spectra of 'H₂SO₄ (0.2M) – HAuCl₄ (2x10⁻⁶M)'

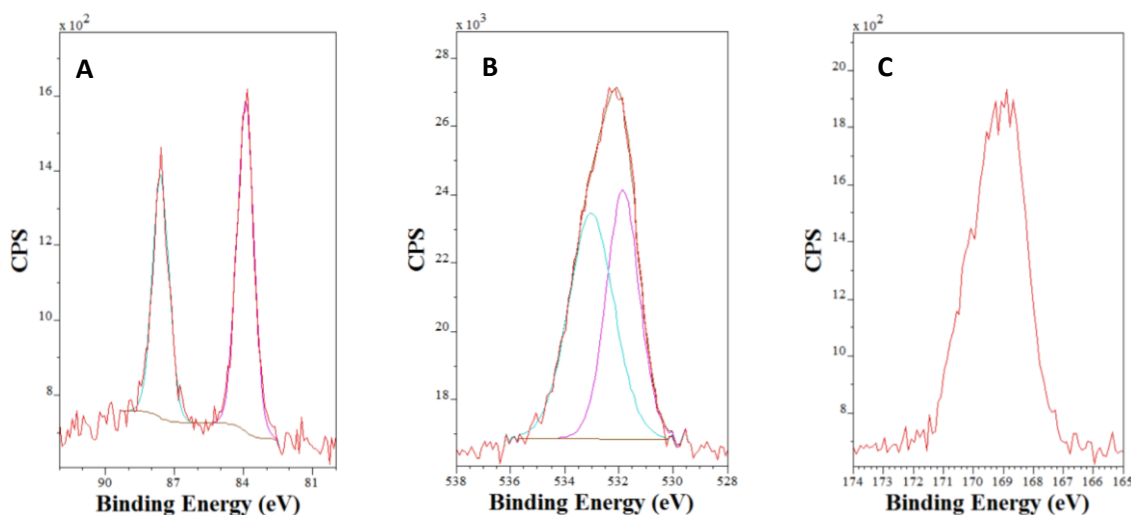


Figure 79 – Narrow scan XPS spectra of 'H₂SO₄ (0.2M) – HAuCl₄ (2x10⁻⁶M)' where A is the Au^{4f} narrow scan, B is the O^{1s} narrow scan and C is the S^{2p} narrow scan.

XPS data of 'H₂SO₄ (0.2M) – HAuCl₄ (2x10⁻⁶M)' shows very little difference in quantities of either nitrogen or sulfur incorporated into the sample. Au(0) is shown to be the only gold species present.

3.9.4 $2 \times 10^{-6} \text{M}$ HAuCl_4 on 0.3M H_2SO_4 Treated HOPG

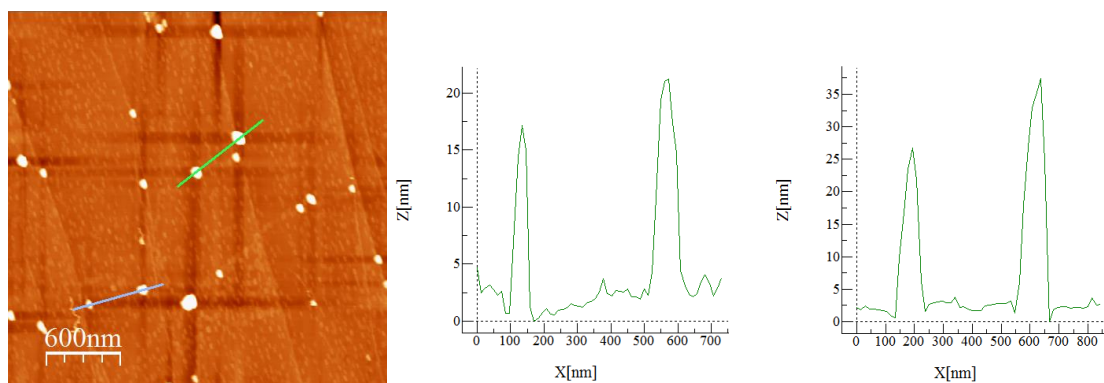


Figure 80 – $3.0 \times 3.0 \mu\text{m}$ AFM image of H_2SO_4 (0.3M) – HAuCl_4 ($2 \times 10^{-6} \text{M}$) with line profile going from bottom left to top right. The grey line refers to the left profile and the green line the right profile.

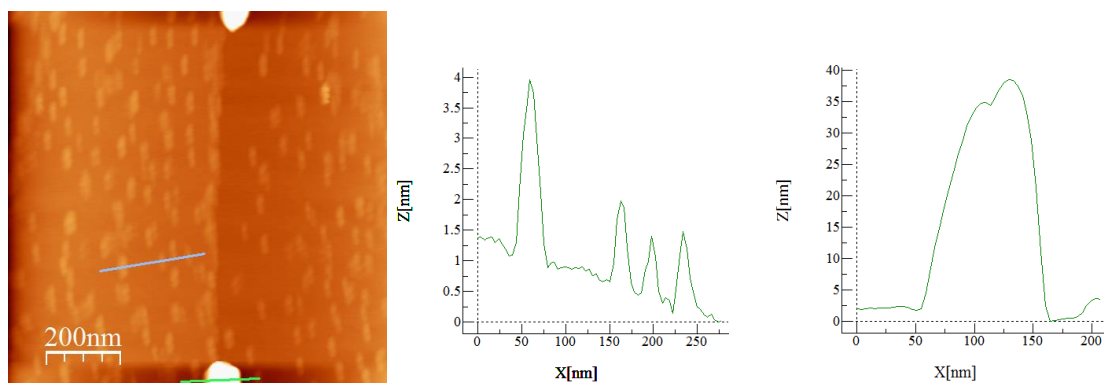


Figure 81 – $1.0 \times 1.0 \mu\text{m}$ AFM image of H_2SO_4 (0.3M) – HAuCl_4 ($2 \times 10^{-6} \text{M}$) with line profile going from bottom left to top right. The grey line refers to the left profile and the green line the right profile.

Issues with the AFM images obtained for ' H_2SO_4 (0.3M) – HAuCl_4 ($2 \times 10^{-6} \text{M}$)' can be seen by the small islands and their elongation. This is likely a result of a dirty or contaminated tip. This results in repeating shapes causing the elongated islands seen in Figure 81.

Small Islands ($X = 20 - 30 \text{ nm}$, $Z = 1 - 3 \text{ nm}$)

Large Islands ($X = 50 - 100 \text{ nm}$, $Z = 15 - 40 \text{ nm}$)

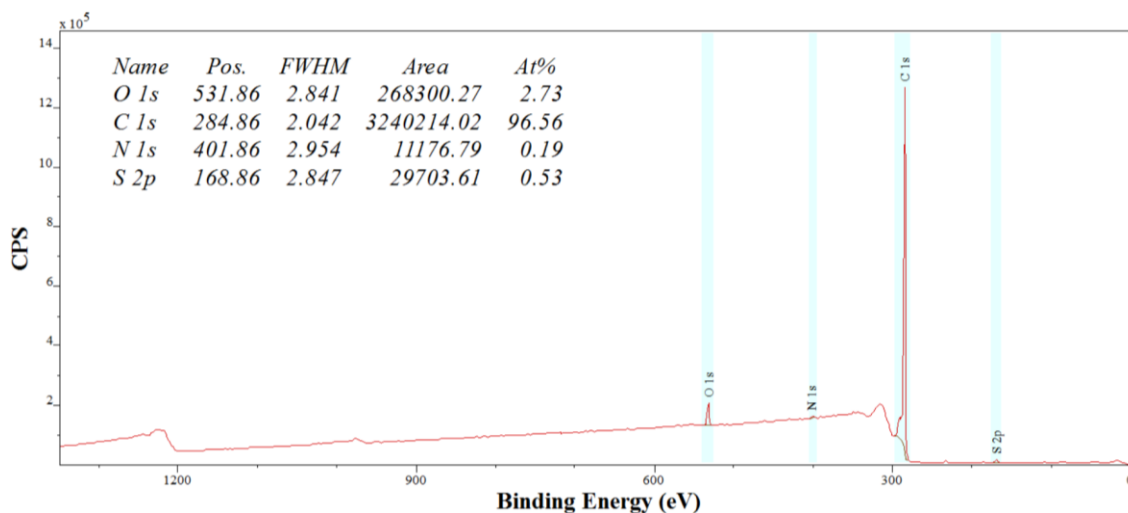


Figure 82 – Wide scan XPS spectra of ' H_2SO_4 (0.3M) – $HAuCl_4$ ($2 \times 10^{-6}M$)'

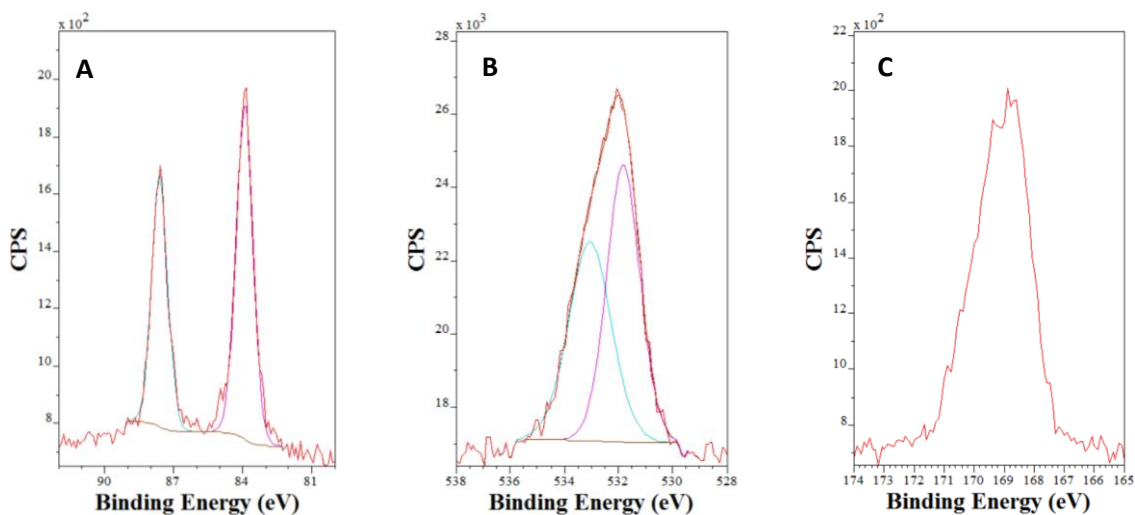


Figure 83 – Narrow scan XPS spectra of ' H_2SO_4 (0.3M) – $HAuCl_4$ ($2 \times 10^{-6}M$)' where A is the Au^{4f} narrow scan, B is the O^{1s} narrow scan and C is the S^{2p} narrow scan.

Wide scan XPS spectra shows the incorporation of both nitrogen and sulfur into the sample surface. Gold for all samples exists only in the form of Au(0) showing full reduction of Au(III) to Au(0).

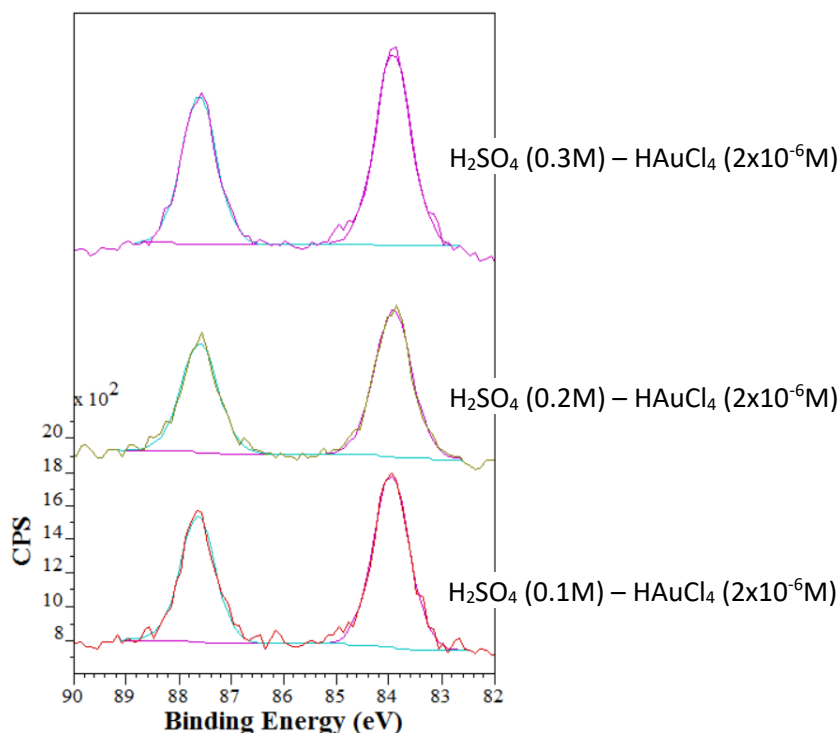


Figure 84 – Overlay of the narrow scan XPS spectra of Au^{4f} peaks in H₂SO₄ (2x10⁻⁶ moldm⁻³) Treatment of H₂SO₄ Treated HOPG.

Concentration of H ₂ SO ₄ (moldm ⁻³)	Concentration of Adsorbate on the Surface.
0.1M	$\sigma_{Au(0)} = 1.59 \times 10^{14} \text{ atoms/cm}^2$
0.2M	$\sigma_{Au(0)} = 1.44 \times 10^{14} \text{ atoms/cm}^2$
0.3M	$\sigma_{Au(0)} = 1.80 \times 10^{14} \text{ atoms/cm}^2$

Table 6 – data showing the coverage of gold on the surface of HOPG activated with H₂SO₄ before treatment with H₂SO₄ determined using the peak areas of the synthetic components of the Au_{4f} peaks.

Quantities of gold formed on the surface after activation with dilute H₂SO₄ were equal to the quantities of gold deposited on the surface of medium to high concentrations of HNO₃ and aqua regia (0.1M & 2.0M) the difference in concentration of the H₂SO₄ and HNO₃/AR used for activation to produce the same quantity of gold on the surface is roughly a magnitude of 10. This along with the large surface deformations shown in H₂SO₄ activated HOPG suggests a much more vigorous reaction occurring on the surface during activation.

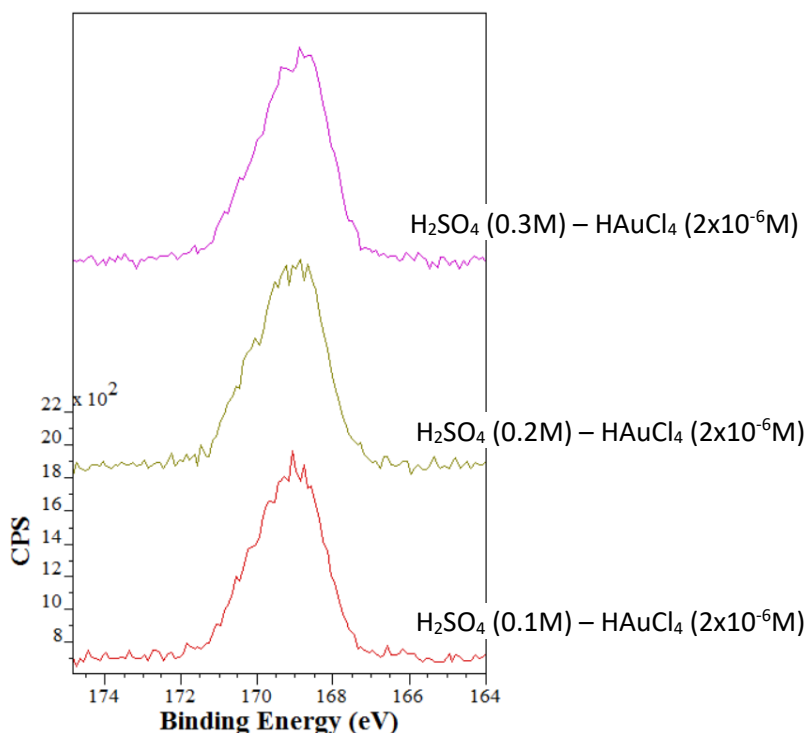


Figure 85 – Overlay of the narrow scan XPS spectra of S^{2p} peaks in $HAuCl_4$ (2×10^{-6} $mol\ dm^{-3}$) Treatment of H_2SO_4 Treated HOPG.

H_2SO_4 Concentration	Ratio of O to S Atomic Percentages	Ratio of S to C Atomic Percentages
0.1M	5.6 : 1	0.052
0.2M	5.2 : 1	0.058
0.3M	5.2 : 1	0.055

Table 7 - Ratio of O to S for different H_2SO_4 determined by atomic percentages in survey scans

The overlay data in Figure 84 and Figure 85 shows no clear increase in the quantities of gold or sulfur in the samples respectively. The ratio of S to C atomic percentages were taken to show a quantitative example of how sulfur doesn't change with increasing H_2SO_4 as shown in Table 7.. The ratio of sulfur to oxygen shows an increase from that seen in Table 5 suggesting that chloroauric acid has introduced oxygen groups onto the surface in addition to the sulphate ions. The wide breadth of the sulfur peaks show varying identities of the sulfur groups, this suggests that the sulphate ions probably bind to the surface through both the sulfur and oxygen groups.

3.10 Effect of H₂SO₄ on the bulk of HOPG

After data was obtained for graphite surfaces treated with H₂SO₄. The surfaces were stripped and treated with HNO₃ for a repeat experiment of HNO₃ treated HOPG. These samples were then analysed by XPS and it was found that sulfur was still present in all samples as shown below. Many of these samples were stripped multiple times with adhesive tape in an attempt to produce a clean surface. The wide scan XPS spectra of the samples showed the presence of sulfur, as such further narrow scan spectra were obtained and shown in Figure 86.

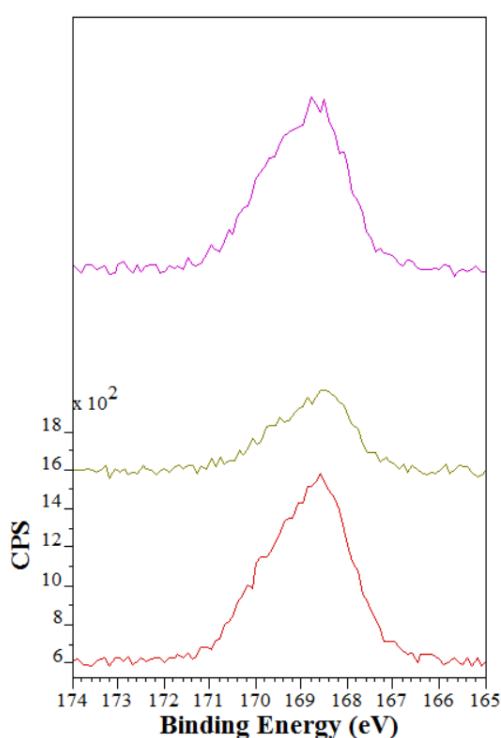


Figure 86 – Overlay of the narrow scan XPS spectra of S_{2p} peaks in HNO₃ treated HOPG after stripping of HAuCl₄ ($2 \times 10^{-6} \text{ mol dm}^{-3}$) Treatment of H₂SO₄ Treated HOPG

Unfortunately, it is not known which HAuCl₄ ($2 \times 10^{-6} \text{ mol dm}^{-3}$) treatment of H₂SO₄ treated HOPG samples were used. That combined with the different extents of stripping with adhesive tape meant that quantitative information of sulfur on the surface cannot be determined. However this data does confirm that sulfur penetrates through the surface layers and into the bulk of the sample. This prompted the concept that if sulfuric acid was able to penetrate deep into the graphite structure, then it is possible that gold atoms or even small gold particles may be able to permeate through the holes created by the sulfuric acid and become incorporated into the graphite structure. As such a narrow scan XP spectrum of Au^{4f} was also obtained and is shown in Figure 87. However, no gold was found in the sample. This suggests that the holes created by sulfuric acid treatment are too small for

gold atoms to pass through, or that all gold has reacted with the higher layers of the sample. However, the cleaning process did involve a very thorough stripping of the surface layers and therefore it is entirely possible that gold did penetrate into the sample but not deep enough to still be seen.

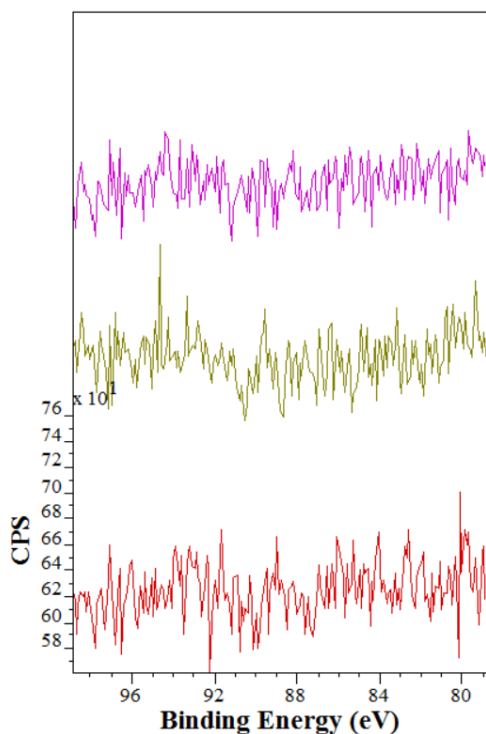


Figure 87 – Overlay of the narrow scan XPS spectra of Au^{4f} peaks in HNO₃ treated HOPG after stripping of HAuCl₄ ($2 \times 10^{-6} \text{ mol dm}^{-3}$) Treatment of H₂SO₄ Treated HOPG

3.11 H₂SO₄ & HAuCl₄ ($2 \times 10^{-6} \text{ mol dm}^{-3}$) Solution Treatment of HOPG

HOPG samples were treated with 100 μl of different concentrations of H₂SO₄ mixed with HAuCl₄ ($2 \times 10^{-6} \text{ mol dm}^{-3}$) in UPW for 30 minutes. These samples were then blow dried under a clean Helium stream for 1 minute. This was done to observe how simultaneous treatment of H₂SO₄ and HAuCl₄ compares to HOPG surfaces treated step by step, first by sulfuric acid followed by chloroauric acid. AFM and XPS studies of these surfaces were done to observe the changes in the quantity, dispersion and oxidation states of gold deposits on the surface.

All samples were prepared in exactly the same way but with a change in the concentration of H₂SO₄ being used for treatment of the HOPG. Samples are labelled as follows.

H₂SO₄ (0.1M)/HAuCl₄ ($2 \times 10^{-6} \text{ M}$)

H₂SO₄ (0.2M)/HAuCl₄ ($2 \times 10^{-6} \text{ M}$)

H₂SO₄ (0.3M)/HAuCl₄ (2x10⁻⁶M)

3.11.1 H₂SO₄ (0.1 moldm⁻³) & HAuCl₄ (2x10⁻⁶ moldm⁻³) Solution Treatment of HOPG

H₂SO₄ (0.1M)/HAuCl₄ (2x10⁻⁶M)

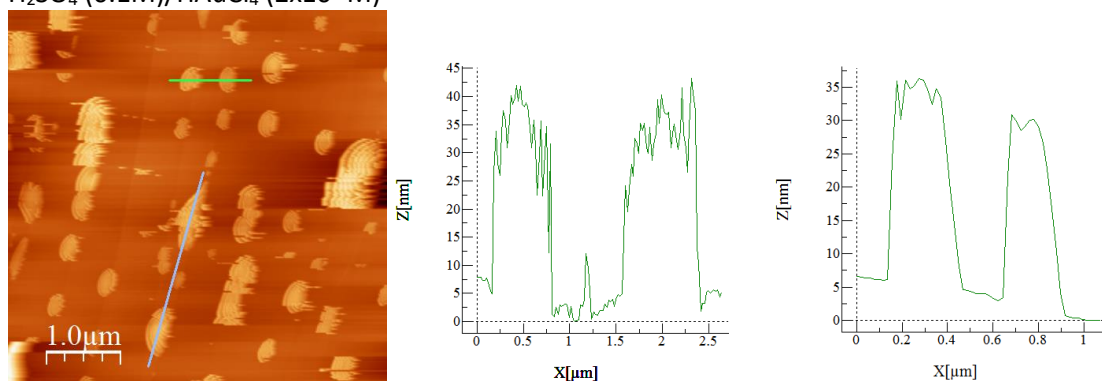


Figure 88 – 5.0x5.0μm AFM image of H₂SO₄ (0.1M)/HAuCl₄ (2x10⁻⁶M) with line profile going from bottom left to top right. The grey line refers to the left profile and the green line the right profile.

Islands shown in Figure 88 are of much larger size than those shown in samples treated step by step with sulfuric acid followed by chloroauric acid. The extent of surface deformation was on a macroscopic scale and whilst these deformations couldn't be seen by the naked eye, they could be seen under a microscope. This microscope was attached to a video camera that was viewed on a monitor and a photo taken from the monitor. This photo is shown in Figure 89.

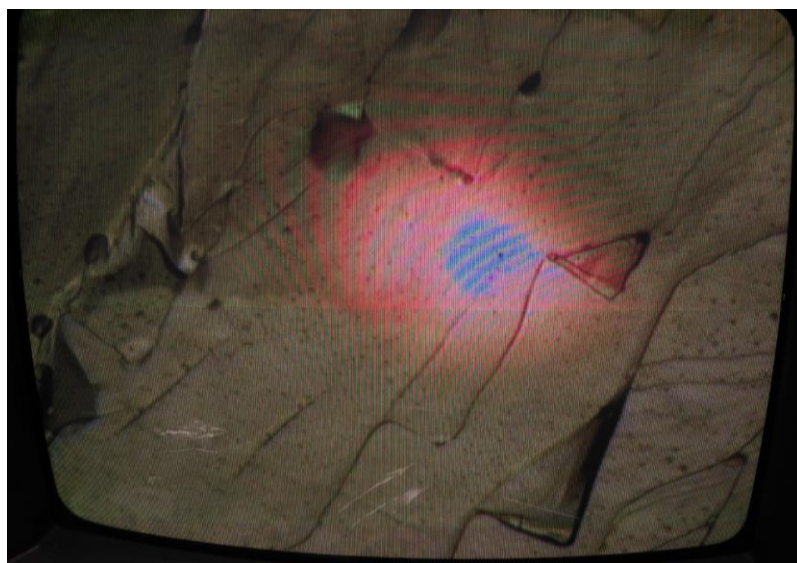


Figure 89 – Photograph of H₂SO₄ (0.1M)/HAuCl₄ (2x10⁻⁶M) as imaged under a x10 microscope.

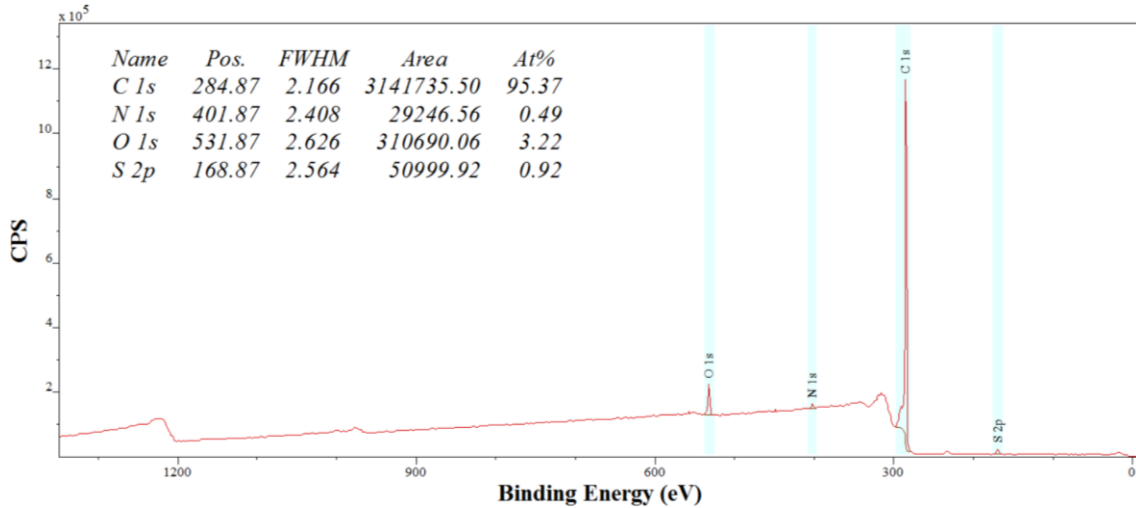


Figure 90 – Wide scan XPS spectra of 'H₂SO₄ (0.1M)/HAuCl₄ (2x10⁻⁶M)'

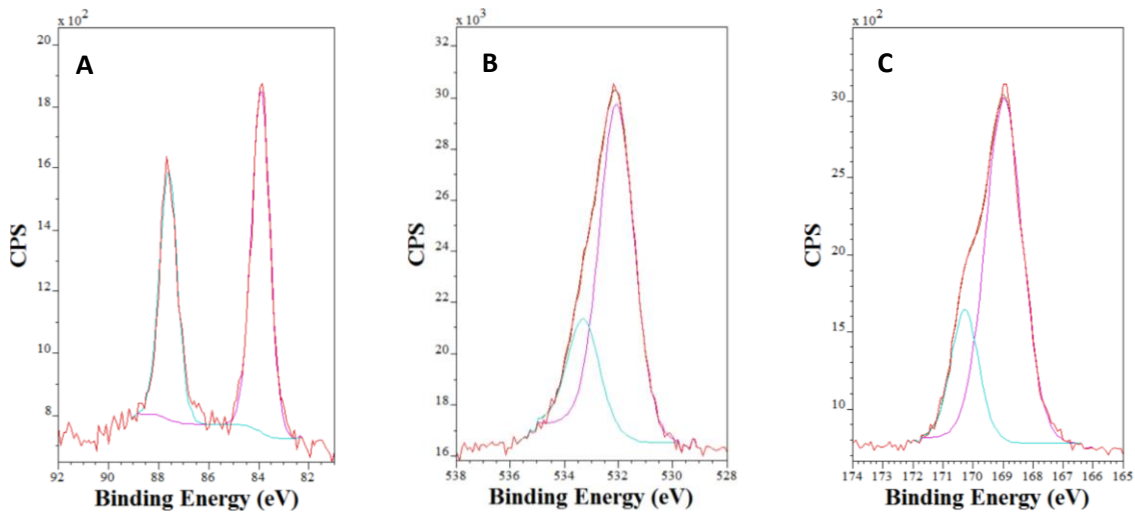


Figure 91 – Narrow scan XPS spectra of 'H₂SO₄ (0.1M)/HAuCl₄ (2x10⁻⁶M)' where A is the Au^{4f} narrow scan, B is the O^{1s} narrow scan and C is the S^{2p} narrow scan.

3.11.2 H₂SO₄ (0.2 moldm⁻³) & HAuCl₄ (2x10⁻⁶ moldm⁻³) Solution Treatment of HOPG

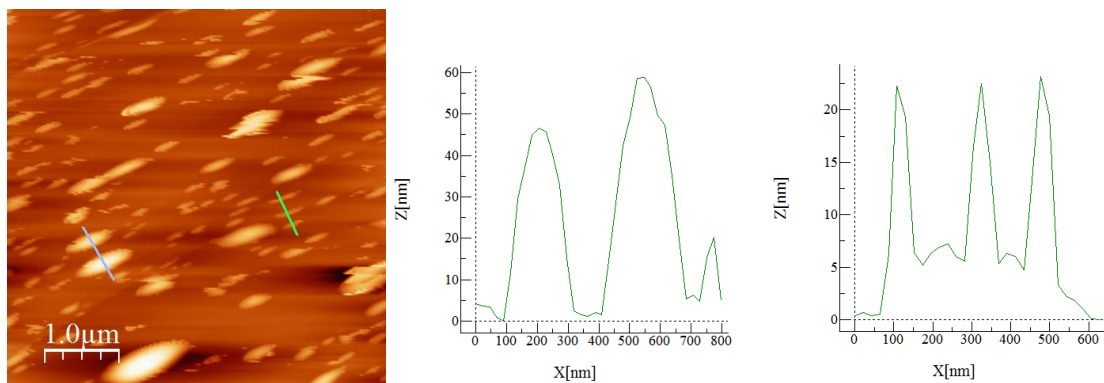


Figure 92 – 5.0x5.0μm AFM image of H₂SO₄ (0.2M)/HAuCl₄ (2x10⁻⁶M) with line profile going from top left to bottom right. The grey line refers to the left profile and the green line the right profile.

Islands shown in Figure 92 are again of much larger size than those shown in samples treated step by step with sulfuric acid followed by chloroauric acid. The extent of surface deformation was on a macroscopic scale and whilst these deformations couldn't be seen by the naked eye, they could be seen under a microscope. Whilst the best effort was made to obtain a clear AFM image on the clearest parts of the sample, islands were too large for the AFM tips high sensitivity causing uncontrolled tip deflections and image drift.

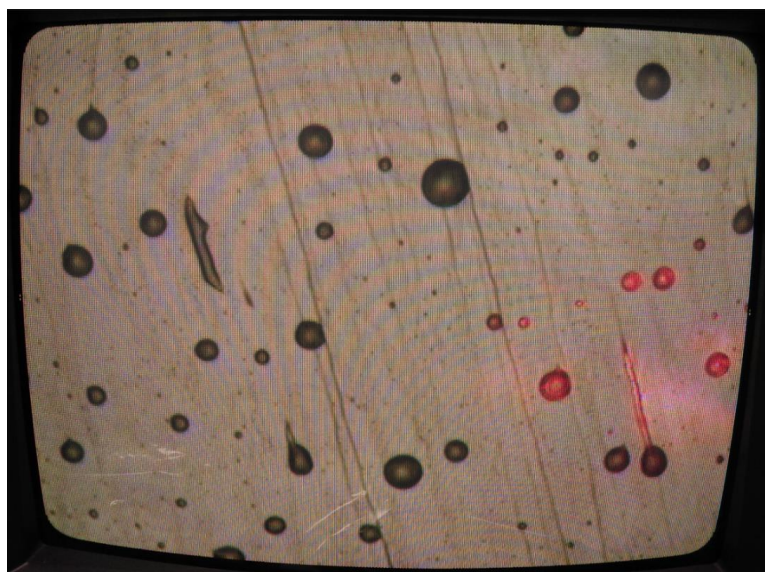


Figure 93 – Photograph of H_2SO_4 (0.1M)/ $HAuCl_4$ ($2 \times 10^{-6}M$) as imaged under a $\times 10$ microscope.

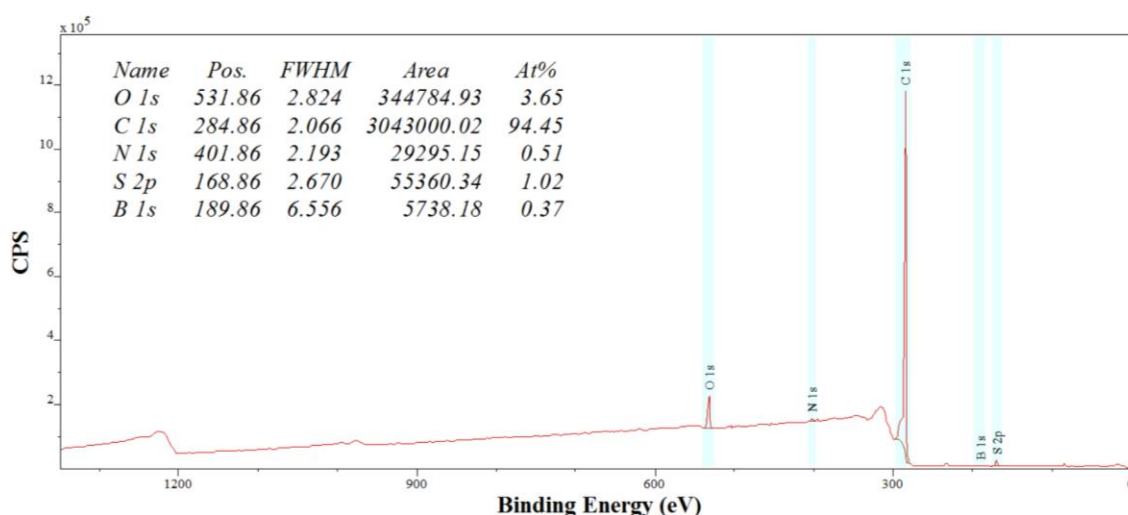


Figure 94 – Wide scan XPS spectra of ' H_2SO_4 (0.2M)/ $HAuCl_4$ ($2 \times 10^{-6}M$)'

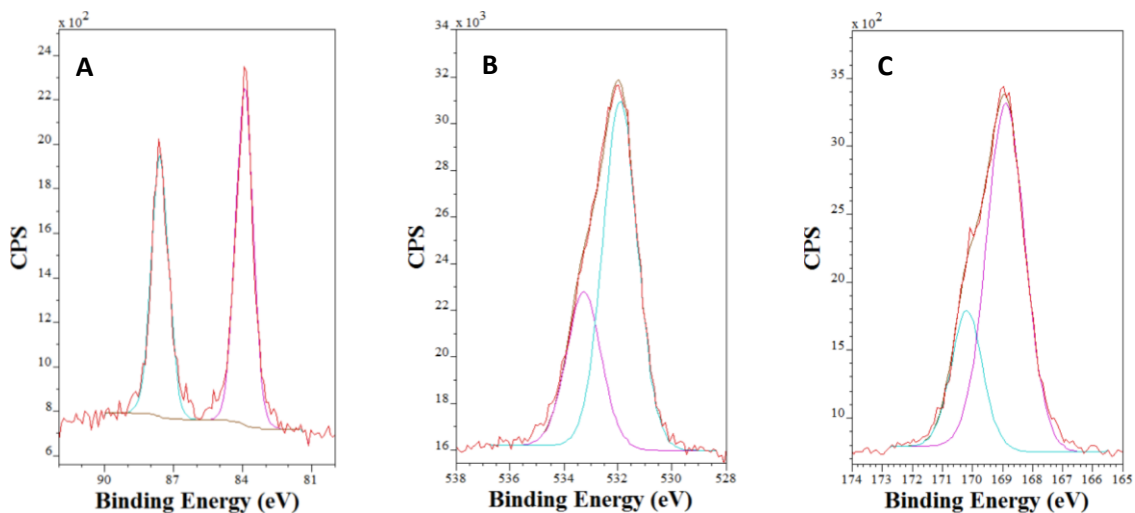


Figure 95 – Narrow scan XPS spectra of ‘ H_2SO_4 (0.2M)/ $HAuCl_4$ ($2 \times 10^{-6}M$)’ where A is the Au^{4f} narrow scan, B is the O^{1s} narrow scan and C is the S^{2p} narrow scan.

3.11.3 H_2SO_4 (0.3 moldm^{-3}) & $HAuCl_4$ ($2 \times 10^{-6} \text{ moldm}^{-3}$) Solution Treatment of HOPG

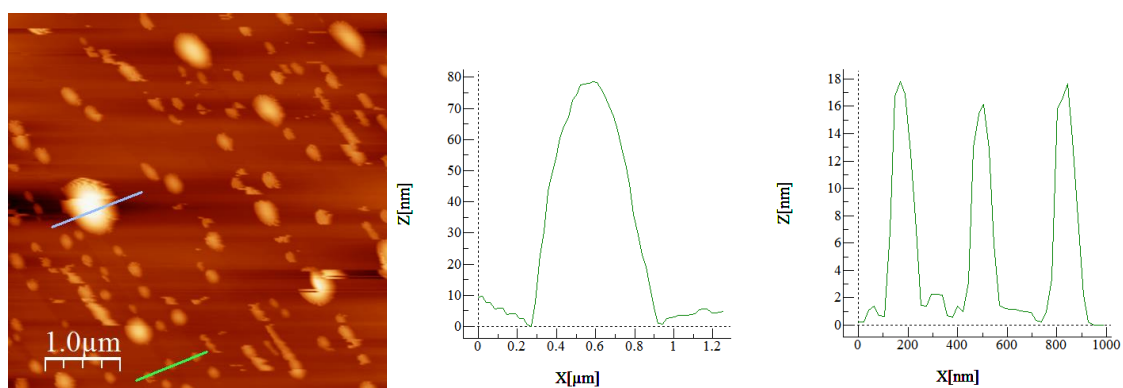


Figure 96 – $5.0 \times 5.0 \mu m$ AFM image of H_2SO_4 (0.3M)/ $HAuCl_4$ ($2 \times 10^{-6}M$) with line profile going from bottom left to top right. The grey line refers to the left profile and the green line the right profile.

Islands shown in Figure 96 have very large diameters, following the pattern of increasing island size when treating surfaces with a mixture of sulfuric acid and chloroauric acid then those treated step by step with sulfuric acid followed by chloroauric acid. The extent of surface deformation was on a macroscopic scale and whilst these deformations couldn't be seen by the naked eye, they could be seen under a microscope. Despite the large surface deformation, a clear AFM image was able to be obtained and island sizes can be considered accurate.

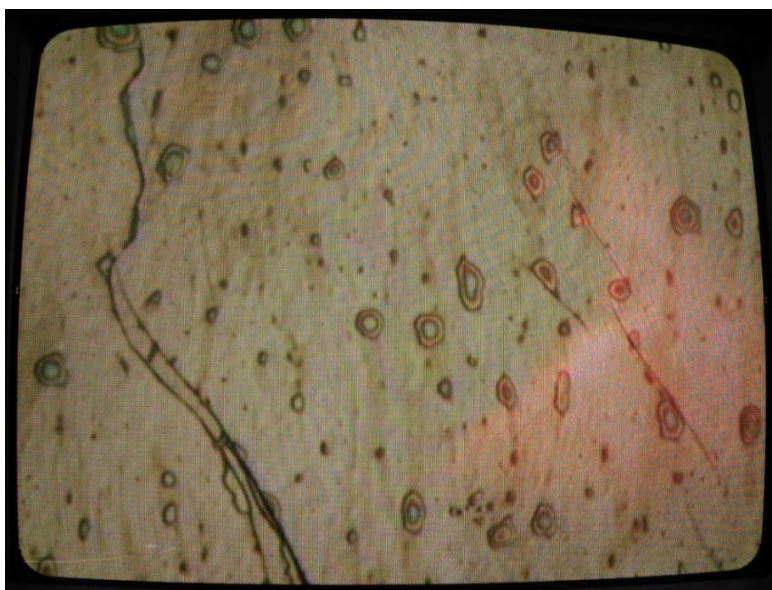


Figure 97 – Photograph of H_2SO_4 (0.1M)/ $HAuCl_4$ ($2 \times 10^{-6}M$) as imaged under a $\times 10$ microscope.

Figure 97 shows the macroscopic deformations that occur upon treatment with a mixture of chloroauric acid and sulfuric acid. This higher sulfuric acid concentration has created small rings around the large deformations.

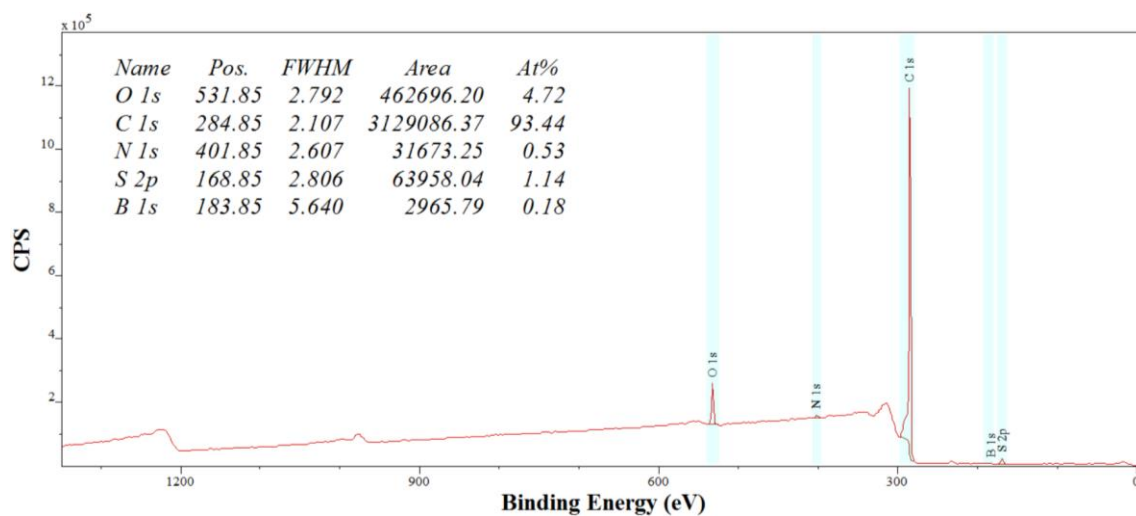


Figure 98 – Wide scan XPS spectra of ' H_2SO_4 (0.3M)/ $HAuCl_4$ ($2 \times 10^{-6}M$)'

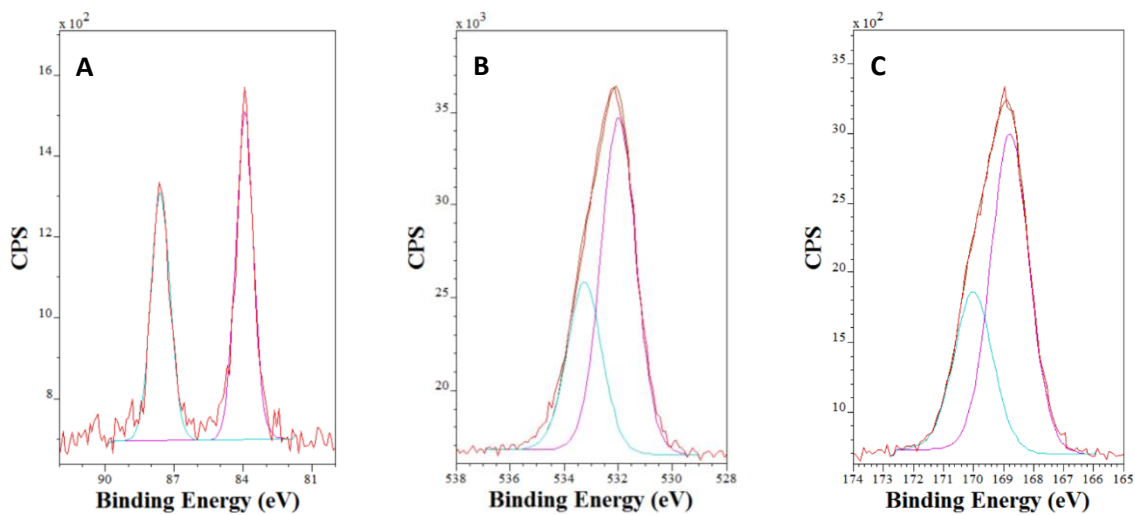


Figure 99 – Narrow scan XPS spectra of ‘ H_2SO_4 (0.2M)/ HAuCl_4 ($2 \times 10^{-6}\text{M}$)’ where A is the Au^{4f} narrow scan, B is the O^{1s} narrow scan and C is the S^{2p} narrow scan.

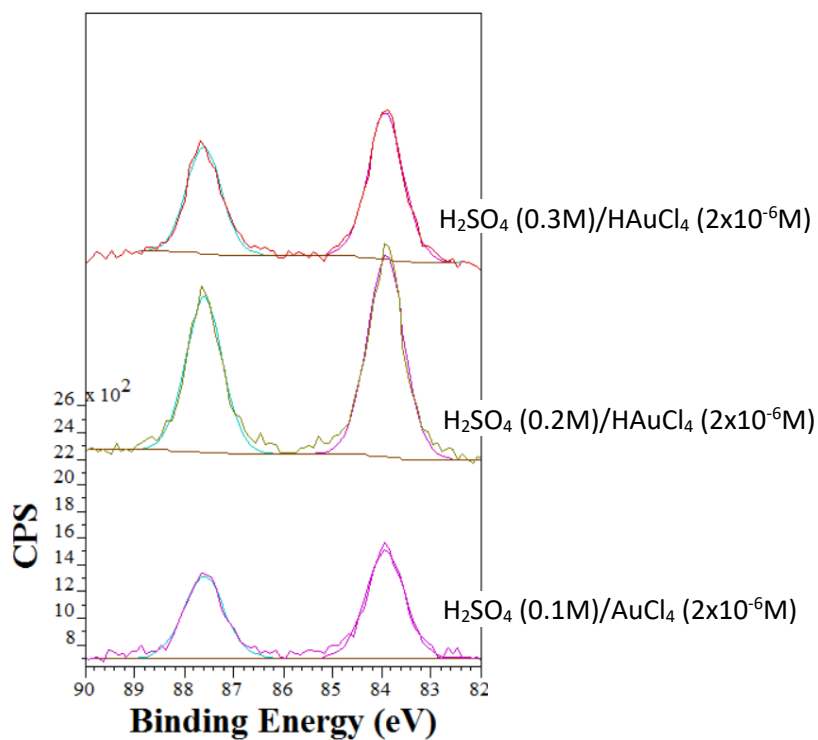


Figure 100 – Overlay of the narrow scan XPS spectra of Au^{4f} peaks in $\text{H}_2\text{SO}_4/\text{HAuCl}_4$ treated HOPG.

<i>Concentration of H₂SO₄ in (mol dm⁻³)</i>	<i>Concentration of Au(0) on the Surface of H₂SO₄ Treated Surfaces.</i>	<i>Concentration of Au(0) on the Surface of HOPG Treated with a Solution of H₂SO₄ & H₂AuCl₄.</i>
0.1M	$\sigma_{Au(0)} = 1.59 \times 10^{14} \text{ atoms/cm}^2$	$\sigma_{Au(0)} = 1.97 \times 10^{14} \text{ atoms/cm}^2$
0.2M	$\sigma_{Au(0)} = 1.44 \times 10^{14} \text{ atoms/cm}^2$	$\sigma_{Au(0)} = 2.75 \times 10^{14} \text{ atoms/cm}^2$
0.3M	$\sigma_{Au(0)} = 1.80 \times 10^{14} \text{ atoms/cm}^2$	$\sigma_{Au(0)} = 1.48 \times 10^{14} \text{ atoms/cm}^2$

Table 8 – data showing the coverage of gold on the surface of HOPG activated with H₂SO₄ before treatment with H₂AuCl₄ (H₂SO₄ – H₂AuCl₄) and coverage of gold on the surface of simultaneous acid activation and gold deposition (H₂SO₄/H₂AuCl₄)

Gold treatment involving a mixture of H₂SO₄ and H₂AuCl₄ created a very different sample surface to surfaces treated step by step with H₂SO₄ followed by H₂AuCl₄. The samples that involved a combination of acid activation and gold treatment simultaneously created much larger islands on the surface and much larger surface deformations that were visible on a microscope. This suggests a very different mechanism between the solution and the surface in simultaneous treatment.

Despite the different XPS data between the concentrations of H₂SO₄ used and the concentration of gold on the surface as shown in Figure 100 there is no correlation and no clear change in the quantities of Au(0) deposited between samples activated with H₂SO₄ and treated with H₂AuCl₄ step-by-step or simultaneously as shown in Table 8.

4 Conclusion

AFM images of HNO₃ treated surfaces showed an increase in the size of blisters on the surface of graphite with an increasing concentration of HNO₃. XPS results showed no significant change in the concentration of oxygen groups from HNO₃ treated surfaces to surfaces treated with UPW. As discovered by R Burgess[46] these oxygen groups were identified as hydroxyl groups however in this study only 0.5M HNO₃ was used and there is therefore the potential for these oxygen groups to vary with treatment with the higher concentrations of nitric acid used. Because of the breadth of the oxygen peaks, a further study involving fluorinating acid treated surfaces with fluorine containing molecules that interact specifically with one type of oxygen functionality is the only method to identify the exact identity of the oxygen functionalities on either nitric acid or aqua regia treated surfaces. XPS peak fitting results show that only one side of the O^{1s} peak increases in size significantly with increasing HNO₃ concentration. This suggests that one type of oxygen functionality remains constant whilst other oxygen functionalities increase in concentration. The different binding energies (BE) of different oxygen functionalities are as follows hydroxyl BE = 532.8 eV, Ketone BE = 532 eV, Ether BE = 533.3 eV. Because of the two oxygens present in carboxylic acid groups, any O1s peak components present from carboxylic acid would span the breadth of the binding energies unless strong resonance occurs.[67]

HAuCl₄ treatment of HNO₃ activated HOPG resulted in very little gold deposition on the surface when using low concentrations of nitric acid or no nitric acid. At nitric acid concentrations of 1.0M or higher there is a large increase in the quantities of gold on the surface. In particular Au(0) (84.0 eV), this suggests that the hydroxyls found on the surface of HNO₃ treated surfaces cause a reduction of the gold from Au(III) (86.0 eV) to Au(0). At nitric acid concentrations of 1.0M to 5.0M the concentration of Au(III) increases significantly and Au(0) concentrations decrease. This supports the conclusions from Figure 31 'overlay narrow scan O1s XPS spectra of nitric acid treated HOPG,' which shows that at high concentrations of nitric acid, hydroxyls become oxidized further to ketone and ether groups. These oxygen groups lack the reductive potential to reduce Au(III) to Au(0) and instead are likely to create an ion-dipole bond with the Au(III) ions showing the increase in the presence of Au(III) with increasing HNO₃ concentrations.

In aqua regia treated samples selective derivatization was conducted to determine if there are any change in the identities of the oxygen groups on the surface. There was no clear change in the concentration of hydroxyl groups with increasing concentrations of aqua regia used. However there was a large increase in the amount of ketone present, showing a clear change in the chemistry of the surface due to aqua regia activation. The F1s peak area in samples selectively derivatised with TFH is

directly proportional to the concentration of ketone groups on the surface. The increase in ketone concentration is likely a result of the oxidising ability of higher concentrations of aqua regia treatment. It also explains why AFM images showed very little change in the topography of the surface, studies done on heated hydrochloric acid treated surfaces showed a decrease in the number of islands formed upon heating and an increase in the quantity of ketone groups observed through selective derivatization.[47] This study supports the observation that increasing numbers of ketone groups result in a flattening of the surface, or that the change from HO groups to C=O groups decreases the number of islands.

After determining that treating HOPG with increasing concentrations of aqua regia resulted in increasing quantities of ketone groups, gold treatment was conducted on these samples to determine how the increased concentration of ketone groups may affect gold deposition. These samples showed increasing concentrations of Au(0) with increasing concentrations of aqua regia. The Au(0) forms in small islands and shows a high preference for step edges over terraces. This is a result of Au(III) being reduced to Au(0) by oxidizing surface hydroxyl groups to ketone groups. The change of hydroxyl groups on graphite to ketone has previously been seen through heating graphite samples treated with 0.5 M nitric acid.[46] Beyond 1.0 M aqua regia the quantity of Au(0) remains constant but further quantities of gold are deposited as Au(III). At higher concentrations of aqua regia activation the number of hydroxyl groups on the surface was shown to remain constant but an increase in ketone groups was shown. This suggests that ketone groups result in the deposition of Au(III) and hydroxyl groups results in the deposition of Au(0).

The effect of heat treatment on aqua regia activated surfaces and its effect on gold deposition was studied. The main difference in the XPS of AR-Heat-HAuCl₄ compared with the XPS of AR-HAuCl₄ is the decrease in the amount of Au seen and the smaller increases in the concentration of Au on the surface with increasing concentrations of aqua regia. This suggests that the numbers of functional groups introduced on the surface may have decreased upon heating possibly due to thermal decomposition or delamination of the surface layers on the graphite. With a disproportionate amount of deactivation occurring to the more heavily activated samples (higher aqua regia treated samples).

Sulfuric acid activated samples showed sulfur present in all samples, this shows a very different mechanism for the reaction of HOPG through acid washing when using sulfuric acid as opposed to hydrochloric or nitric acid. Neither hydrochloric nor nitric acid treatment resulted in incorporation of the chloride or nitride anion. Sulfur peaks are broad suggesting two or more sulfur environments.

These environments may possibly be due to the sulphate ion binding to the graphite through the sulfur atom in some instances and the oxygen atom in others.

Samples treated with HAuCl_4 after activation with dilute H_2SO_4 showed equal quantities of gold deposited between samples. The total amount of gold deposited when using H_2SO_4 was greater in almost all samples to the amount of gold deposited when using 10x the concentration of nitric or hydrochloric acid. This along with the large surface deformations in H_2SO_4 activated HOPG suggests a much more vigorous reaction occurring on the surface during activation.

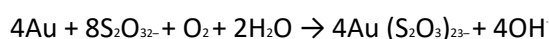
When attempting to do further studies on HNO_3 treated surfaces the samples activated with H_2SO_4 before treatment with HAuCl_4 were cleaned with adhesive tape multiple times to create a brand new surface for activation with HNO_3 . When XPS data was collected sulfur was found on the surface suggesting that sulfur was able to penetrate deep into the bulk of the sample during activation by sulfuric acid. A narrow scan XPS spectra was obtained for Au^{4f} but no gold was discovered suggesting that the holes created by sulfuric acid were not large enough for gold to penetrate into the bulk of the sample.

Gold treatment involving a mixture of H_2SO_4 and HAuCl_4 created a very different sample surface to surfaces treated step by step with H_2SO_4 followed by HAuCl_4 . The samples that involved a combination of acid activation and gold treatment simultaneously created much larger islands on the surface and much larger surface deformations that were visible on a microscope. This suggests a very different mechanism between the solution and the surface in simultaneous treatment. But despite the different mechanism on the surface there was no clear change in the quantities or charge of the Au.

5 Further Work

The activation of graphite substrates to create effective catalysts has potential when looking at thiosulfate leaching which removes gold from gold bearing ores. Thiosulfate leaching is a process that has many advantages over cyanide leaching which is currently used such as lower toxicity and greater efficiency with gold deposits associated with preg-robbing ores.

The leaching process involves a chemical reaction between metallic gold and the thiosulfate anion using oxygen as the oxidant and ammonium and copper ions as unconsumed catalysts in the reaction. A suggested scheme for the overall reaction is presented below.



The gold thiosulfate complex is very poorly adsorbed by activated carbon, negating the use of the traditional carbon-in-pulp (CIP) or carbon-in-leach (CIL) processes for the recovery of gold directly from leach pulps. This provides an opportunity to determine if different methods of carbon activation can create stronger bonds with the gold thiosulfate complex. TPD can be used to determine the bond strength of the gold thiosulfate complex on the activated graphite surface.[69]

When nanoparticles of palladium are spread out on a surface such as graphite, palladium forms a versatile catalyst; palladium on carbon catalysts are used for catalytic hydrogenation in organic synthesis such as reductive amination[70], carbonyl reduction, nitro compound reduction and the reduction of imines and Schiff bases.[71] When palladium is dispersed on conductive materials such as graphite it becomes a great electro catalyst for the oxidation of primary alcohol in alkaline media.[72]

Palladium (II) chloride is a common starting material in palladium chemistry and is soluble in ultra-pure water. As such a solution of PdCl₂ in UPW can be drop treated onto acid activated HOPG for determination of how the different functional groups determined in this thesis effect the deposition and ionisation states Pd nanoparticles on the surface.

In order to investigate the different ways gold bonds to the different functional groups on acid treated graphite. IR spectroscopy and Raman spectroscopic studies could be conducted, however HOPG crystals do not provide a large enough surface area to provide a high enough concentration of functional groups for adequate detection. Performing acid treatment and attaching gold to graphite powders could provide the required surface area for IR and Raman investigation. The determination of metal bonding to oxidized graphite powders has been used in the study of ozone modified graphite bonding with lithium. IR treatment of graphite powders oxidised using O₃/O₂ flow was used to create a variety of oxygen-containing groups on the graphite surface such as ozonides, carboxylic

acid and epoxy groups and IR spectroscopy was able to determine the formation –COLi and –COOLi groups after treated with LiOH. This shows the potential of using ozone to create different functional groups and attaching gold to these samples [73]

Because of the wide varieties of oxygen functionalities that can be introduced onto the surface of graphite, there is scope for continued research into using different methods of oxidising the surface. These oxidation groups need to be identified and their effect on the adsorption of catalytically active metals determined. This provides the potential for a wide variety of different treatments to further study the interactions between different metal nanoparticles and these surface functionalities and their effect on the nucleation, stability and the chemistry of the metal nanoparticles on the surface.

6 References

- [1] G. C. Bond, *Heterogeneous Catalysis - Principles and Applications*, Second. Clarendon Press Oxford, 1987.
- [2] 'Wiley: Concepts of Modern Catalysis and Kinetics, 2nd, Revised and Enlarged Edition - I. Chorkendorff, J. W. Niemantsverdriet'. [Online]. Available: <http://eu.wiley.com/WileyCDA/WileyTitle/productCd-3527316728.html>. [Accessed: 15-Jul-2016].
- [3] E. Schwab, 'Lehrbuch der Katalyse: Fundamentals of Industrial Catalytic Processes', *Nachrichten aus Chemie*, vol. 46, no. 10, pp. 988–988, Apr. 2010.
- [4] 'Wiley: Introduction to Surface Chemistry and Catalysis, 2nd Edition - Gabor A. Somorjai, Yimin Li'. [Online]. Available: <http://eu.wiley.com/WileyCDA/WileyTitle/productCd-047050823X.html>. [Accessed: 15-Jul-2016].
- [5] C. G. Bond, C. Louis, and Thompson D. T., *Catalysis by Gold*, vol. 6. Imperial College Press.
- [6] M. Nič, J. Jiráč, B. Košata, A. Jenkins, and A. McNaught, Eds., *IUPAC Compendium of Chemical Terminology: Gold Book*, 2.1.0. Research Triangle Park, NC: IUPAC, 2009.
- [7] M. Bowker, *The Basis and Applications of Heterogeneous Catalysis*. Oxford University Press, 1998.
- [8] 'Wiley: Principles and Practice of Heterogeneous Catalysis - John Meurig Thomas, W. John Thomas'. [Online]. Available: <http://eu.wiley.com/WileyCDA/WileyTitle/productCd-352729239X.html>. [Accessed: 15-Jul-2016].
- [9] G. C. Bond, *Principles of Catalysis*, Second. The Chemical Society, 1972.
- [10] M. P. Seah and W. A. Dench, 'Quantitative electron spectroscopy of surfaces: A standard data base for electron inelastic mean free paths in solids', *Surf. Interface Anal.*, vol. 1, no. 1, pp. 2–11, Feb. 1979.
- [11] M. Haruta, S. Tsubota, T. Kobayashi, H. Kageyama, M. J. Genet, and B. Delmon, 'Low-Temperature Oxidation of CO over Gold Supported on TiO₂, α -Fe₂O₃, and Co₃O₄', *Journal of Catalysis*, vol. 144, no. 1, pp. 175–192, Nov. 1993.
- [12] M. Haruta, 'Size- and support-dependency in the catalysis of gold', *Catalysis Today*, vol. 36, no. 1, pp. 153–166, Apr. 1997.
- [13] M. Valden, X. Lai, and D. W. Goodman, 'Onset of Catalytic Activity of Gold Clusters on Titania with the Appearance of Nonmetallic Properties', *Science*, vol. 281, no. 5383, pp. 1647–1650, Sep. 1998.
- [14] M. Valden, S. Pak, X. Lai, and D. W. Goodman, 'Structure sensitivity of CO oxidation over model Au/TiO₂ catalysts', *Catalysis Letters*, vol. 56, no. 1, pp. 7–10.
- [15] S.-J. Lee and A. Gavriilidis, 'Supported Au Catalysts for Low-Temperature CO Oxidation Prepared by Impregnation', *Journal of Catalysis*, vol. 206, no. 2, pp. 305–313, Mar. 2002.
- [16] M. Haruta, 'Catalysis of Gold Nanoparticles Deposited on Metal Oxides', *CATTECH*, vol. 6, no. 3, pp. 102–115, Jun. 2002.
- [17] M. Haruta and M. Daté, 'Advances in the catalysis of Au nanoparticles', *Applied Catalysis A: General*, vol. 222, no. 1–2, pp. 427–437, Dec. 2001.
- [18] L. Kesavan *et al.*, 'Solvent-Free Oxidation of Primary Carbon-Hydrogen Bonds in Toluene Using Au-Pd Alloy Nanoparticles', *Science*, vol. 331, no. 6014, pp. 195–199, Jan. 2011.
- [19] V. A. Bondzie, S. C. Parker, and C. T. Campbell, 'The kinetics of CO oxidation by adsorbed oxygen on well-defined gold particles on TiO₂(110)', *Catalysis Letters*, vol. 63, no. 3–4, pp. 143–151.
- [20] C. Lemire, R. Meyer, S. Shaikhutdinov, and H.-J. Freund, 'Do Quantum Size Effects Control CO Adsorption on Gold Nanoparticles?', *Angewandte Chemie International Edition*, vol. 43, no. 1, pp. 118–121, Jan. 2004.
- [21] N. Lopez, 'On the origin of the catalytic activity of gold nanoparticles for low-temperature CO oxidation', *Journal of Catalysis*, vol. 223, no. 1, pp. 232–235, Apr. 2004.

- [22] R. Zanella, 'Characterization and reactivity in CO oxidation of gold nanoparticles supported on TiO₂ prepared by deposition-precipitation with NaOH and urea', *Journal of Catalysis*, vol. 222, no. 2, pp. 357–367, Mar. 2004.
- [23] A. Sanchez *et al.*, 'When Gold Is Not Noble: Nanoscale Gold Catalysts', *The Journal of Physical Chemistry A*, vol. 103, no. 48, pp. 9573–9578, Dec. 1999.
- [24] J. Guzman and B. C. Gates, 'Simultaneous Presence of Cationic and Reduced Gold in Functioning MgO-Supported CO Oxidation Catalysts: Evidence from X-ray Absorption Spectroscopy', *The Journal of Physical Chemistry B*, vol. 106, no. 31, pp. 7659–7665, Aug. 2002.
- [25] Q. Fu, 'Active Nonmetallic Au and Pt Species on Ceria-Based Water-Gas Shift Catalysts', *Science*, vol. 301, no. 5635, pp. 935–938, Aug. 2003.
- [26] D. T. Thompson and G. C. Bond, 'Catalysis by Gold', *Catalysis Reviews*, vol. 41, no. 3–4, pp. 319–388, Jan. 1999.
- [27] G. C. Bond, 'The origins of particle size effects in heterogeneous catalysis', *Surface Science*, vol. 156, pp. 966–981, Jun. 1985.
- [28] J. R. Anderson, *Structure of metallic catalysts*. London; New York: Academic Press, 1975.
- [29] P. Johnston, N. Carthey, and G. J. Hutchings, 'Discovery, Development, and Commercialization of Gold Catalysts for Acetylene Hydrochlorination', *J. Am. Chem. Soc.*, vol. 137, no. 46, pp. 14548–14557, Nov. 2015.
- [30] G. Hutchings and D. Grady, 'Effect of Drying Conditions on Carbon Supported Mercuric-Chloride Catalysts', *Applied Catalysis*, vol. 16, no. 3, pp. 411–415, 1985.
- [31] G. Hutchings and D. Grady, 'Hydrochlorination of Acetylene - the Effect of Mercuric-Chloride Concentration on Catalyst Life', *Applied Catalysis*, vol. 17, no. 1, pp. 155–160, 1985.
- [32] K. Shinoda, 'The Vapor-Phase Hydrochlorination of Acetylene Over Metal Chlorides Supported on Activated Carbon', *Chemistry Letters*, vol. 4, no. 3, pp. 219–220, 1975.
- [33] G. J. Hutchings, 'Vapor phase hydrochlorination of acetylene: Correlation of catalytic activity of supported metal chloride catalysts', *Journal of Catalysis*, vol. 96, no. 1, pp. 292–295, Nov. 1985.
- [34] B. Nkosi, N. J. Coville, and G. J. Hutchings, 'Vapour phase hydrochlorination of acetylene with group VIII and IB metal chloride catalysts', *Applied Catalysis*, vol. 43, no. 1, pp. 33–39, Jan. 1988.
- [35] G. Qin, Y. Song, R. Jin, J. Shi, Z. Yu, and S. Cao, 'Gas-liquid acetylene hydrochlorination under nonmercuric catalysis using ionic liquids as reaction media', *Green Chem.*, vol. 13, no. 6, pp. 1495–1498, Jun. 2011.
- [36] G. J. Hutchings, 'Catalysis: A golden future', *Gold Bull*, vol. 29, no. 4, pp. 123–130, Dec. 1996.
- [37] L.-F. Gutiérrez, S. Hamoudi, and K. Belkacemi, 'Synthesis of Gold Catalysts Supported on Mesoporous Silica Materials: Recent Developments', *Catalysts*, vol. 1, no. 1, pp. 97–154, Dec. 2011.
- [38] B. Nkosi, M. D. Adams, N. J. Coville, and G. J. Hutchings, 'Hydrochlorination of acetylene using carbon-supported gold catalysts: A study of catalyst reactivation', *Journal of Catalysis*, vol. 128, no. 2, pp. 378–386, Apr. 1991.
- [39] M. Conte, A. F. Carley, and G. J. Hutchings, 'Reactivation of a Carbon-supported Gold Catalyst for the Hydrochlorination of Acetylene', *Catal Lett*, vol. 124, no. 3–4, pp. 165–167, Aug. 2008.
- [40] F. Rodriguez-Reinoso, 'The role of carbon materials in heterogeneous catalysis', *Carbon*, vol. 36, no. 3, pp. 159–175, 1998.
- [41] J. L. Figueiredo and J. A. Moulijn, Eds., *Carbon and Coal Gasification*. Dordrecht: Springer Netherlands, 1986.
- [42] H. L. David Appy, 'Transition metals on the (0 0 0 1) surface of graphite: Fundamental aspects of adsorption, diffusion, and morphology', *Progress in Surface Science*, vol. 89, no. s 3–4, pp. 219–238, 2014.
- [43] E. Bouleghlimat, P. R. Davies, R. J. Davies, R. Howarth, J. Kulhavy, and D. J. Morgan, 'The effect of acid treatment on the surface chemistry and topography of graphite', *Carbon*, vol. 61, pp. 124–133, Sep. 2013.

- [44] P. Albers, K. Deller, B. M. Despeyroux, G. Prescher, A. Schafer, and K. Seibold, 'SIMS/XPS Investigations on Activated Carbon Catalyst Supports', *Journal of Catalysis*, vol. 150, no. 2, pp. 368–375, Dec. 1994.
- [45] S. Wang and G. Q. (Max) Lu, 'Effects of acidic treatments on the pore and surface properties of Ni catalyst supported on activated carbon', *Carbon*, vol. 36, no. 3, pp. 283–292, 1998.
- [46] R. Burgess *et al.*, 'The functionalisation of graphite surfaces with nitric acid: Identification of functional groups and their effects on gold deposition', *Journal of Catalysis*, vol. 323, pp. 10–18, Mar. 2015.
- [47] C. Buono *et al.*, 'Spectroscopic and atomic force studies of the functionalisation of carbon surfaces: new insights into the role of the surface topography and specific chemical states', *Faraday Discuss.*, vol. 173, pp. 257–272, 2014.
- [48] G. Binnig, C. F. Quate, and C. Gerber, 'Atomic Force Microscope', *Phys. Rev. Lett.*, vol. 56, no. 9, pp. 930–933, Mar. 1986.
- [49] Z. Ma and F. Zaera, 'Heterogeneous Catalysis by Metals', in *Encyclopedia of Inorganic and Bioinorganic Chemistry*, John Wiley & Sons, Ltd, 2011.
- [50] I. Horcas, R. Fernández, J. M. Gómez-Rodríguez, J. Colchero, J. Gómez-Herrero, and A. M. Baro, 'WSXM: A software for scanning probe microscopy and a tool for nanotechnology', *Review of Scientific Instruments*, vol. 78, no. 1, p. 13705, Jan. 2007.
- [51] N. US Department of Commerce, 'NIST Standard Reference Database 71'. [Online]. Available: <http://www.nist.gov/srd/nist71.cfm>. [Accessed: 09-Sep-2015].
- [52] T. Koopmans, 'Über die Zuordnung von Wellenfunktionen und Eigenwerten zu den Einzelnen Elektronen Eines Atoms', *Physica*, vol. 1, no. 1, pp. 104–113, Jan. 1934.
- [53] Y. V. Larichev, B. L. Moroz, and V. I. Bukhtiyarov, 'Electronic state of ruthenium deposited onto oxide supports: An XPS study taking into account the final state effects', *Appl. Surf. Sci.*, vol. 258, no. 4, pp. 1541–1550, Dec. 2011.
- [54] 'Fig. 5 XPS based determination of the oxidation state of copper in Cu-G...' [Online]. Available: https://www.researchgate.net/figure/255772309_fig4_Fig-5-XPS-based-determination-of-the-oxidation-state-of-copper-in-Cu-G-composites-The. [Accessed: 06-Aug-2016].
- [55] *CasaXPS*. Casa Software Ltd, 1999.
- [56] A. F. Carley and M. W. Roberts, 'Proceedings of the Royal Society of London Series a-Mathematical Physical and Engineering Sciences', vol. 363, p. 403, 1978.
- [57] T. E. Madey, J. T. Yates, and Erickson N. E., 'Chemical Physics Letters', vol. 19, p. 487, 1973.
- [58] R. F. Reilman, A. Msezane, and S. T. Manson, 'Relative intensities in photoelectron spectroscopy of atoms and molecules', *Journal of Electron Spectroscopy and Related Phenomena*, vol. 8, no. 5, pp. 389–394, 1976.
- [59] C. D. Batich, 'Chemical derivatization and surface analysis', *Applied Surface Science*, vol. 32, no. 1–2, pp. 57–73, Jun. 1988.
- [60] F. Pippig, S. Sarghini, A. Holländer, S. Paulussen, and H. Terryn, 'TFAA chemical derivatization and XPS. Analysis of OH and NHx polymers', *Surf. Interface Anal.*, vol. 41, no. 5, pp. 421–429, May 2009.
- [61] J. L. Figueiredo and M. F. R. Pereira, 'Carbon as Catalyst', in *Carbon Materials for Catalysis*, P. Serp and J. L. Figueiredo, Eds. John Wiley & Sons, Inc., 2008, pp. 177–217.
- [62] D. Everhart and C. Reilley, 'Chemical Derivatization in Electron-Spectroscopy for Chemical-Analysis', *Anal. Chem.*, vol. 53, no. 4, pp. 665–676, 1981.
- [63] A. Chilkoti, B. D. Ratner, and D. Briggs, 'Plasma-deposited polymeric films prepared from carbonyl-containing volatile precursors: XPS chemical derivatization and static SIMS surface characterization', *Chem. Mater.*, vol. 3, no. 1, pp. 51–61, Jan. 1991.
- [64] X. Yang *et al.*, 'Au/CNTs catalyst for highly selective hydrodeoxygenation of vanillin at the water/oil interface', *RSC Adv.*, vol. 4, no. 60, pp. 31932–31936, 2014.

- [65] R. Heyrovská, 'Atomic Structures of Graphene, Benzene and Methane with Bond Lengths as Sums of the Single, Double and Resonance Bond Radii of Carbon', *arXiv:0804.4086 [physics]*, Apr. 2008.
- [66] R. J. Hamers, R. M. Tromp, and J. E. Demuth, 'Surface Electronic Structure of Si (111)-(7 \times 7) Resolved in Real Space', *Phys. Rev. Lett.*, vol. 56, no. 18, pp. 1972–1975, May 1986.
- [67] A. Cossaro, D. Cvetko, and L. Floreano, 'Amino–carboxylic recognition on surfaces: from 2D to 2D + 1 nano-architectures', *Phys. Chem. Chem. Phys.*, vol. 14, no. 38, pp. 13154–13162, Sep. 2012.
- [68] D. Gao *et al.*, 'Supported single Au(III) ion catalysts for high performance in the reactions of 1,3-dicarbonyls with alcohols', *Nano Res.*, vol. 9, no. 4, pp. 985–995, Apr. 2016.
- [69] A Blockbolten, 'THIOSULFATE LEACHING OF GOLD FROM SULFIDE WASTES', *METALL*, vol. 40, no. 7, pp. 687–689.
- [70] S. Nishimura, *Handbook of Heterogeneous Catalytic Hydrogenation for Organic Synthesis*. Wiley, 2001.
- [71] 'ETHYL p-DIMETHYLAMINOPHENYLACETATE', *Organic Syntheses*, vol. 47, p. 69, 1967.
- [72] J. Tsuji, *Palladium Reagents and Catalysts: New Perspectives for the 21st Century*. Wiley, 2004.
- [73] N. A. Asrian *et al.*, 'IR Study of Ozone Modified Graphite Matrix', *Mol. Cryst. Liquid Cryst.*, vol. 340, pp. 331–336, 2000.